AD-A122 076 RESEARCH PROGRAM REVIEW AIRCREW PHYSIOLOGY(U) NAVAL AIR 1/2
DEVELOPMENT CENTER WARMINSTER PA AIRCRAFT AND CREW
SYSTEMS TECHNOLOGY DIRECTORATE G T CHISUM ET AL.
UNCLASSIFIED JUN 82 NADC-82232-60 F/G 6/19 NL

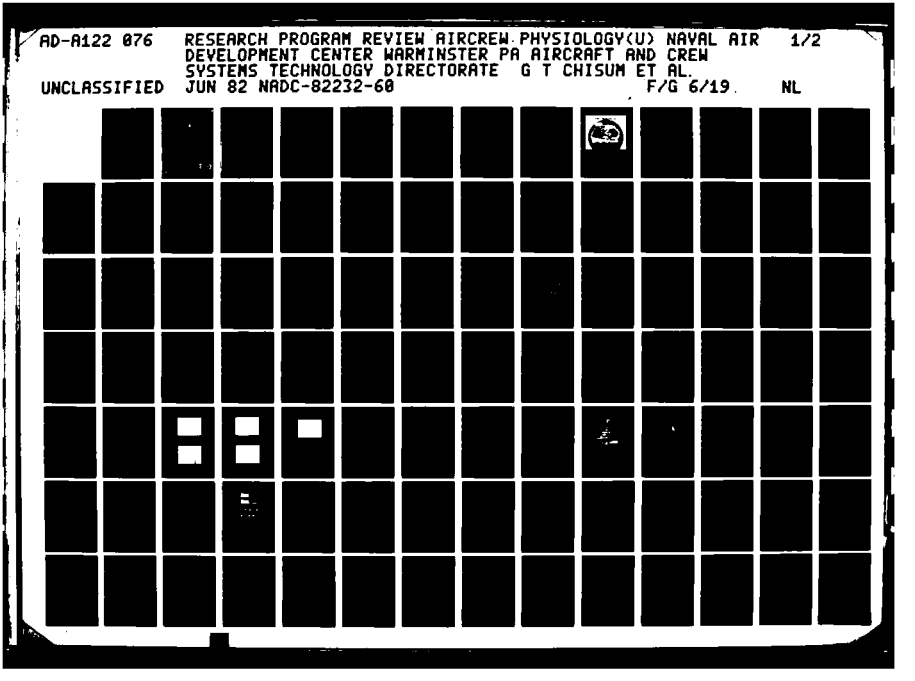

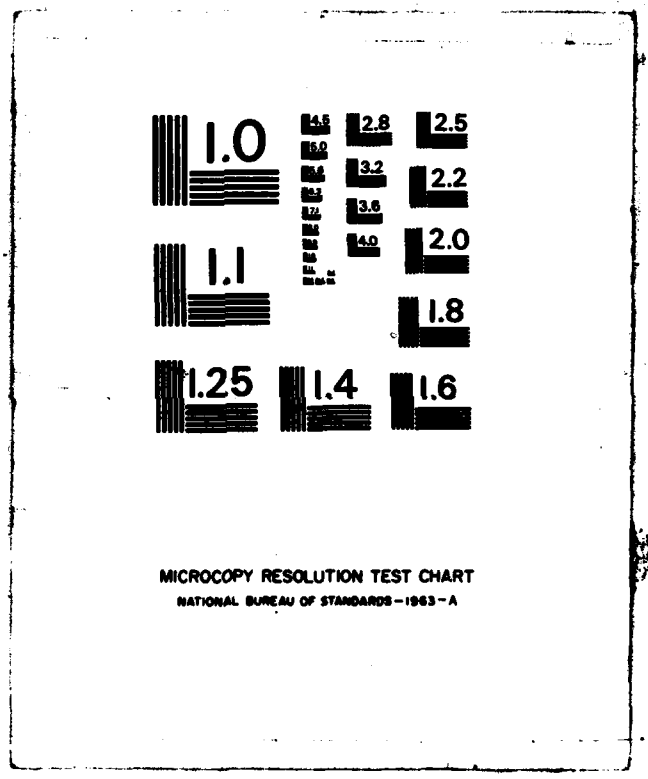
1.0
1.1
1.25
1.4
1.6
2.8
2.5
3.2
2.2
3.6
2.0
4.0
1.8
MICROCOPY RESOLUTION TEST CHART
NATIONAL BUREAU OF STANDARDS-1963-A

Report NO. NADC-82232-60

RESEARCH PROGRAM REVIEW: AIRCREW PHYSIOLOGY

Gloria T. Chisum and Phyllis E. Morway (Editors)
Aircraft and Crew Systems Technology Directorate
NAVAL AIR DEVELOPMENT CENTER
Warminster, Pennsylvania 18974

Hyman Rosenwasser (Editor)
NAVAL AIR SYSTEMS COMMAND
Department of the Navy
Washington, DC 20361

JUNE 1982

PROGRAM REVIEW
AIRTASK NO. A310310C/001A/2R04101001
Work Unit No. DG 127

Prepared for
NAVAL AIR SYSTEMS COMMAND
Department of the Navy
Washington, DC 20361

NOTICES

REPORT NUMBERING SYSTEM – The numbering of technical project reports issued by the Naval Air Development Center is arranged for specific identification purposes. Each number consists of the Center acronym, the calendar year in which the number was assigned, the sequence number of the report within the specific calendar year, and the official 2-digit correspondence code of the Command Office or the Functional Directorate responsible for the report. For example: Report No. NADC-78015-20 indicates the fifteenth Center report for the year 1978, and prepared by the Systems Directorate. The numerical codes are as follows:

CODE	OFFICE OR DIRECTORATE
00	Commander, Naval Air Development Center
01	Technical Director, Naval Air Development Center
02	Comptroller
10	Directorate Command Projects
20	Systems Directorate
30	Sensors & Avionics Technology Directorate
40	Communication & Navigation Technology Directorate
50	Software Computer Directorate
60	Aircraft & Crew Systems Technology Directorate
70	Planning Assessment Resources
80	Engineering Support Group

PRODUCT ENDORSEMENT – The discussion or instructions concerning commercial products herein do not constitute an endorsement by the Government nor do they convey or imply the license or right to use such products.

APPROVED BY: _____ DATE: 1 November 1982

T. J. GALLAGHER
DEPUTY DIRECTOR

UNCLASSIFIED

SECURITY CLASSIFICATION OF THIS PAGE (When Data Entered)

REPORT DOCUMENTATION PAGE		READ INSTRUCTIONS BEFORE COMPLETING FORM
1. REPORT NUMBER	2. GOVT ACCESSION NO. AD-A222 076	3. RECIPIENT'S CATALOG NUMBER
4. TITLE (and Subtitle) Research Program Review: Aircrew Physiology		5. TYPE OF REPORT & PERIOD COVERED Program Review
		6. PERFORMING ORG. REPORT NUMBER
7. AUTHOR(s) Gloria Twine Chisum Phyllis E. Morway Hyman Rosenwasser (NAVAIRSYSCOM)		8. CONTRACT OR GRANT NUMBER(s)
9. PERFORMING ORGANIZATION NAME AND ADDRESS Aircraft & Crew System Technology Directorate Naval Air Development Center Warminster, PA 18974		10. PROGRAM ELEMENT, PROJECT, TASK AREA & WORK UNIT NUMBERS AIRTASK No. A310310C/001A/ 2R04101001 Work Unit No. DG 127
11. CONTROLLING OFFICE NAME AND ADDRESS Naval Air Systems Command Department of the Navy Washington, D.C. 20361		12. REPORT DATE 13. NUMBER OF PAGES
14. MONITORING AGENCY NAME & ADDRESS(if different from Controlling Office)		15. SECURITY CLASS. (of this report) UNCLASSIFIED 15a. DECLASSIFICATION/DOWNGRADING SCHEDULE

16. DISTRIBUTION STATEMENT (of this Report)

Approved for Public Release; Distribution Unlimited.

17. DISTRIBUTION STATEMENT (of the abstract entered in Block 20, if different from Report)

18. SUPPLEMENTARY NOTES

19. KEY WORDS (Continue on reverse side if necessary and identify by block number)

Vision Research
Vision
Visual Requirements
Aircrew Vision
Research

20. ABSTRACT (Continue on reverse side if necessary and identify by block number)

The Aircrew Physiology Research Program Review was organized to provide a forum for the exchange of ideas and information between researchers involved in basic visual research and research directly applicable to visual problems in the Naval Air community. This volume includes the prepared texts of the formal presentations.

DD FORM 1 JAN 73 1473 EDITION OF 1 NOV 65 IS OBSOLETE
S/N 0102-LF-014-6601

UNCLASSIFIED
SECURITY CLASSIFICATION OF THIS PAGE (When Data Entered)

TABLE OF CONTENTS

OVERVIEW

Gloria Twine Chisum, Ph.D.

The AIR 310C Aircrew Physiology Research Program Review was sponsored by the Naval Air Systems Command and was organized and coordinated by the Naval Air Development Center, Vision Laboratory and the Cornell University School of Applied and Engineering Physics.

The purposes of the research performed under the program are to develop knowledge which can be used by those who are charged with providing conditions which will enhance the performance capability of aircrew and related personnel. The environment in which naval aircrew personnel operate places a variety of stresses on the personnel. The stresses may result from the accelerations which the aircraft are capable of achieving, conditions within the aircraft created by on-board equipment, personal equipment worn by the personnel, or aircraft carrier deck conditions, such as lighting, to which the personnel are exposed before launch or after recovery of the aircraft. In addition, aircraft handlers and other associated personnel may be exposed to some of the same conditions, and will be required to perform their functions with accuracy and dispatch.

The papers presented and discussed deal with a number of aspects of visual functioning which will broaden our knowledge and understanding of eye movements, visual acuity, sensory localization, adaptation and acceleration related visual phenomena and responses.

AN OVERVIEW OF THE

HELMET MOUNTED DISPLAY

John H. Allen

Advanced Simulation Concepts Laboratory
Code N-731
Naval Training Equipment Center
Orlando, Florida 32813

As demands on visual simulation increase, the costs for simulation climb proportionately. Most wide angle, high resolution visual simulation systems rely upon several computer image generator channels, each driving a separate display. The displays, when butted together, form a single wide angle field of-view. Increasing the number of displays enlarges the field-of-view and generally improves the fidelity of the visual simulation. Of course, the greater the number of computer generated displays, the higher the cost of the final system. There is a more modest approach.

The proposed Helmet Mounted Display System (now entering the 6.3 phase of development) contains only two computer generated displays, yet it provides both a wide angle field-of-view and high resolution. One display, containing both high resolution and high detail, is presented only at the observer's point of gaze, or area-of-interest. The second display, containing less resolution and less detail, surrounds the area-of-interest and fills the remainder of the observer's field-of-view. Visually, then, the total display tends to follow the acuity profile of the human eye by generating high resolution imagery only along the fiveal axis, and low resolution imagery in the periphery.

An artist concept of the proposed Helmet Mounted Display System is depicted below. A simulator cockpit is enclosed by a spherical screen. Two displays are projected onto the highly retro-reflective interior surface of the sphere. The imagery, both in the Area-of-Interest display and the surrounding Instantaneous-Field-of-View display are computer generated according to the pilots viewpoint. His viewpoint is determined from his head and eye position, as well as the velocity, attitude and position of the simulated aircraft. Each display has the appearance of a standard 1023 line interlaced full color video raster. However, the rasters are formed from modulated laser beams, which are projected from the pilot's helmet.

The computer generated red, green and blue video drives for each displayed channel modulate blue and green beams from a remotely located argon laser and a red beam from a companion dye laser which is pumped with excess power from the argon laser. The modulated laser beams are then horizontally line scanned and suitably focused onto the ends of two coherent flat fiber optic ribbons for subsequent relay to the helmet mounted projector.

The far end of each flat fiber optic ribbon is attached to the pilot's helmet. There, the two separate, full color line scans are vertically frame scanned by scanning mirrors and eventually projected onto the interior surface of the spherical screen.

The highest resolution will occur in the Area-of-Interest display – approximately two arc minutes. The lowest resolution is in the Instantaneous-Field-of-View display – about 10 arc minutes. Covering an area of 90 degrees horizontally by 70 degrees vertically, the Instantaneous-Field-of-View display will blend gradually into the 25 by 25 degree Area-of-Interest. It is hoped that the blending will alleviate any obvious effects caused by low detail low resolution forms transitioning into high detail, high resolution forms. Further study is required to determine the severity of the problem if indeed, one exists at all.

Most image generating systems utilize some form of pipeline processing to create the displayed video images. The 17 millisecond video field, as displayed by the Helmet Mounted Projector and viewed by the pilot, typically requires 100 milliseconds or so for formation. The current displayed video field, then, has been generated for a 100 millisecond old viewpoint. If the pilot/trainee fixates at a single spot on the spherical screen, the viewpoint is simply a consequence of simulator aircraft attitude, velocity and position, and a tenth of a second lag in image

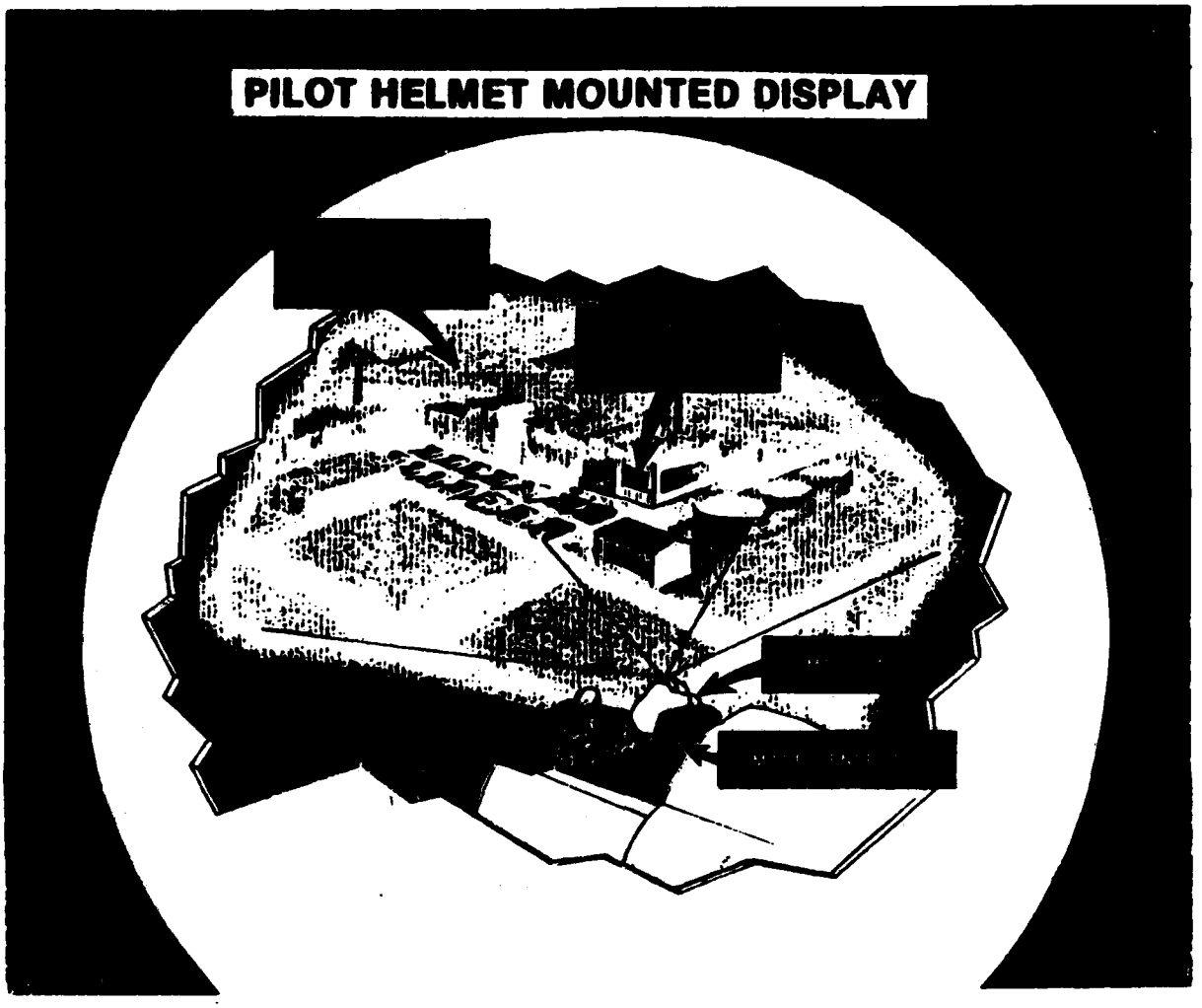

Figure 1 - Artist Concept

update is tolerable due to the inherent delays in real aircraft dynamics. Perceptually, an entirely different situation arises when the pilot wearing the helmet mounted projector makes a rapid head/eye movement. To be unobtrusive, an image must be created for his instantaneous viewpoint and displayed at the viewpoint for which it was created. Given the aforementioned delays in pipeline processing, the problem appears to be impossible to solve until faster image generators become available. There is an interim solution, however. If the imagery is always projected at the viewpoint it was created for, regardless of current viewpoint, the display will appear stable to the viewer. Since the high detail Area-of-Interest display covers a larger area than the equivalent area available to the human eye, considerable latitude can exist between the correctly displayed image viewpoint and the actual instantaneous viewpoint of the pilot/viewer. Further, if the pilots viewpoint or point of gaze can be predicted, the image generator may be given an equivalent "head start" in processing, and the effects of pipeline delay reduced accordingly. Research on eye movements performed at Carnegie Mellon has strongly indicated that the endpoint of a saccade is

predictable, given some allowable tolerance for error. To date, though, the data is for fixed head position. Additional investigation is required to determine the feasibility of predicting head and eye coupled motion.

Despite these areas of concern, the Helmet Mounted Display offers a reasonable, low cost alternative to traditional, multi-channel wide field-of-view displays. It presents a high detail, eye resolution limited display only where the pilot chooses to look and, by so doing, provides a more economic and effective visual simulation.

PREDICTING FINAL EYE POSITION HALFWAY THROUGH A SACCADE

A. Terry Bahill
and
Jeffrey S. Kallman

Biomedical Engineering Program,
Department of Electrical Engineering,
Carnegie-Mellon University,
Pittsburgh, PA 15213.
(412) 578-2536

INTRODUCTION

To save money and lives pilots sometimes fly simulators rather than airplanes. To be realistic, the visual display must change in response to a pilot's actions. This precludes the use of motion pictures for visual displays in simulators. Simulators typically produce the visual scene with computer image generators (CIGs).

Present CIGs cannot display a full 360° image. The human, however, does not have uniform visual acuity: he only sees with fine detail where the fovea of the eye is directed. So, in the simulator under development at the Navy Training Equipment Center in Orlando, Florida one CIG channel controls a laser projector covering the 20° by 20° area directly in front of the subject with eye limited resolution and another CIG channel displays the 90° by 70° peripherial field of view with lower resolution.

When a pilot makes a head or eye movement, the new area of regard should have detailed resolution when the eye gets there. However, the CIG needs 80 ms to change the display. We have developed an instrument that monitors eye position and, in the middle of a saccadic eye movement, predicts the final eye position. This instrument gives the CIG a 20 to 60 ms head start in computing the detailed foveal display for the pilot's new direction of gaze. This headstart is not as large as the CIGs delay, but coupled with the 20 ms afforded by saccadic suppression (Campbell and Wurtz, 1978; Matin, 1982) it may be sufficient to make the change unnoticeable to the pilot.

We have used two concepts in constructing the predictor; main sequence diagrams and the multiplier factor.

(1) Main sequence diagrams show the relationship between saccadic peak velocity and saccadic magnitude (Bahill, et al., 1975). To predict the end point of a saccade, we computed eye velocity, waited for the peak to occur, used this value of the peak velocity to find the appropriate saccadic magnitude, and then made a prediction of the final eye position. We used a generalized main sequence equation that fit the data of 24 individuals (Bahill, et al., 1981). Variability in the data limited the accuracy of this approach to ± 10%. This is why we became interested in whether nasal saccades or temporal saccades were faster. We were prepared to use two main sequence curves; one for nasal and one for temporal. However, our studies and those cited above showed that although for two consecutive saccades in opposite directions the nasalward one would probably have a higher peak velocity, in general, neither could be said to be faster.

(2) The Saccadic velocity profile is approximately symmetric about peak velocity. Therefore, for our second technique we continuously computed eye velocity, detected the peak velocity of the saccade, noted how far the eye had moved since the start of the saccade, and then predicted that the eye would go twice this distance before it came to rest. However, the saccadic velocity profiles were not exactly symmetric. Most saccades reached peak velocity before the middle of the saccade. Therefore, the distance the eye had gone at the time of peak velocity was not merely doubled, but rather it was multiplied by the multiplier factor defined in Fig. 1. Taking advantage of this asymmetry reduced the prediction time by a few milliseconds and produced more accurate predictions. This paper is primarily about this multiplier factor.

METHODS

We used two different instrumentation systems for measuring eye movements. For horizontal saccades smaller than 20 degrees we used a standard photoelectric system (Bahill, 1981; Bahill, et al., 1981). The linear range extended ±10 degrees from primary position. Linearity was obtained by adjusting the equipment while the subject tracked a sinusoidally moving target. We set the amplifier gains so that 20 degrees represented full scale. Instrumentation noise was then less than ten millivolts, corresponding to an error of 1.2 minutes of arc. The error resulting from the 12 bit analog to digital conversion was 0.3 minutes of arc. Biological noise was about 1.5 minutes of arc. For vertical eye movements and for horizontal saccades larger than 20 degrees a new eye movement measurement system was used. It was based on a German instrument that used the United Detector Technology FPT125 X-Y photodiode. It was easy to adjust the instrument to achieve linearity for 40 degree horizontal saccades, and 20 degree vertical or oblique saccades. For certain subjects (notably those with large astigmatic corrections) linearity could not be achieved. Both instrumentation systems had a 100 Hz bandwidth.

We used two different computer systems for analyzing the data. For off-line calculations (such as those that produced the main sequence data of Fig. 2) floating point arithmetic operations were performed on a PDP 11/34 minicomputer. Target and eye movement data were passed through a 12 bit analog to digital converter sampling at 1000 Hz, and were then stored on a disk for future calculations. Calibration factors were derived from segments of the data when the subject tracked a target that jumped between points ±5 degrees from primary position. Calibration factors for each eye were computed by averaging one to two seconds of data from four to ten manually selected periods when the eye was stationary and looking at the target. For real-time calculations (such as those that produced the predictions shown in Fig. 3) integer arithmetic operations were performed on a LSI-11/2 microcomputer. Eye movement data were sampled at 1000 Hz by a 12 bit analog to digital converter, stored in semiconductor memory, processed by the predictor algorithm, and finally passed through a digital to analog converter.

For the off-line calculations, eye velocity was calculated with the following two-point central difference algorithm.

$$\dot{y}(kT) = \frac{y([k+3]T) - y([k-3]T}{6T} \tag{1}$$

where T is the sampling interval and k is the index for descritized time. This produced velocity records with (for 1 msec sampling) 3 dB bandwidths of 74 Hz (Bahill, et al., 1982). For the on-line real-time velocity calculations we used the following backward difference algorithm.

$$\dot{y}(kT) = \frac{y(kT) - y([k-8]T)}{8T} \tag{2}$$

This produced velocity records with (for 1 msec sampling) 3 dB bandwidths of 55 Hz. This algorithm required no division operation, merely a shift right of three bits.

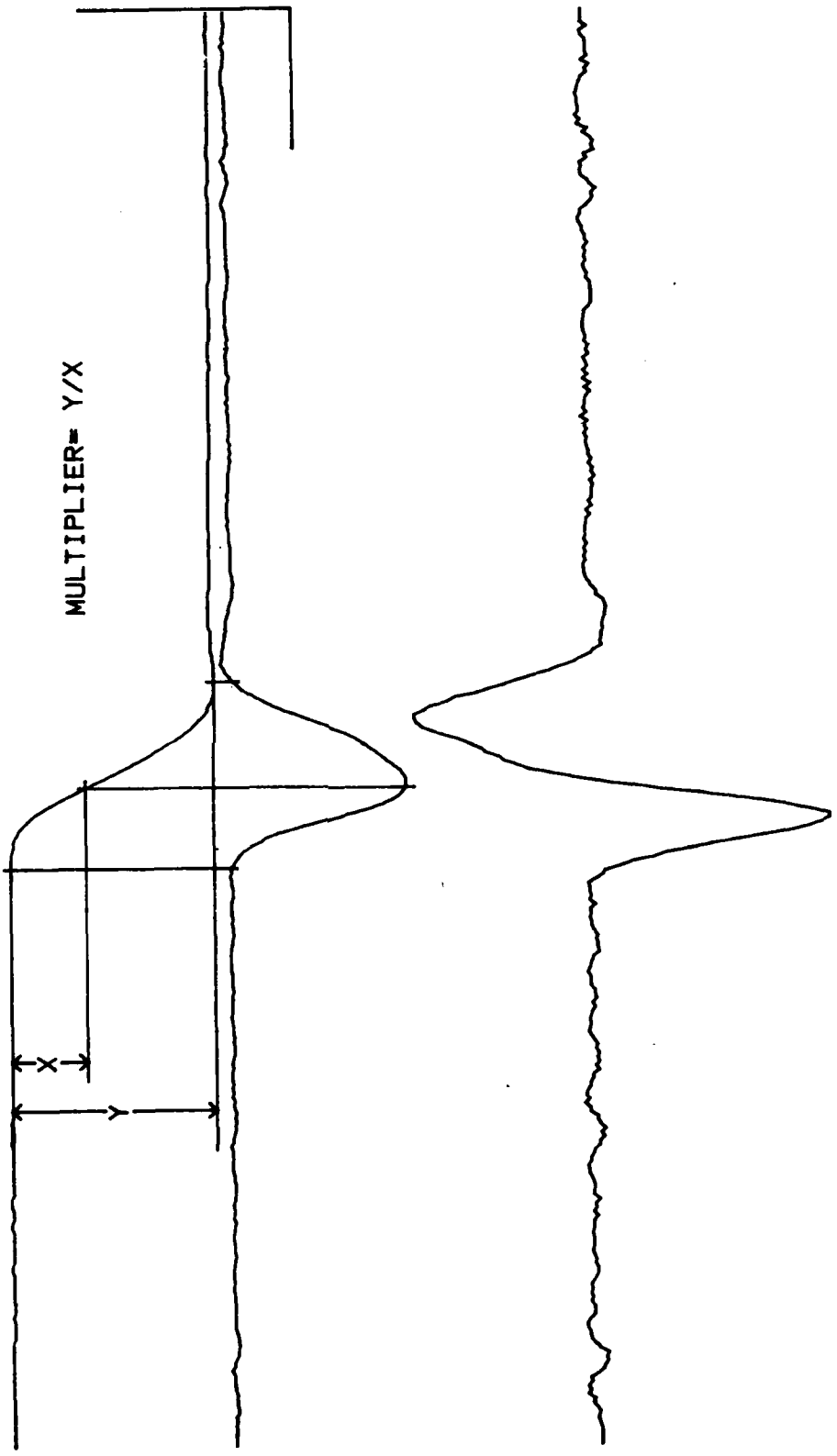

Figure 1 - Definition of the multiplier factor. If the change in eye position at the time of peak velocity is multiplied by the multiplier factor then the final eye position will be predicted. The calibration key represents 10 degrees, 500 deg/sec, 30,000 deg/sec2, and 100 msec. This was a temporal movement of the left eye.

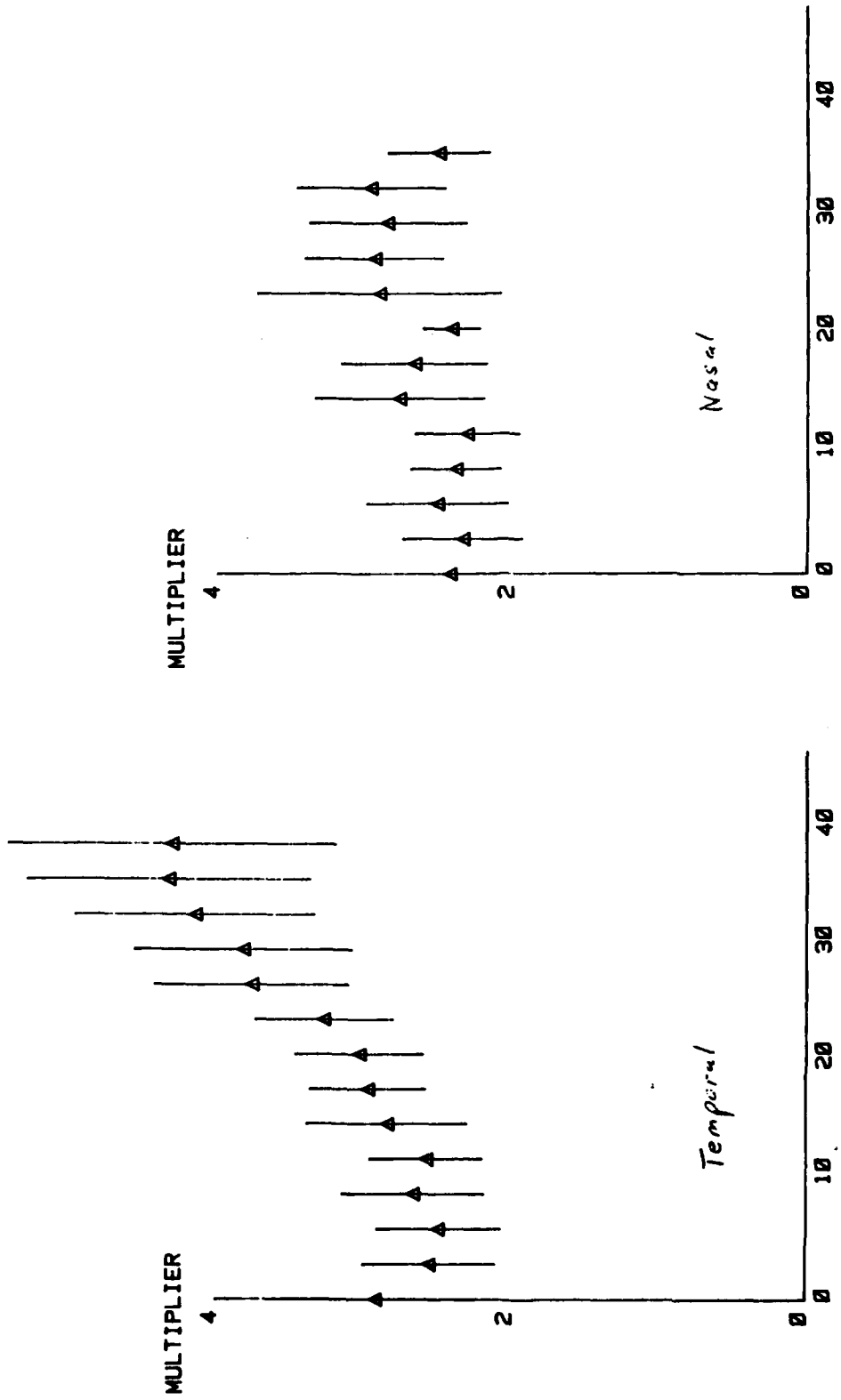

Figure 2 - Multiplier factors for 200 saccades of one subject for (left) temporal saccades and (right) nasal saccades. Multiplier factors are a function of saccadic magnitude.

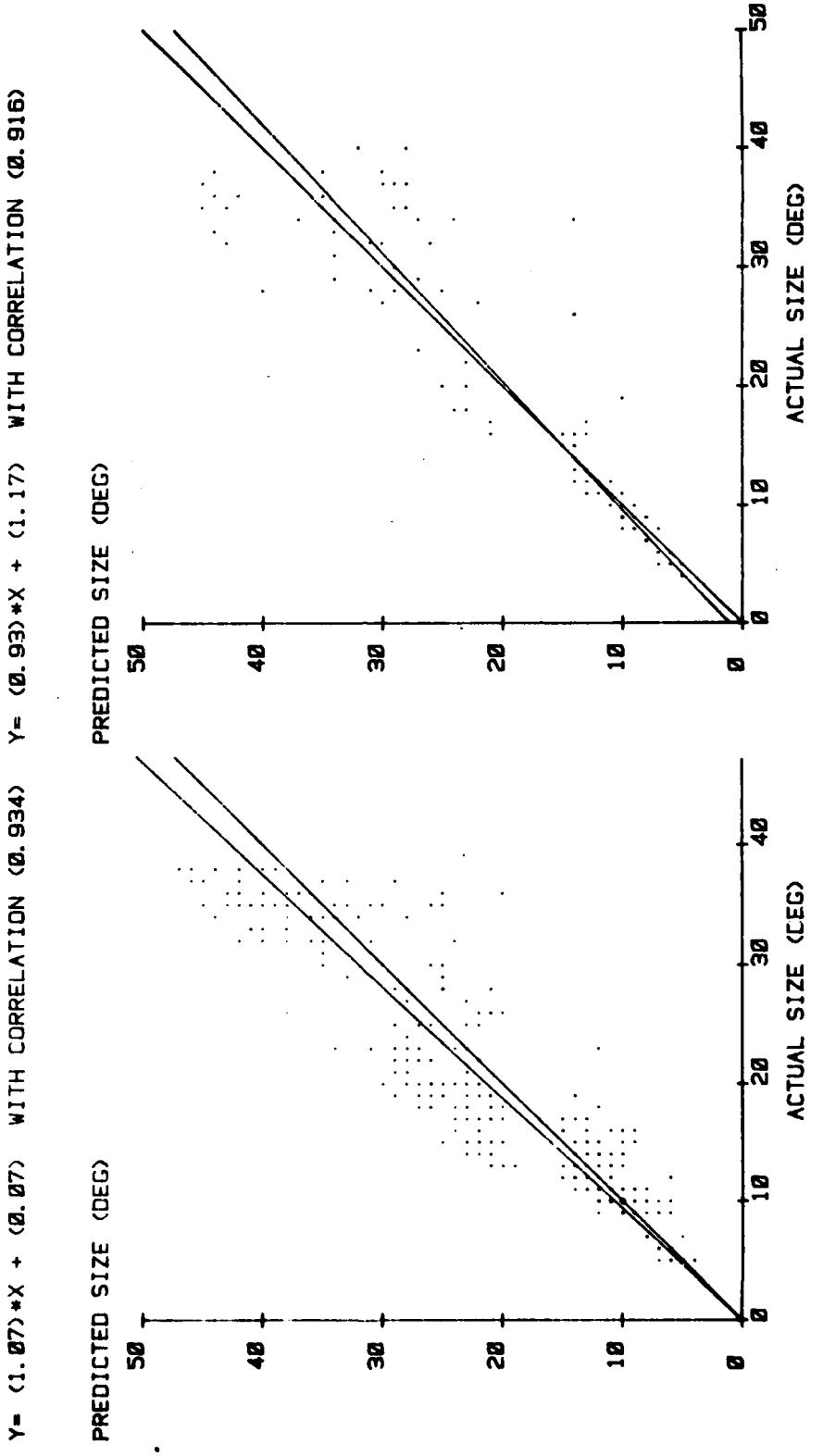

Figure 3 - Predicted versus actual saccadic magnitude for two subjects; the predictor did better for subject A (left) than for subject B (right).

RESULTS

Figure 1 shows the basic definition of the multiplier factor. If a saccade were perfectly symmetric the final position would be twice the position at peak velocity. Because most saccades reached peak velocity before the middle of the saccade the multiplier factor was greater than 2. For small saccades there was little difference between temporal and nasal saccades. As the saccadic magnitude became larger the difference between the multiplier factors for temporal and nasal saccades increased, as shown in Fig. 2.

There was intersubject variability in the multiplier factor. For most subjects the multiplier factor for temporal saccades was greater than two and increased with saccadic magnitude, but not as rapidly as for the subject of Fig. 2. For most subjects the multiplier factor for nasal saccades was not a strong function of saccadic magnitude.

The multiplier factors of Fig. 2 were computed with the zero-phase two-point central difference differentiation algorithm and they were plotted as functions of final saccadic magnitude. For use in the real-time predictor, the multipliers were formulated differently. First, velocity was calculated using the backward difference algorithm. This variation allowed real time implementation, but had the effect of adding a time delay. Second, to avoid prediction on small saccades and to avoid false predictions on noisy data, the eye velocity had to exceed 100 degrees per second before the predictor started operation. This had the effect of making the angle x in Fig. 1 smaller. Third, we calculated the multiplier factor versus the angle x, not the multiplier factor versus saccade size.

Our best general predictor algorithm for all subjects used the following equations. For saccades smaller than 20 degrees the equations for the predicted saccade size were

$$y = (1.4 + 0.05x)x \quad \text{for temporal saccades (positive x)} \tag{3}$$

$$y = (1.4 + 0.04x)x \quad \text{for nasal saccades (negative x)} \tag{4}$$

For saccades larger than 20 degrees the best results were obtained by using a multiplier of 2, i.e.

$$y = 2x \tag{5}$$

Figure 3 shows the results of this predictor operating on data from two subjects; (A) shows some of its best results, (B) shows some of its worst results. The equation at the top of each figure is the linear regression fit to the data; it can be used as a figure of merit for the predictor. If the predictor were perfect the slope of the linear regression line would be 1.0, the intercept would be 0 and the correlation would be 1.0. Predictions of the final position of the eye were made 10 to 60 msec before the eye came to rest.

To make this predictor work at a sampling rate of 60 Hz the multiplier factor for saccades larger than 20 degrees was changed to 1.2, i.e. $y = 1.2x$. Predictions almost as good as with the 1000 Hz sampling rate were obtained. The linear regression estimates for the data of Fig. 3 sampled at 60 Hz were

$$Y = 0.87x + 4.2 \text{ with correlation of } 0.961$$

$$Y = 0.78x + 5.2 \text{ with correlation of } 0.927$$

The 60 Hz sampling rate prevented the predictor from making predictions of saccades smaller than 10 degrees. The final eye position was predicted either 0, 17, or 34 msec before the eye came to rest.

Three versions of the predictor were tried on a data pool from four subjects. The linear regression lines were, for the main sequence predictor

$$Y = 0.86x + 1.7 \text{ with correlation of } 0.856$$

for the multiplier factor predictor

$$Y = 0.73x + 2.7 \text{ with correlation of } 0.887$$

and for the modified multiplier factor predictor described by Eqs. 3-5

$$Y = 1.04x + 0.71 \text{ with correlation of } 0.936$$

The modified multiplier factor technique of Eqs. 3-5 was the best predictor for any random subject.

DISCUSSION

Other derivative algorithms were tried. They substituted complexity for speed and simplicity. They did not allow more accurate predictions to be made.

Acceleration was tried in conjunction with velocity. The acceleration data were too noisy to be used without extensive low-pass filtering. This filtering slowed down the prediction process. The fastest and most accurate predictions were made using velocity alone.

The predictor was set up to operate with no individualization. If a group of points were to be presented for calibration purposes then the multiplier factors could be tailored for each individual.

The multiplier factor had variability from subject to subject, but it had less variability that the main sequence diagrams. Furthermore, it worked for vertical as well as horizontal saccades.

Acknowledgements—— This research was supported by a contract from the U.S. Navy Training Equipment Center, Orlando, Florida administered by John Kulik, Denis Breglia, and John Allan.

REFERENCES

Campbell, F.W. and Wurtz, R.H. (1978) Saccadic omission! Why we do not see a gray-out during saccadic eye movement. **Vision. Res. 18**, 1297-1303.

Matin, E. (1982) Saccadic suppression and the dual mechanism theory of direction constancy. **Vision. Res. 22**, 335-336.

Bahill, A.T., Clark, M.R. and Stark, L. (1975) The main sequence, a tool for studying human eye movements. **Math. Biosci. 24**, 191-204.

Bahill, A.T., Brockenbrough, E.E. and Troost, B.T. (1981) Variability and development of a normative data base for saccadic eye movements. **Invest. Ophthalmol. Vis. Sci. 21**, 116-125.

Bahill, A.T. (1981) **Bioengineering: Biomedical, Medical and Clinical Engineering.** Prentice-Hall Inc., Englewood Cliffs New Jersey.

Bahill, A.T., Kallman, J.S. and Lieberman, J.E. (1982) Frequency limitations of the two-point central difference differentiation algorithm. **Biological. Cybernetics.** in press.

PROGRESS IN REAL-TIME MONITORING OF THE VISUAL EVOKED POTENTIAL

J.G. Nelson, L. Hrebien and M.M. Cohen
Aircraft and Crew Systems Technology Directorate
Naval Air Development Center, Warminster, PA 18974

INTRODUCTION

Modern high-performance aircraft can produce and sustain levels of acceleration ($+G_z$) greater than the pilot's physiologic tolerance limits. These limits, as a joint function of $+G_z$ parameters and numerous protective devices and methods, are studied on human centrifuges such as the Dynamic Flight Simulator at the Naval Air Development Center.

Subjects can experience loss of consciousness (LOC) during exposure to sufficiently high $+G_z$ acceleration. LOC is usually preceeded by visual symptoms: decreased visual sensitivity, dimming of the visual field, peripheral light loss (PLL), and central light loss, ending in complete light loss or blackout. PLL is commonly used as an end point indicator for centrifuge runs [1].

Real-time monitoring of PLL requires an active response by the subject. In contrast, the visual evoked potential (VEP) [2], which also reflects the integrity of the visual system, requires only a relatively passive task of viewing a visual stimulus.

Real-time monitoring of VEP as a measure of visual functioning on the human centrifuge must meet certain criteria, and stay within certain constraints. The most important are that the response-time to loss of vision must be less than approximately four seconds, with a low false-alarm rate and a very low probability of not detecting (and acting upon) a complete loss of vision. The method must not require extended subject preparation time, e.g., a many-electrode montage. The required computer capacity must be less than a full mini-computer and the non-real-time computations must not significantly extend the normal 1-2 minute rest periods between centrifuge runs.

The available real-time methods (e.g., [3, 4, 5]) did not seem to be directly applicable when considered in terms of these criteria and constraints. However, such methods did provide the broad strategy for attempting a solution.

To provide a continuous flow of data, we chose to utilize the steady-state VEP [3]. A monitoring method, staying within these computer capacity and time constraints, was developed [6]. This method was implemented on a desk-top computer (HP 9825T) and an FFT-based low-frequency dual channel signal analyzer (HP 3582A), and tested with six subjects under static (non centrifuge) conditions. The results proved encouraging and potentially useful in general VEP studies [7].

METHOD

Overview

The method requires an initial parameter estimation run, relating system output (VEP & EEG) to input (stimulus). Based on an ensemble of FFT's, calculation provides co-power, cross-power, phase angle, and coherence [8]. These are used to calculate a weighting function to be applied to single FFT's in real-time to produce a single variable which may be labeled "Percent Vision". The weighting function performs magnitude normalization, rotation of axes such that the VEP components become positive-real, and optimal weighting. When summed together, these optimally weighted components become the variable "Percent Vision". Under the restrictive assumptions of our model, this variable should have a maximal S/N, a predicted standard deviation, an expected value of 100 under conditions of normal vision, and 0 under conditions of blackout.

Parameter Determination

In order to determine the basic parameters of the process we collected simultaneous ensembles of input (stimulus) and output (response) FFT's from the dual channel frequency analyzer. Here we designate the input as X(f) and the output at Y(f) were Y(f) is actually VEP + EEG. The computation of the other parameters is as follows: input auto-power spectrum

$$G_{xx}(f) = X(f) \cdot X^{*}(f) \tag{1}$$

output auto-power spectrum

$$G_{yy}(f) = Y(f) \cdot Y^{*}(f) \tag{2}$$

and cross-power spectrum

$$G_{yx}(f) = Y(f) \cdot X^{*}(f) \tag{3}$$

Then, using the ensemble averages, the coherence function

$$\gamma^2 = \frac{|\bar{G}_{yx}(f)|^2}{\bar{G}_{xx}(f) \cdot \bar{G}_{yy}(f)} \tag{4}$$

Simplified Parameter Determination

We are concerned only in regularities in the data, not with veridicality. In real-time, we want to process a raw FFT to produce a single optimized variable. At the level of the FFT, this means that we do not want corrections for phase-shift and pass-band ripple produced by the anti-aliasing and decimation filters in the signal analyzer. Similarly we used a uniform window function for the time function measurement.

By careful design and control of the stimulus, a number of advantages and simplifications occur. For the VEP, using a strobe light driven by a spulse train or trains, each response, whether fundamental or harmonic, is an integral multiple of the stimulus fundamental, which is chosen to be an integer multiple of the bin spacing. This eliminates "picket-fence" effects and places the response at specific harmonically related spectral points.

The stimulus and measurement processes are slaved such that each stimulus time-frame is identical

$$[x_i(t)]_j = [x_i(t)]_{j+1}$$

Since the stimulus is thus constant, then for our relativistic approach in the detection process we define the input amplitude spectrum as uniform and unity magnitude with zero phase angle over the band of interest. This eliminates the need to calculate the FFT for the input and greatly simplifies the calculations required later on. Thus

$$X(f) = 1 \tag{5}$$

and therefore

$$G_{xx}(f) = 1. \tag{6}$$

Then, by substituting into equation (3):

$$G_{yx}(f) = Y(f) \tag{7}$$

and, finally

$$\gamma^2 = |\bar{Y}(f)|^2 \; / \; \bar{G}_{yy}(f). \tag{8}$$

Also, note that $\bar{Y}(f)$ directly specifies the phase angle of the response.

Since a response will be obtained at the fundamental and possibly harmonic frequencies of the stimulus X(f), the FFT need only be processed at those frequencies. Thus, in our application, with a 0.8 Hz spacing of a 128 point FFT over the 0-100 Hz band, using a mixed pulse train of stimuli (12.8 and 16 Hz) synchronized with a missing fundamental of $f_o = 3.2$ Hz, we analyzed at every fourth non-zero point, for a total of 31 points.

To summarize, our simplified computational requirements consist of:

1) For each time frame of the ensemble, compute Y(F) and decimate to include only multiples of the missing fundamental: $Y(Nf_o)$ where $N = 1, \ldots, 31$. For each time-frame, compute auto-power spectrum, $G_{yy}(Nf_o)$.

2) Compute ensemble averages, $\bar{Y}(Nf_o)$ and $\bar{G}_{yy}(Nf_o)$

3) Compute coherence,

$$\gamma^2(Nf_o) = |\bar{Y}(Nf_o)|^2 \; / \; \bar{G}_{yy}(Nf_o) \tag{9}$$

Unless the number of frames in the ensemble (N_f) is quite large, coherence should be corrected for bias. Thus, setting $1/N_f$ as the threshold criterion,

$$\text{if } \gamma^2 (Nf_o) \leq 1/N_f, \text{ then } \gamma_c^2 = 0 \text{ and}$$

$$\text{if } \gamma^2 (Nf_o) > 1/N_f, \text{ then}$$

$$\gamma_c^2 = \frac{\gamma^2 - 1/N_f}{1 - 1/N_f} \tag{10}$$

(All further reference to coherence assumes this correction).

Creation of Normalized Real Variables

The corrected coherence permits us to partition the power (variance about the origin) into signal,

$$s = \gamma^2 \, \bar{G}_{yy} \tag{11}$$

and noise,

$$N = (1 - \gamma^2)\bar{G}_{yy} = \bar{G}_{yy} - s \tag{12}$$

components. Since the noise, which is predominently background EEG, is phaseless, its variance (which is produced by squaring and summing two zero mean, equal variance, orthogonal, linear variables) is equal to N/2 along any arbitrary axis. That is, phase sensitive detection rejects ½ of the incoherent noise. Then, defining a new axis system where the positive real axis is aligned with and of the same sense as $\bar{Y}(Nf_o)$, the new real component can be determined by defining a rotational weight,

$$W_1 = \frac{\bar{Y}(Nf_o)}{|\bar{Y}(Nf_o)|} \tag{13}$$

and calculating the function,

$$(\text{Re } W_1)(\text{Re } Y) + (\text{Im } W_1)(\text{Im } Y). \tag{14}$$

Using the expected standard deviation about the origin we derive a normalizing weight,

$$W_2 = 1/((\gamma^2 + \tfrac{1}{2}(1-\gamma^2))\ \bar{G}_{yy})^{1/2} = 1/(\tfrac{1}{2}(1+\gamma^2)\ \bar{G}_{yy})^{1/2} \tag{15}$$

Then, these weights may be combined as,

$$W_3 = \text{Re}(W_1 W_2), \text{Im}(W_1 W_2). \tag{16}$$

We may then calculate real, positive mean, unity power variables, using single FFT's in real-time,

$$R = (\text{Re } W_3)(\text{Re } Y) + (\text{Im } W_3)(\text{Im } Y) \tag{17}$$

which have the enhanced coherence,

$$\gamma_E^2 = \frac{\gamma^2}{\gamma^2 + \frac{1}{2}(1-\gamma^2)} = \frac{2\gamma^2}{1+\gamma^2} \quad . \tag{18}$$

(All further use of coherence assumes γ_E^2).

By combining decimation across frequency with phase sensitive detection, we have improved overall S/N by a factor of eight. By conversion to normalized, positive mean, real variables, we are in a position to optimally weight and sum these variables for further S/N improvement.

Optimal Weighting

In the most general form, the variance of a weighted sum of variables involves a full variance-covariance matrix [9]. It was decided that, while multiple regression [10] and/or linear discriminant [11] models could be applied, the required computation would exceed our capacity-time constraints. If we assume that all of the structure of the covariance of the variables is due to unity correlation of signal components with each other and zero correlation of noise components with each other and with signal, then a step-wise process may be used. Here, two variables are combined, the compound is then combined with the third, the resulting compound is then combined with the fourth, and so on. Computational requirements increase as a linear function of the number of variables to be combined.

For two variables [9], setting $W_1 = 1$, we may solve for relative weight ($W_1 = 1$, $W_2 = W$):

$$\sigma^2_{x_1 + Wx_2} = \sigma_1^2 + W^2 \sigma_2^2 + 2r_{12} W \sigma_1 \sigma_2. \tag{19}$$

The variables which we are weighting and summing are real and each have two components with variances (powers) S_R and N_R, such that $S_R + N_R = 1$. The signal variance of the resultant compound is,

$$S_{RC} = S_{R1} + W^2 S_{R2} + 2W(S_{R1}S_{R2})^{\frac{1}{2}} \tag{20}$$

the standard deviation is,

$$S_{RC}^{\frac{1}{2}} = S_{R1}^{\frac{1}{2}} + W S_{R2}^{\frac{1}{2}} \tag{21}$$

and the noise variance is,

$$N_{RC} = N_{R1} + W^2 N_{R2} = (1-S_{R1}) + W^2(1-S_{R2}). \tag{22}$$

To find the weight W producing the maximum S_{RC}/N_{RC}, we differentiate it with respect to W and set the result equal to zero,

$$0 = [(S_{R2}-1)\,(S_{R1}S_{R2})^{1/2}]\,W^2 + [S_{R2}-S_{R1}]\,W + [(1-S_{R1})\,(S_{R1}S_{R2})^{1/2}]. \quad (23)$$

This quadratic equation is then solved for W.

Some rather tedious change-of-scale arithmetic is involved in getting from W as delivered by equation (23) to the actual weighting function to be used for optimization. In our application, we take the first of the compressed spectral points and set $W_1 = 0$ if $\gamma_1^2 < 0.15$, and arbitrarily set $W_1 = \gamma_1^4$ if not. This defines values "S_{RC}" = $W_1^2\gamma_1^2$; "N_{RC}" = $W_1^2(1-\gamma_1^2)$; and "γ_{RC}^2" = γ_1^2. The γ_{RC}^2 is passed as S_{R1} to the optimization equation along with γ_2^2 (if > 0.15) as S_{R2}. The delivered weight, W_D, which assumes that $S_1 + N_1 = 1$, is rescaled to,

$$W_2 = (S_{RC1} + N_{RC1})^{1/2} W_D. \quad (24)$$

W_2 is then used to produce the first genuine compound. Since signals add as standard deviations (eq. 21) and noises as variances (eq. 22),

$$S_{RC2} = (S_{RC1}^{1/2} + WS_2^{1/2})^2,$$

$$N_{RC2} = N_{RC1} + W^2(1-S_2), \text{ and}$$

$$\gamma_{RC2}^2 = S_{RC2} / (S_{RC2} + N_{RC2}).$$

This step-wise process continues until all useable points are exhausted.

Final values of S_{RC} and N_{RC} are used to rescale the entire weighting function, to produce an expected value of 100%. This weighting function is combined with the normalization and rotation weights to produce the weighting function for use in real time runs. The final value of $1-\gamma_{RC}^2$ is used to set confidence limits for the variable "Percent Vision", which is computed and displayed in real time.

The final γ_{RC}^2 also provides a simple figure-of-merit for evaluation of any change in experimental method. Changes in electrode placement, changes in stimulus parameters (e.g., intensity, frequency composition, spatial structure), or any other changes in method may be evaluated.

A paper detailing the above detection method will be presented as reference [12].

Application

This approach was tested on six male Naval Enlisted and Officer volunteers under static (non-centrifuge) conditions. The subjects sat in front of a diffuse strobe light flickering simultaneously at 12.8 and 16.0 Hz. This was timed and controlled from the internal clock signal of an HP 3582A low frequency spectrum analyzer which was set to retrigger every 1.5625 seconds and generated an FFT for each of these time frames in the frequency range of 0-100 Hz, with a spectral resolution of 0.8 Hz. Standard scalp electrodes (Oz, Cz, mastoid ref.) were used to monitor the EEG. Each subject sat through four runs lasting about one minute each on two different days. The first of each four runs was a parameter estimation run and the next three, taken less than two minutes apart, were used for determination of "Percent Vision". For these three runs the strobe light was occluded for about five seconds and then exposed again near the end of each run to simulate an episode of loss of vision.

During the parameter estimation runs, we collected 32 FFT's and estimated the copower, cross-power, phase angle, and coherence of the ensemble. These parameters were used to calculate a complex weighting function to be applied to single FFT's in real-time to produce the single variable, "% Vision". The weighting function performs magnitude normalization, rotation of axis such that the VEP component becomes positive real, and produces scalars which when summed result in a variable which has maximal signal-to-noise ratio. (This method assumes stationarity, normal distribution, uncorrelated "noise", correlated "signal").

Results and Conclusions

In all runs, a five second delay of the data collection, after turning on the strobe, was used to permit the response to reach a steady-state. In Figure 1, the first 2-3 plotted points indicate that a total delay of 8-10 seconds should be used in further applications. In the real-time runs, the strobe was occluded for three times beginning approximately at frame 34. In Figure 1, the values for Frames 35-38 indicate that a three frame loss of stimulus has a major effect on only four frames. Frames 36-37, clustering as they do at zero, indicate that coherent electronic noise was not corrupting the measurement.

Taking Frames 4-34 as quasi-stationary, Table 1 presents the summary results for each of the 3[illegible] real-time runs. The expected standard deviation, based upon the parameter estimation runs, ranges from 17.0 to 30.4, while the obtained values ranged from 15.4 to 36.8. The correlation between E[SD] and real-time SD was +.62.

Mean Percent Vision, ranging from 59.6 to 106.5, was not related to either expected or obtained SD (r = +.12 and +.07 respectively). This reduced signal amplitude would seem to require a non-stationarity of the VEP's phase angles and/or relative magnitudes (magnitude as a function of frequency). Further data and analysis are required to estimate the source of this effect, and appropriate methods for dealing with it.

Figure 2, in addition to showing that the monitoring method is useable with the "better" subjects, also shows the effectiveness and cost of using a "Two-Point Smooth": the displayed result at frame 35 is delayed by one frame-time. Since we cannot simply reject time-frames contaminated by eye-blink or other artifacts such smoothing provides a simple and reasonably effective method.

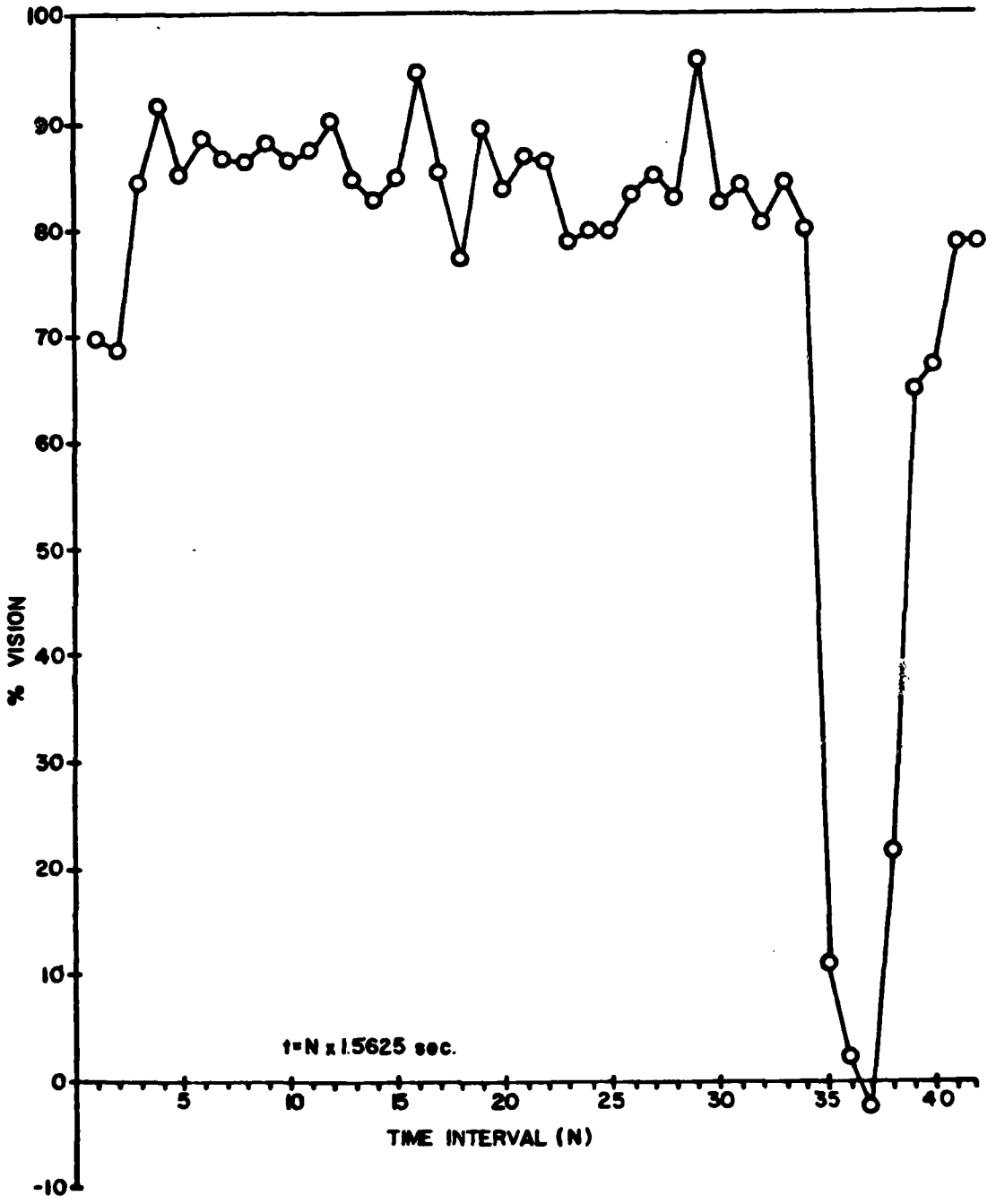

Figure 1 - Mean Percent Vision For All Real-Time Runs.

Table I. The Expected Standard Deviations, Obtained Standard Deviations, and Mean Percent Vision for Real-Time Runs (Frames 4-34).

SESSION-SUBJECT	EXPECTED SD	RT-1 SD	RT-2 SD	RT-3 SD	RT-1 MEAN	RT-2 MEAN	RT-3 MEAN
1-1	24.9	29.6	27.6	27.2	82.1	106.3	90.5
1-2	18.2	24.5	22.9	16.7	99.7	80.6	67.9
1-3	18.5	15.4	21.8	19.1	85.9	77.9	74.7
1-4	21.6	31.0	28.4	21.1	79.1	64.8	59.6
1-5	17.0	18.3	19.1	20.4	94.1	83.7	77.1
1-6	22.0	25.8	19.2	20.1	86.3	73.4	79.7
2-1	30.4	24.9	26.3	33.9	64.8	79.2	97.9
2-2	18.0	19.5	26.7	22.5	91.7	81.7	69.5
2-3	24.0	22.8	28.8	20.0	106.5	95.2	105.2
2-4	29.5	24.7	30.1	32.8	97.6	86.2	90.5
2-5	17.5*	21.0	18.6	17.5*	101.2	91.3	93.3*
2-6	21.8	23.8	22.5	36.8	80.9	89.0	79.7

*: SPECIMEN RUN OF FIG. 2

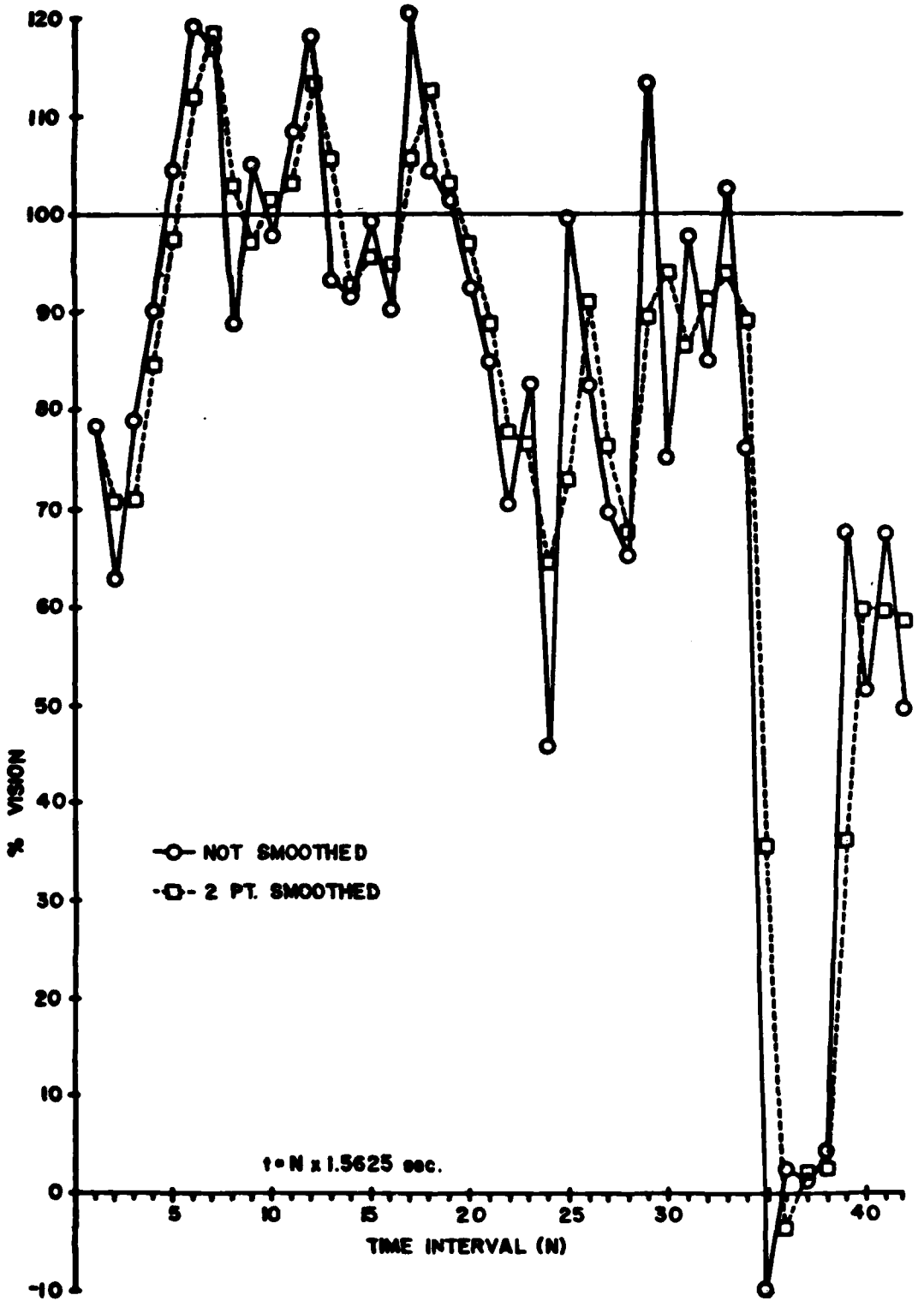

Figure 2 - Specimen real-time run for subject with low predicted and obtained standard deviation. (See Table 1)

Overall, the results of this experiment indicate that while improvements in the method are required, if we are to have an effective real-time monitor for visual functioning, such improvements are not only possible, but feasible. Procedure modification, changes in stimulus parameters and provision of auditory or tactile feedback to the subject, all promise some improvement. Measurement of the separate responses at O_1 and O_2, instead of just O_z, should give a considerable improvement in detection.

The above experiment has been reported as reference [7]. A preliminary analysis of the complete spectra collected in the experiment show some interesting features. The first of these is that the average coherence across subjects shows 14 spectral points with coherence greater than .20, indicating that some multivariate approach is required to efficiently utilize this data.

When the average power spectrum of the data was computed, after removal of the VEP component, a small but consistent elevation of the presumed EEG was noted for those spectral points at which the VEP was found. The most parsimonious interpretation of this result is that a small part of the VEP, due to phase and/or amplitude instability, is not recoverable. These results contravert the idea of "entrainment" or "capture" or "photic-driving" [2] of the EEG, to the extent that these ideas imply that components of the EEG are brought into frequency and phase lock, to produce the VEP.

Work in Progress

A centrifuge program designed to evaluate two different electrode placements and four different frequencies of stimulation is now in progress. In this experiment, the onset rate of the acceleration is low (1g/15 sec), and subjects are relaxed and do not wear a g-suit. The end-point is loss of central vision. The measurement of the VEP will be in real-time. With present computer capacity, such real-time operation limits data collection.

A larger, faster, more sophisticated computer capability has been purchased and installed. When programmed for this application, it will permit more complete data collection and analysis.

REFERENCES

[1] M.M. Cohen, "On the additivity of acceleration protection", in Aerospace Medical Assoc. Annual Meeting Preprints, May 1981, pp. 9-10.

[2] D. Regan, **Evoked Potentials in Psychology, Sensory Physiology and Clinical Medicine**, London, Chapman and Hall, 1972.

[3] D. Regan, "Steady-state evoked potentials", **J. Opt. Soc. Amer.**, vol. 67, 1977, pp. 1475-1489.

[4] T.F. Collura, "Real-time evoked potential correlates of directed attention", in Proc. ACEMB, Oct. 1978, p. 10.

[5] R.W. Sencaj, J.I. Aunon, and C.D. McGillem, "Discrimination among visual stimuli by classification of their single evoked potentials", **Med. Biol. Eng. Comput.**, vol. 17, 1979, pp. 391-396.

[6] J.G. Nelson, J.J. Palumbo, and M.M. Cohen, "Use of the coherence function in analysis of steady-state visual evoked potential (VEP)", in Research Program Review, Aircrew Physiology, Naval Air Systems Command Research and Technology Group, Oct, 1980, pp. 15-24.

[7] J.G. Nelson and L. Hrebien, "Real-time monitoring of the visual evoked potential", in Aerospace Medical Assoc. Annual Meeting Preprints, pp. 169-170, May 1982.

[8] J.S. Bendat and A.G. Piersol, **Random Data: Analysis and Measurement Procedures**, New York, Wiley-Interscience, 1971.

[9] J.P. Guilford and B. Fruchter, **Fundamental Statistics in Psychology and Education** (6th Ed.), New York, McGraw-Hill, 1977.

[10] N.P. Draper and H. Smith, **Applied Regression Analysis** (2nd Ed.), New York, Wiley, 1981.

[11] D.F. Morrison, **Multivariate Statistical Methods** (2nd Ed.), New York, McGraw-Hill, 1976.

[12] J.G. Nelson and L. Hrebien, "Real-time detection of steady-state evoked potentials", Frontiers of Computers in Medicine: COMPMED 82, Sep 22, 1982.

VISUAL AND AUDITORY LOCALIZATION: NORMAL AND ABNORMAL RELATIONS

Leonard Matin

Department of Psychology
Columbia University
New York, N.Y. 10027

When we see an object, hear a sound it emits, and touch it, all three impressions appear to be coming from a single object at a single location in space. Yet the three impressions have entered the nervous system through three entirely different sensory avenues. These different sensory avenues receive and transduce entirely different forms of energy from the object, carry the results of the separate transductions through three different sets of afferent neural channels to three different sensory projections centers at three different locations in the brain. The phenomenological unitariness of the perception of spatial location of the object implies mechanisms for coordination of information via the three sensory avenues and also implies the existence of physiological connections either beyond the projection centers or in regions that are alternate pathways to the normal projection centers. My talk today will be concerned with mechanisms by which coordination of localizations through different sensory avenues is effected. In order for us to study this I am making measurements on groups from three populations of abnormal individuals in addition to a group of normal observers. These three groups are: (1) Individuals who are strabismic; these in some cases are being examined both before and after corrective extraocular muscle surgery (2) Individuals with bilaterally asymmetric hearing deficits; and (3) Normal individuals whose musculature — both limb musculature and extraocular muscles — has been weakened by systemically injected curare.

Figure 1 shows a portion of the apparatus used for most of the experiments. Twenty-five loudspeakers were horizontally arranged 2.5° apart 6 feet away from the observer and centered on the observer's median plane. I am showing three target lights; each was a circular diffusely illuminamed 9' disc. In fact, each target light was movable to any position along the circumference in the horizontal array. In most of the later experiements there was a separate fixed visual target at each loudspeaker location.

Most of the experiments involved auditory/visual matching. The auditory stimulus in all cases was either a 32, 64, or 128 cycle portion of a 3.5 khz sinewave repeated three times a second (Figure 2). This sounded like a set of 3 clicks/second. [So far we have found no effect of employing different sinewave frequencies in the range from 500 hz to 4000 hz nor any effect of varying the number of cycles from 32 to 128.] Almost all of the energy in the auditory stimulus was in a narrow frequency range as shown by the experimentally measured power spectrum which itself corresponded to the theoretical spectrum fairly well. (The theoretical spectrum shown here is the envelope of peaks of the Fourier coefficients).

Only one target light was on (continuously) at a time. The observer, who foveally fixated the light, picked the loudspeaker that sounded as if it was in the same horizontal location as the light. He did this by use of standard psychophysical techniques.

Figure 3 shows some theoretical curves. Data which fall on the main diagonal are veridical; that is, the loudspeaker chosen by the observer (ordinate) appears to be at the same horizontal location as the fixated light at each of the horizontal eccentricities of the fixated light. Suppose we put a wedge prism in front of the observer's eye which visually displaces the entire visual field to

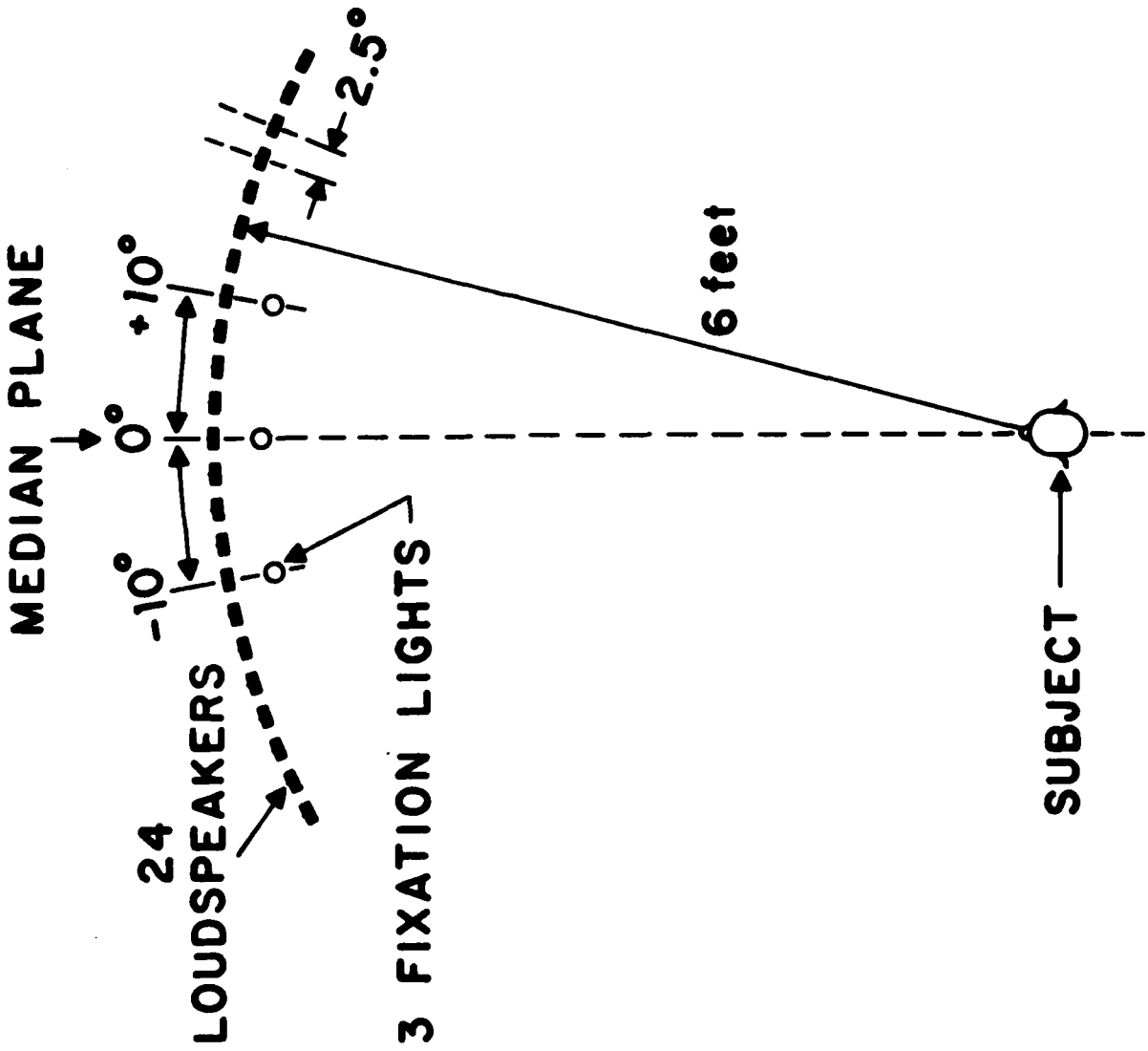

Figure 1 - Diagram of apparatus used to measure auditory-to-visual localization matches.

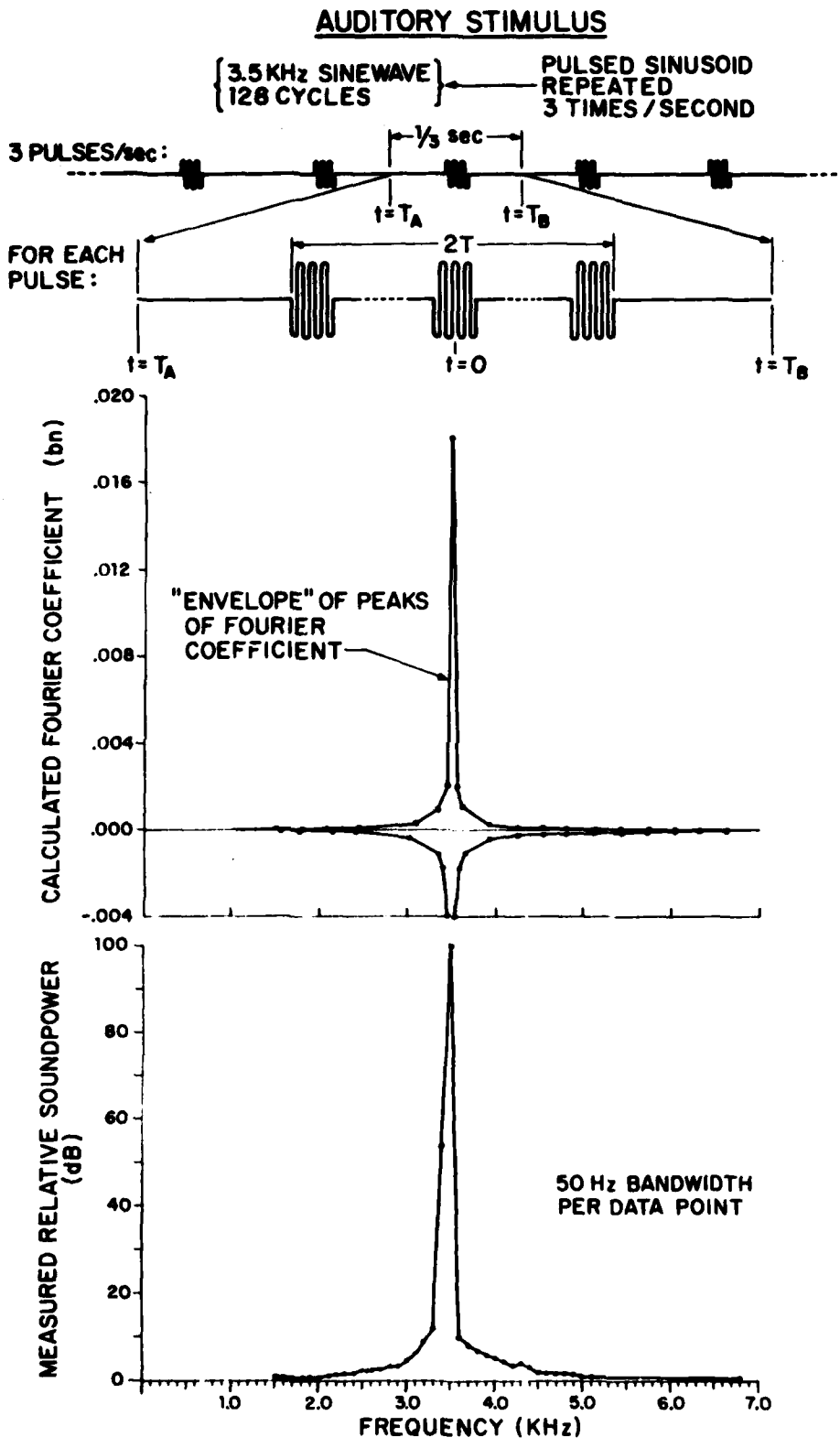

Figure 2 - The auditory stimulus employed for auditory-to-visual localization matches.

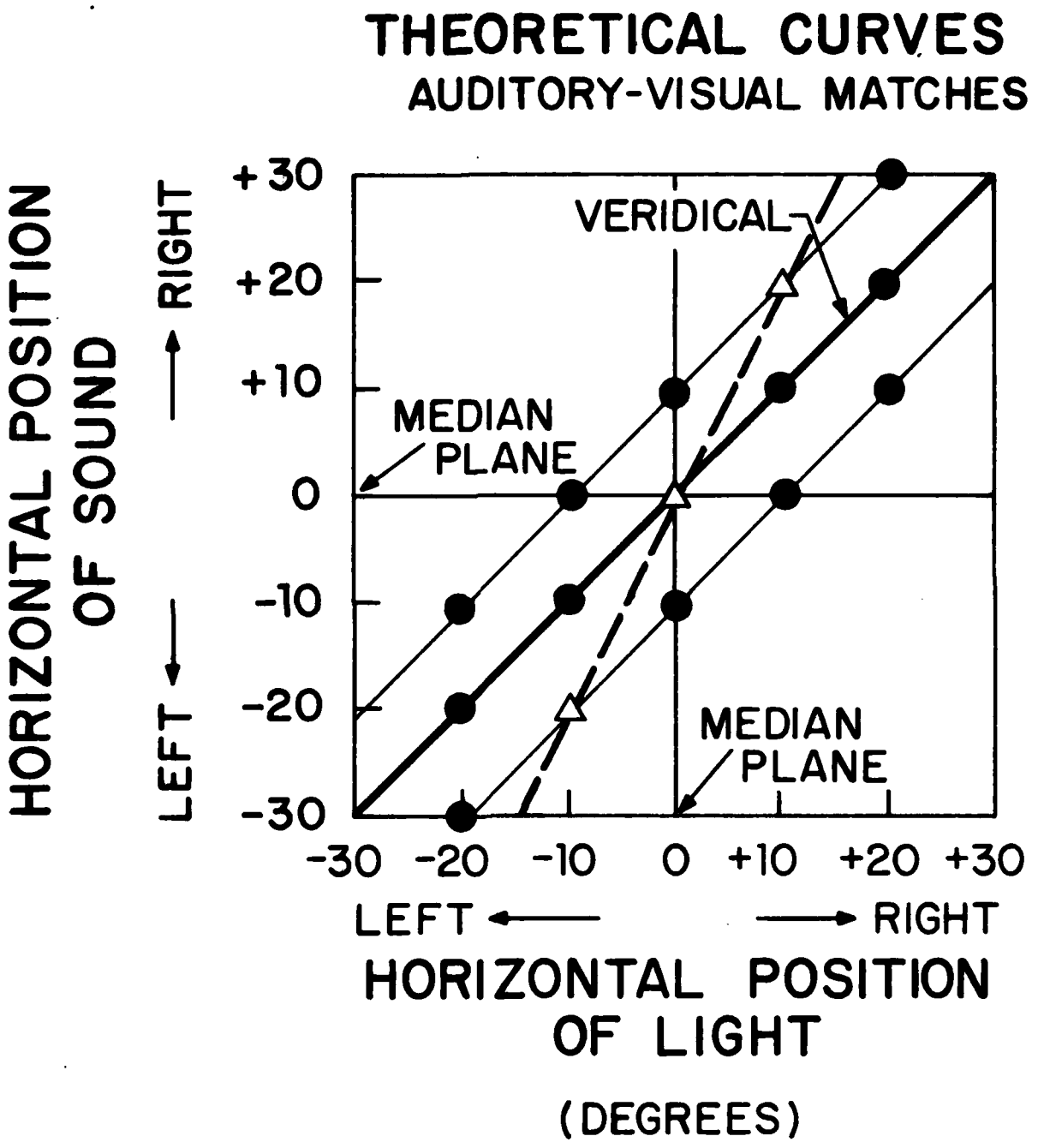

Figure 3 - Theoretical curves relating auditory-to-visual localization matches under different conditions; see text for description.

the left by exactly 10°. Then the rays from a light that is truly on his median plane will enter the eye of the observer from a different direction – the direction at which rays from an object that is actually 10° to the left normally enter the eye on occasions when no wedge prism is present. If the observer's data fell on the veridical line before, it should fall on the parallel line 10° below the veridical line with the wedge prism in place. This is because the light is displaced but not the sound. If the wedge prism were to displace the visual field to the right by 10°, the data should fall on the parallel line 10° above the veridical line.

However, if the visual stimulus being displaced by the wedge prism is a face talking, the sound from the talking face will appear displaced as well. No dissociation of sound and sight occurs even though only the visual stimulus has been displaced and not the auditory stimulus. This fact is referred to as visual capture; it is a pervasive fact: We go to the movies, look at the screen, and never doubt that the sound is coming from the same direction as the lips of the character on the movie screen whereas it typically arises from loudspeakers on the sides of the auditorium, sometimes at 90° from the screen.

So the first principle relating auditory and visual localizations is "visual capture". It is not the one I wish to discuss today however, but it was necessary to mention it here. My interest today is in comparing visual and auditory localizations in situations in which the two are independent. We thus had to eliminate visual capture. This is easy to do. Even though the basis for visual capture is not yet clear, it's elimination is easily effected, and our procedure, in which there was no temporal correlation between the fluctuations of auditory and visual stimuli was effective in eliminating visual capture.

Thus, the expectation of a displacement of the match locus as I talked about in relation to the graph is only for the case in which visual capture is removed.

Now then, suppose visual capture is removed in all of the rest of today's talk, let's look again at the expectations regarding the relation of visual and auditory localizations. The use of a wedge prism was my way of showing a simple means for producing a shift in this relation. But, go back a step. With visual capture out of the way how can visual and auditory localizations bear any determinate relation to each other at all? For a determinate relation to be present there must be (1) a mechanism for the auditory system to localize – to process sounds differently from different directions differently, and (2) a mechanism for the visual system to localize – to process lights from different directions differently:

We know a lot about the mechanism for auditory localization by itself and I want to say as little as possible about it. But just to establish a baseline I will refresh your memories quickly: A sound from my left arrives at my left ear more quickly than it arrives at my right ear. The difference in time of arrival increases monotonically with leftward eccentricity of the sound direction to reach a maximum when it is on a line with my two ears (i.e., 90° to my median plane). Similarly with sounds to the right: Time of arrival is increasingly earlier at the right ear as the the rightwardness of the direction of the sound source increases. Also a sound from my left proceeds directly to my left ear but my head obstructs the sound on its way to my right ear, and so it reaches the right ear with less intensity than it reaches the left ear. Time of arrival difference to the two ears and intensity difference to the two ears are the two main bases for localizing sounds within a horizontal plane. These cues are used fairly precisely. We can reliably tell whether one sound is to the left of a second sound if the time of arrival difference is as little as 6 microseconds, a difference that would be produced by a difference in angular direction of the sound source of 1°.

That's all for auditory localization by itself.

Visual localization is another matter. Since the eye is mobile relative to the head, at least two pieces of information must be available to the observer if he is to localize the position of a light in space: (1) For a given position of the eye he must be able to process stimulation at different retinal locations as if they arose from different spatial locations. (2) He must be able to integrate this retinal information with extraretinal eye position information (EEPI).

Figure 4 shows the typical cancellation model by which visual localization is thought to be carried out (see Matin, 1972, 1982 for reviews). A neural comparator treats EEPI and retinal location signals (RI) algebraically and arrives at a value of perceived visual direction. The source of EEPI may be inflowing information from muscle spindles, tendon organs, and so on in the region of the extraocular muscles, or outflowing information regarding the command to turn the eye, or a hybrid. Figure 5 shows these three versions of cancellation theory. As things stand now we don't know which version is the correct one. *I am working on it – setting up some experiments* – and expect to have the answer in a couple of years. But regardless of which one of the theories is correct, we have shown in an article that just came out in Science (Matin, Picoult, Stevens, Edwards, Young and MacArthur, 1982) that the cancellation mechanism applies to visual localization only in darkness. In a normally illuminated and structured visual environment visual localization is not determined by the cancellation mechanism. The use of cancellation for visual localization is suppressed by a normal visual field.

So now we have an additional mechanism that is part of the picture: Visual-field suppression of cancellation.

Thus, up to now I've briefly mentioned four mechanisms involved in the relations between visual and auditory localization: (1) The means by which auditory localization itself is effected; (2) Visual capture; (3) Cancellation mechanism for visual localization; (4) Visual-field suppression of cancellation. These four provide the basis for a determinate relation between auditory and visual localizations.

Let's go back to Figure 3. I noted earlier how the introduction of a wedge prism would be expected to modify relations between auditory and visual localizations when visual capture is eliminated. Now that we've got the rudiments of the mechanisms determining visual localization and auditory localization separately out in front of us we can ask how changes in any of the components of these mechanisms influence the relation between visual and auditory localization: Thus, let's consider as a first example a case in which an auditory attenuator is placed over the left ear of an individual whose auditory-to-visual localization matches are normally veridical; this should influence the localization of all sounds in a horizontal plane so that they appear horizontally displaced by the same fixed amount to the right, and thus should result in loudspeaker locations chosen to the left of a veridical match by the observer; this would yield a parallel shift of the auditory-to visual match line downward on the graph. An attenuator over the right ear of the observer would be similarly expected to produce a shift from veridicality to the line above the veridical line. These are exactly the same shifts that, as we noted earlier, could be produced by the introduction of a wedge prism. Now, in fact, if an individual had a fixed bias in visual localization – an equivalent prism in his visual system – he would produce an auditory-to-visual match curve that also would be parallel shifted from veridiciality. Thus, a parallel shift from veridicality could be produced by a fixed bias in either vision or audition. This presents us with the problem of how to tell when it is one or the other. *I'll answer that question*, but first I want to show you some data: Figure 6 shows on the left some data of a normal subject, and also

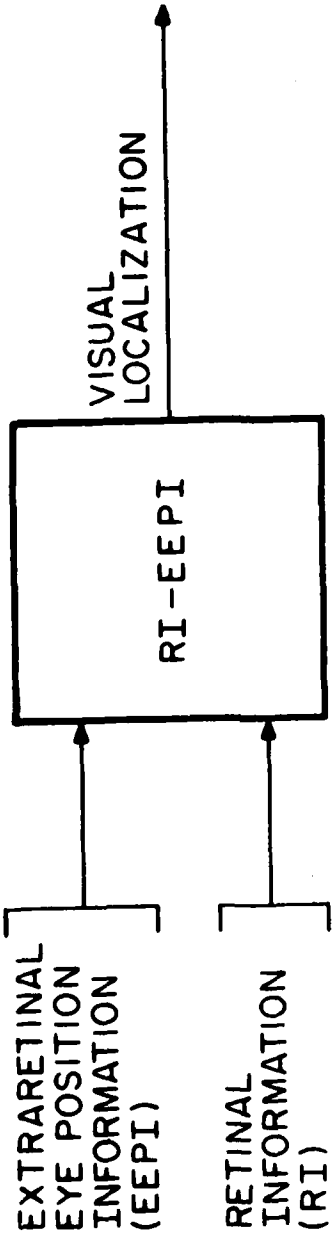

Figure 4 - Theoretical cancellation mechanism governing visual localization.

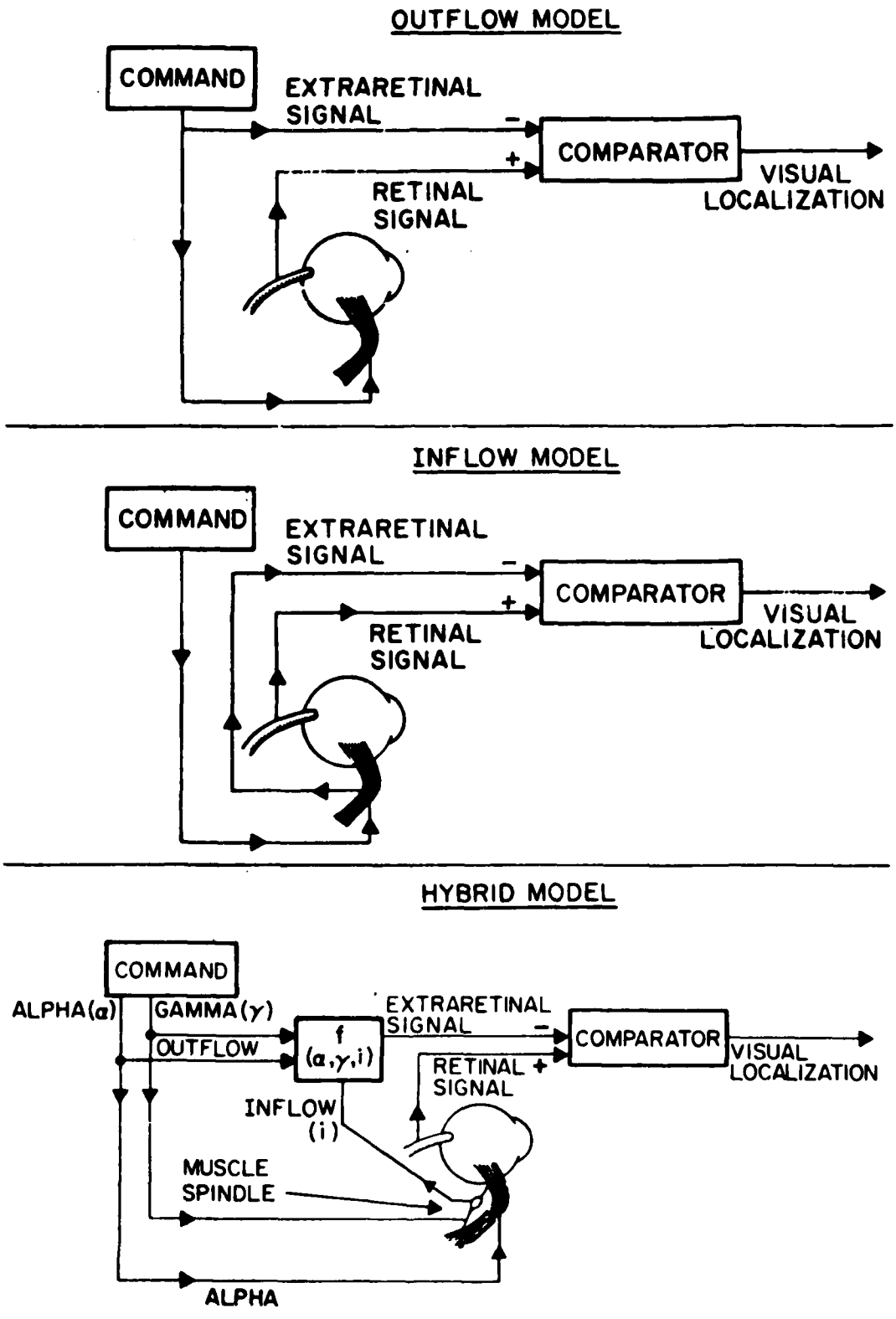

Figure 5 - Three varieties of theoretical cancellation mechanisms.

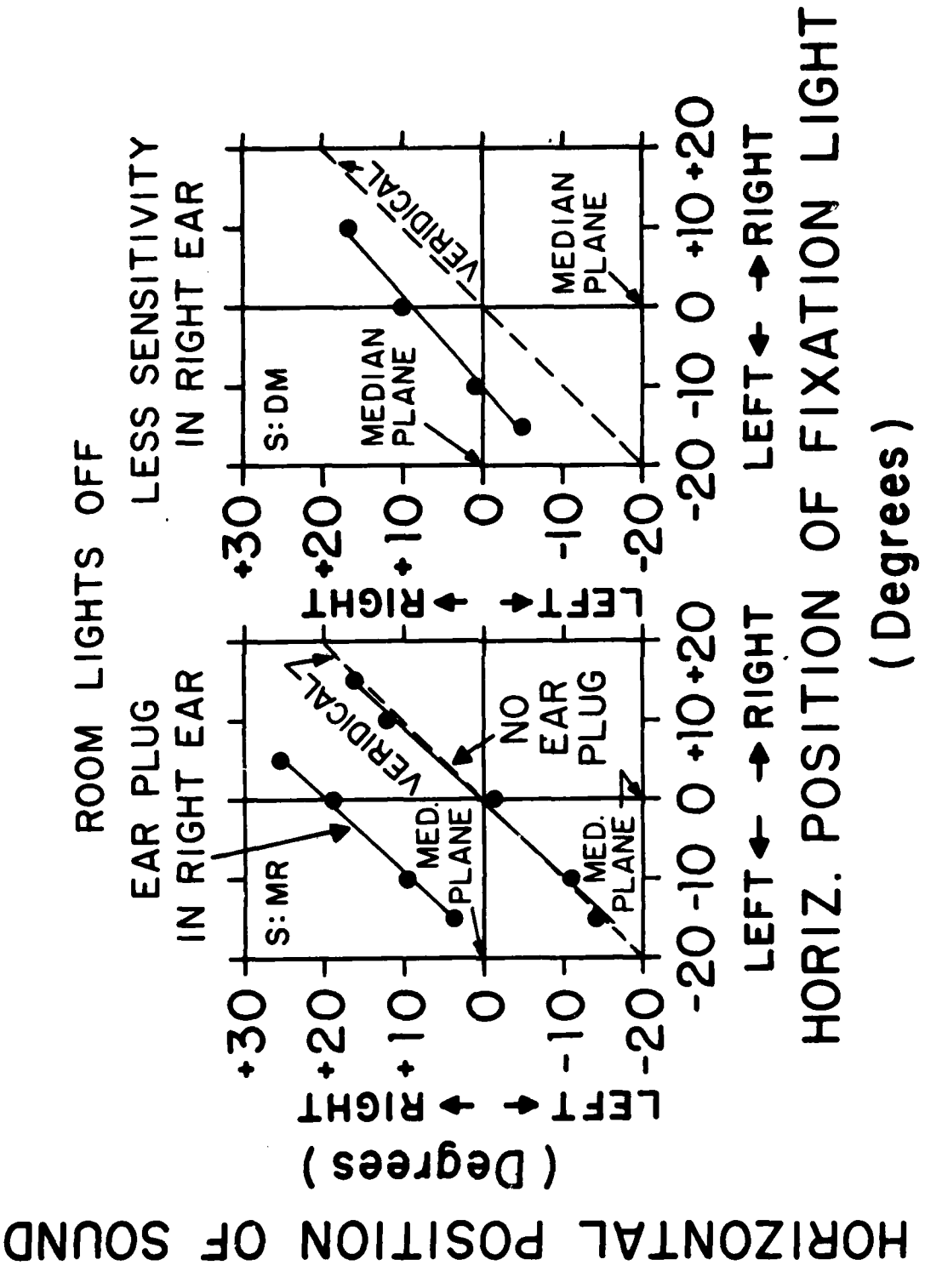

Figure 6 - Auditory deficit data.

his data with an attenuator over one ear. The parallel shift is there just as we thought it would be. We also show some data of an individual drawn from one of our clinical populations who had a differential threshold loss; one ear had lost more sensitivity (it had a higher threshold than the other); again the parallel shift is there. [I call your attention to one interesting and unexpected fact: this individual had been walking around with this deficit for at least twenty years and her auditory localization had not adapted to the deficit.]

Now, I want to ask what might seem like a peculiar question. Although in one case I introduced the auditory deficit experimentally, and in the other we were dealing with a clinical deficit, I can still ask: how do we know that the errors in matching in either or both cases was really an error in auditory localization – it is entirely possible that introducing an auditory deficit produces errors in visual localization (I'm not going to try to give you the line of reasoning that makes this more than just a plausibility argument – I'm only interested in pointing out that I have not yet truly proved to you that the error in localization produced by the auditory deficits is one of auditory localization, and not of visual localization.) The next figure shows the proof: The proof is the outcome of using a different method: Name the Speaker. In this method the loudspeakers were numbered from 1 to 25. The observer listens to one speaker and reports on its number. Figure 7 plots the average number report against the actual loudspeaker number for the same normal observer whose data was shown on the previous slide. You can see that the attenuator on one ear offsets his report of speaker number in one direction and the attenuator on the other ear offsets the report of speaker number in the other direction. Since vision is not directly involved in these reports the error has got to be one of audition.

A second element of the proof that the error in Figure 6 is one of auditory localization and not visual localization is to ask the observer to pick the sound location that corresponds to his median plane. For observers with auditory deficits their errors in setting the median plane corresponds quantitatively to their errors in the auditory-to-visual match. In addition, they set a light to their median planes in darkness with accuracy. This conjunction of errors in auditory median plane setting with accuracy in visual median plane setting provides another way of determining when the error is one of audition.

At this point it is worth noting an important result: The auditory-to-visual matches we obtain with any given observer are essentially identical when they are obtained with the observer in complete darkness, or in a normally illuminated and structured visual environment. This is shown in Figure 8 where the data for four individuals are presented. The left panel shows the data obtained in normal illumination; the right panel shows the data collected in darkness. There is no difference in the data of the two panels. This is actually to be expected. Since our method removes the influence of visual capture, there is no reason to expect that providing a structured visual field would influence the auditory-to-visual matches, and indeed it does not.

Let's return to Figure 3 again. This time, note the line whose slope is steeper than the slope of the veridical line. This could be produced by EEPI that overestimates the distance of the eye from some zero position and this overestimation is by a constant factor. For example, suppose the observer underestimates his eyeturn by a factor of 2: when he turns his eye 5° to the right he treats it as if he has turned it 10° to the right; when he turns his eye 10° to the right he treats it as if he has really turned it 20° to the right; and so on. Since for the purposes of this example we assume that auditory localization is accurate, an auditory/visual match would result in auditory targets that are set further to the right than the visual targets to which the normal observer has matched them.

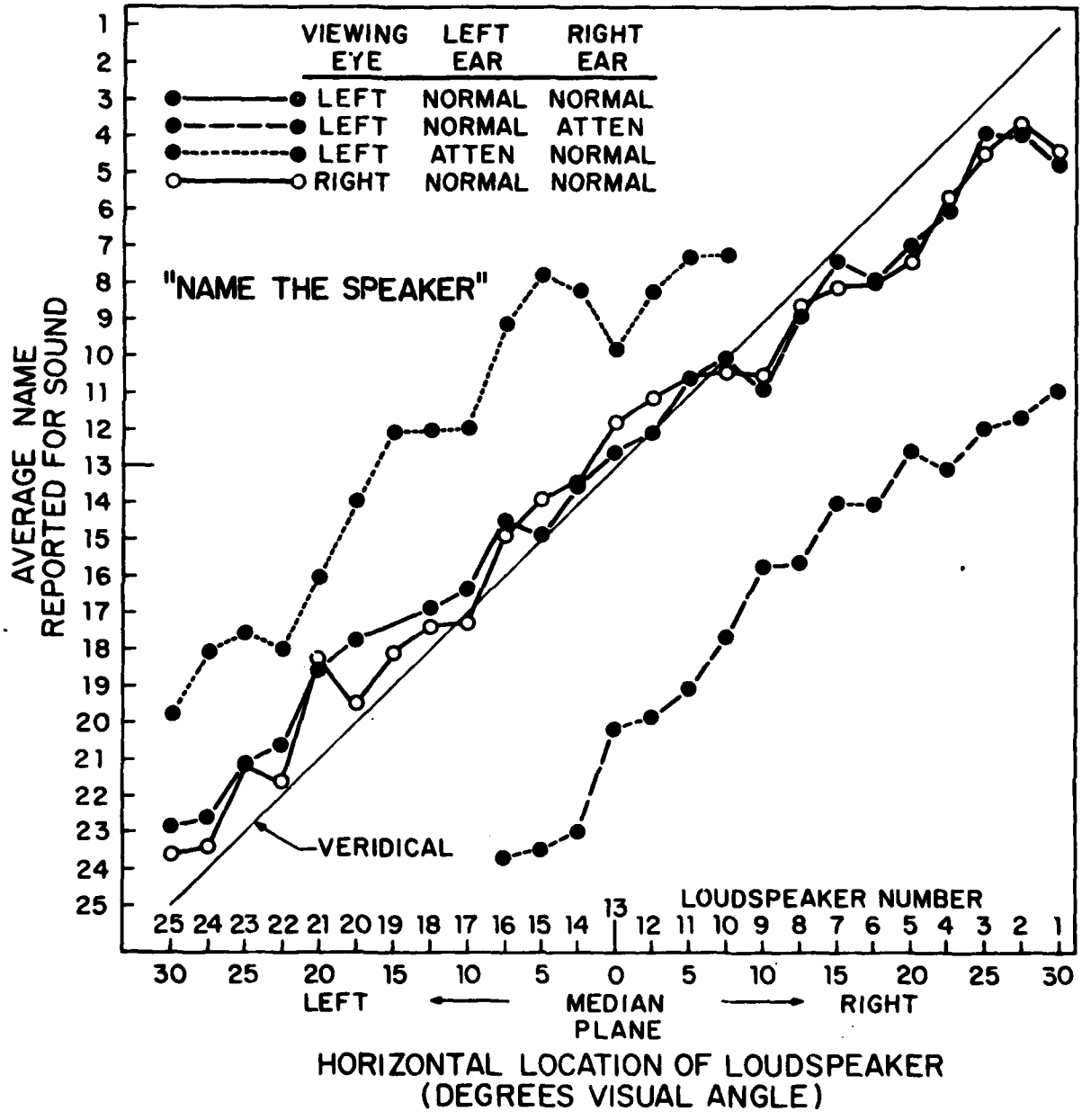

Figure 7 - Name-the-speaker data.

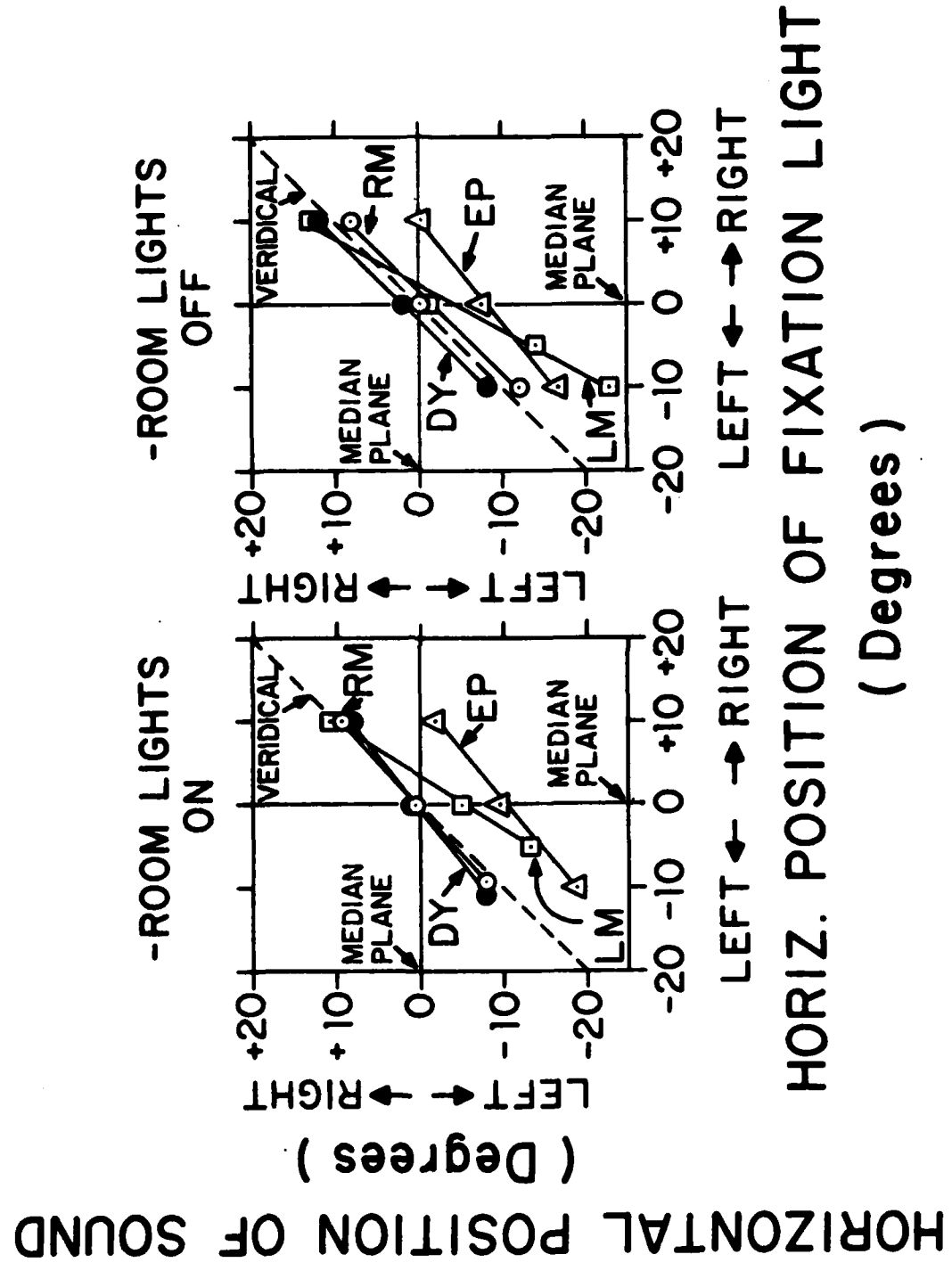

Figure 8 - Auditory-to-visual matches made in light and darkness.

Figure 9 (from Matin et al, 1982) shows a set of data in a condition in which the observers did indeed do just that. Each of these two observers was partially paralyzed by curare at the time the data with steep slope were collected. The observers were in their normal noncurarized state when the nearflat data were collected. The data are auditory-to-visual match data of the kind I've been discussing; the ordinate, however, plots errors in the match; the abscissa plots eccentricity of the visual target just as it has in previous figures. And so data that falls on a horizontal line is error free; to the degree that the data fall along a line that slopes away from the horizontal, the observer's EEPI is in error relative to reality by a scale factor greater than 1. What is happening here is that the curare has weakened transmission at the neuromuscular junction of the extraocular muscles with the result that when the observer directs his gaze at a position 10° to the right, for example, he must generate an effort pattern that normally gets his eye to a much farther rightward position, for example, to 20°. He treats his eye as if it is actually farther out than it actually is, and the auditory-to visual-mismatch is the sign of that error in EEPI. So, up to now, I've described the utilization of auditory/visual matching to measure errors that are, on the one hand, primarily reflections of auditory deficits, and on the other hand, primarily the reflection of visual deficits. For the case of auditory deficits I've talked about both normally occurring and experimentally-produced deficits. For the visual case I've only talked about experimentally-produced deficits so far.

In the interest of working with naturally-occurring visual deficits in visual localization we have begun to work with individuals who are strabismic. We have collected enough data on them to be certain of several results. The results are surprising. In fact, there are two kinds of surprises. The first kind of surprise was obtained with the strabismics when we measured them prior to their undergoing corrective surgery. The second surprise was when we measured them after corrective surgery.

Surprise #1: The central fact about individuals who are strabismic is that when they look at a particular point in space their two eyes point in different directions. In order for a strabismic to look at a given point in physical space with one eye, then, the positions of the two eyes must be very different than when he looks at the same point in physical space with the other eye. Since EEPI must be very different for the two positions of the two eyes, it would seem to follow that the auditory/visual matches would also be very different, and that this difference would equal the difference in eye posture between the conditions when one eye is fixating and when the other eye is fixating. Nothing could be farther from the truth. The bottom line, leaving out all frills and details, is that the auditory/visual matches are very similar, in a few cases essentially the same with either eye.

There is only one inescapable conclusion from this result – and even though we are just beginning this work, and can't show you slides of the results, and even though I still have many many qualms about what we've done so far that are related to difficulties in dealing with patients where we have limited time in which to make measurements – the conclusion is the following: It's in two statements: (1) When the strabismic looks at the world with one eye, he "knows" which eye he is looking with. Now, although for a long time it had been thought that such utrocular discriminations were impossible – and for the most of us – they are, more recent experiments in several other laboratories have turned up somewhat positive results on the matter. Of course, in our case he need not be able to report on which eye is receiving the stimulus; the difference in processing need only occur for localization (2) The second statement is even more surprising. The strabismic uses eye position information regarding the position of the left eye when a stimulus impinges on his left eye, and eye position information regarding the right eye when a stimulus impinges on his right eye.

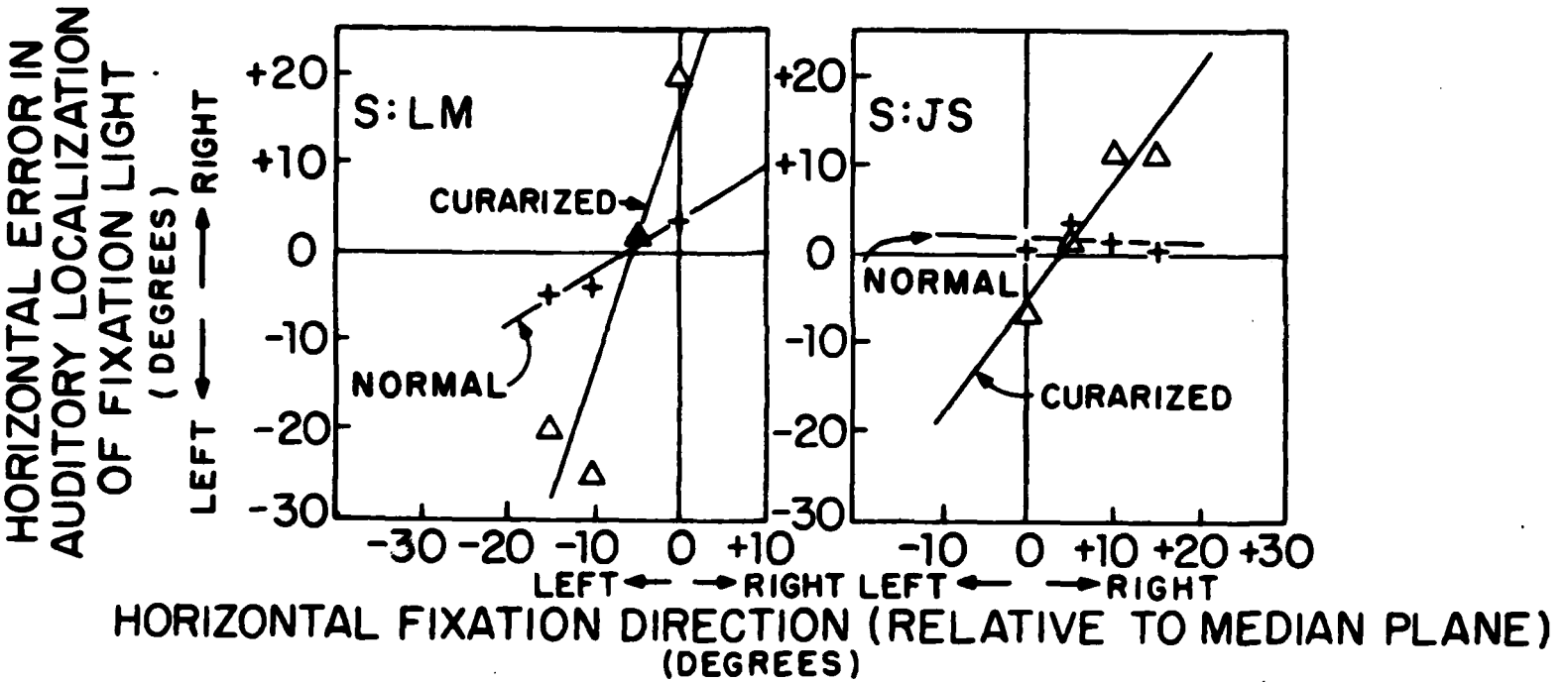

Figure 9 - Errors in auditory-to-visual matches for observers whose extraocular muscles were partially paralyzed by curare is shown along with data for the same observers in their normal, unparalyzed condition.

NADC-82232-60

The combination of the above two statements derives from out still-new work with strabismics. They are equivalent to saying that when the strabismic senses with one eye he does it the way we sense with one arm. Just as we localize independently with our two arms – touch one arm and we know which one is touched, and that the touch came from a different position independently with his two eyes.

Surprise #2: A day or so after the operation the strabismic is localizing with his operated eye just about in the same way that he did before the operation in spite of the fact that his eye may be assuming a very different position in relation to the other eye than it did before the operation. Since these are still new things and the work is just beginning I will leave surprise #2 without any further comment now.

REFERENCES

Matin, L. (1972). Eye Movements and Perceived Visual Direction. Chapter 13 in Handbook of Sensory Physiology, vol VII/4, D. Jameson and L. Hurvich (eds.), Springer-Verlag, Berlin.

Matin, L. (1982). Visual Localization and Eye movements in: Tutorials on Motion Perception. A. Wertheim, W.A. Wagenaar, H.W. Leibowitz (eds.), Plenum, New York, in press.

Matin, L., Picoult, E., Stevens, J., Edwards, M. Jr., Young, D., and MacArtther, R. (1982). Oculoparalytic Illusion: Visual-Field Dependent Mislocalizations by Humans Partially Paralyzed with Curare. SCIENCE, 216, 198-201.

DETECTION OF RETINAL ISCHEMIA PRIOR TO BLACKOUT BY ELECTRICAL EVOKED CORTICAL RESPONSE

by M.L. Wolbarsht
Duke University

1. INTRODUCTION

The objective of this program is to detect as early as possible any distrubances in cortical blood flow that will lead to blackout and unconsciousness. The specific sign that has been used is occurrence of retinal ischemia which is detected by monitoring cortical responses. External electrical stimulation of the eye has been used to evoke responses from the peripheral retina while keeping disturbances of normal visual function to a minimum. The purpose of the present work is to advance our knowledge of techniques to furnish early warning of loss of brain function or blackout resulting from high positive G forces or other types of maneuvers that produce circulatory stasis in the head, particularly in the brain or eye. During the present period, background information was acquired to use for the design of such operational techniques and to compare our proposed electrical stimulation techniques with those using visual stimulation. The investigation was carried out on cats to determine if a decrease in peripheral blood flow would be equated with loss of responsiveness to electrical stimulation to peripheral portions of the retina from external electrodes. The electrically evoked cortical responses (EER or EECR) were monitored by scalp electrodes in the region of the inion in a manner similar to the responses evoked by visual stimulation (VER). The data gathered during this program suggests the EER approach is more favorable than others, as the electrical stimulation may be delivered to stimulate the peripheral portion of the retina preferentially. This is in contrast to optical stimulation which preferentially evokes cortical responses from the central or macular portion of the retina. In order for the visual evoked response to be useful as the criterion for the positive detection of the effects of high G forces, the loss of visual function should occur as early as possible. Also, as the electrical responses stimulate mainly the peripheral retina, any changes in the perception of visual space due to a combination of the electrical stimulation with the optical signal in the most peripheral portion of the environment will be less noticeable and degrade visual function in the less important portions of the visual field.

2. SCIENTIFIC BACKGROUND OF THE PROGRAM

The scientific background can be considered under two headings: the current state of research on the use of visual evoked cortical potentials to monitor retinal function; and the scientific background for the electrical stimulation of the retina from external sources.

2A. Current status of research on the use of visual evoked cortical potentials to monitor retinal function as an indicator of "G" tolerance.

The limitations of "G" tolerance by pilots can be far exceeded by modern high performance jet aircraft. The driving force of the heart is often not sufficient to force blood into the brain against the downward thrust of blood resulting from acclerations attendant upon aircraft maneuvers. As the blood pools in the legs and abdomen, the eyes and brain are not supplied with freshly oxygenated blood. This results in loss of visual sensitivity, first in the periphery, and then in the central areas. This can be followed by total blackout and unconsciousness, all in a rapid sequence.

The Naval Air Development Center has an extensive program on blackout detect on, and much of the following background material is based on an extensive review of that program by Cohen (1979).

Normal intraocular pressures are between 8 and 20 mm Hg, usually about 12 mm Hg. This intraocular pressure means that the blood flow to the retina is impeded with respect to that through the cortex, to a certain extent. Because of this the retina becomes ischemic at about one G less downward acceleration than the brain itself. Thus, with downward G forces visual changes generally precede the loss of CNS functioning, and human tolerance to downward G forces has often been based on visual performance criteria.

In general, total anoxia affects the cortex first and progesses to the lateral geniculate nucleus, then to the retina, working its way peripherally to the photoreceptors (Brown & Watanabe, 1965). However, during downward acceleration, the effect of blood stagnation is first manifested in the inner layers of the retina where, as the local arterial pressure falls, the normal intraocular pressure occludes the blood vessels beginning with the capillaries. As the resistance to blood flow is higher in smaller vessels, and the caliber of the capillaries generally decreases towards the periphery, the peripheral vessels are more sensitive to blood changes than the more central ones, and function is lost first in these peripheral regions (Ward, 1968). This loss of peripheral vision, progressing to loss of central vision and blackout, is attributed to retinal ischemia. These retinal events have long been considered to be the precursors of unconsciousness due to cerebral hypoxia (Doolittle, 1924; Duane. 1954; Fraser, 1966; Leverett, Kirkland, Schermerhorn & Newsom, 1966; and Mercier and Duguet, 1947).

Visual blackout in unprotected and uncompensated human subjects in acceleration environments is probably not a simple process due only to mechanical consideration and blood flow (Betz, 1972; Krutz, Rositano, & Mancini, 1975). Nevertheless, a consideration of blood flow in the eye and brain is sufficient to show how some currently employed methods for enhancing human resistance to downward acceleration may act.

The simplest method to enhance resistance to downward acceleration is to place the subject with his back toward the acceleration. This replaces the head-to-toe accelerative forces by chest-to-spine forces. In this position the subject can tolerate more than 11 Gs. Enhanced resistance to blackout also results when the blood is prevented from pooling in the lower extremities and the abdomen. This increases the circulating blood volume. Blood pooling can be prevented by inflation of the bladders in a conventional G-suit. This can provide between 1.5 and 2.0 Gs additional protection. Straining maneuvers in which the subject exhales against a closed or partially closed glottis (the L1 and N1 maneuvers) increase intrathoracic pressure, diminish blood pooling, and can provide up to two Gs protection.

In order to use these protective measures, it is necessary to obtain methods for evaluating G tolerance that have the following characteristics:

1. High reliability and reproducibility.
2. Physically and behaviorally non-invasive.
3. Provides objective end points.
4. Relatively insensitive to experimental artifacts.
5. Give rapid on-line, real time discrimination.
6. Have a margin of safety for determining G tolerance without undue risk of approaching unconsciousness.

Behavorial measures of the visual system function lack stability and in a functional sense are usually quite invasive in a functional sense. Only objective measures of the integrity of the visual system during retinal ischemia seem able to meet these criteria.

The NADC program (Cohen, 1979) is based upon the work of Duane et al, 1961, who demonstrated visually discriminable photic driving of the filtered EEG which followed the frequency of this test light. Although all subjects did not demonstrate these phenomena, pilot results were encouraging. Subjects were exposed to accelerative force in the human centrifuge while measures of peripheral light loss, photic driving of the EEG, and ophthalmoscopically observed collapse of the retinal arterioles were associated with both loss of photic driving of the EEG and peripheral light loss. Blackout coincided with systolic collapse of the arterioles. In this study, photic driving appeared to be lost approximately one second before the subject signalled grayout (dimming of the peripheral visual field). Electrophysiological measurements such as the ERG or VER may give other objective tests for G tolerance.

Visual evoked responses (VER) recorded from scalp electrodes are a non-specific cortical response to light. Recent advances in bioelectronics, such as high gain steady state lock-in amplifiers, fast Fourier transform techniques, and improved real time digital computer processing methods have combined to make feasible the continuous real time analysis of small amplitude bioelectrical signals, that, in the past, could not be recovered from background noise. Since changes in visual function should provide a reliable indicator of G tolerance (Coburn, 1970; Gillingham & Krutz, 1974) and since both the visual evoked cortical responses (Donmchin & Lindsley, 1969; Richards, 1977) and electroretinograms (Tepas, Armington & Kropfl, 1962; Ward, 1968) have been shown to provide reliable indicators of visual functioning, it appears these techniques may furnish a simple, yet reliable, approach to the determination of human tolerance to acceleration. To some extent recent work at NADC has borne this out (Nelson and Hrebien, 1982).

The electroretinogram (ERG) consists of a negative a-wave generated by the retinal receptors and a positive b-wave arising from the neural activity of the inner layers of the retina (Ward, 1968). The presence or absence of the ERG and its various components, to some degree, gives an objective measure of retinal ischemia and thus, G tolerance. Also, the averaged ERG to a high luminance stimulus is much easier to detect than the VER. However, as stimulus luminance decreases,the ERG virtually disappears while the VER remains detectable. Thus, the ERG may provide a more sensitive index of retinal function than the VER. Ward (1968) has observed that the amplitude of the ERG b-wave was markedly diminished in anesthetized beagles exposed to downward acceleration, and disappeared completely when the acceleration was doubled. Also, the ERG is an area effect, and thus photometrically represents peripheral retinal responses. In this point, the ERG has an advantage over the VER. Unfortunately, research equivalent to that with the VER has not yet been conducted with human subjects with the ERG. For this reason the value of the ERG as an end point remains to be determined

The ERG and the VER both depend upon potentially annoying visual stimulation. However, recent work at NADC (Nelson and Hrebien, 1982) shows that the VER may be much less dependent than the ERG responses. On the other hand, the VER preferentially represents the central retinal responses. Thus, it may be that an alternative electrical response which combines the minimal visual distraction of the VER with the high sensitivity to peripheral retinal integrity of the ERG, such as the electrical stimulated cortical response (EER), could be a suitable measure of visual system function in an acceleration field to be used operationally as an early warning of blackout. This program was designed to evaluate the possible development of the EER as an early warning for blackout during positive G.

2B. Scientific background for electrical stimulation of the retina from external sources.

The response of the visual system to electrical stimulation has been reviewed by K. Motokawa (1949) in a comprehensive fashion. Previous investigations have been devoted to the perceptual responses of electrical stimulation of the eye, and to the perceptual assessment of electrical stimuli presented in conjunction with flashes of light in various patterns within visual space. Most subjects perceive stimulation of the retina as equivalent to a diffusely presented light in the peripheral portion of the retina. The threshold of this electrical response in the retina is greatly lowered by the ambient illumination. Also, the electrical excitability of the retina varies with a fixed time course after illumination (Motokawa, 1949). This indicated that the frequency of electrical stimulation and its relation to the frequency content of illumination of the eye must be considered as interactive elements and will greatly modify the response.

The electrical excitability of the retina has been used as an indicator of oxygen deficiency (Motokawa & Iwama, 1949). In these experiments, the perceived response to electrical stimulation was measured as the inspired 0_2 partial pressure was changed. However, this data is ambiguous. The tests were conducted on dark-adapted subjects in order to get maximum sensitivity. Nevertheless, there was a difference between the threshold levels with ascending and descending 0_2 levels, as compared with a normally oxygenated subject. Only three thousand meters were achieved in the decompression chamber, with minimum oxygen saturation of the blood still well above that where additional oxygen is normally administered. The administration of oxygen to the whole body prevented the low ocular and cortical levels which are achieved during or just before blackout, which are the levels really needed for operational purposes. The responses to visual stimulation were very similar to those elicited by electrical stimulation, although electrical stimulation seemed to be more sensitive.

Flickering light has been used in conjunction with pulsating electrical stimulation. The quantified approach to interaction used indwelling electrodes to stimulate the retina. The cortical responses to this type of stimulation have been investigated in some detail by Dawson and Radtke (1977). They have an extensive bibliography of previous attempts to do the same thing. On the basis of this review and their own experimental data, they have concluded that the eye is comparatively refractory to electrical stimulation in the dark. However, when the retinal threshold dropped, the responses did not allow positive identification of the active region of the retina.

3. METHODS USED IN THIS PROJECT

3A. Experimental Approach Used in the Present Program

We have examined the cortical responses to visual and electrical stimulation of the retina, and also the electroretinograms (ERGs) which accompany evoked cortical responses to visual stimuli and to electrical stimuli of the eye. All of these responses were recorded with normal intraocular pressure, and with elevated intraocular pressure. Some experiments were also made recording with intraocular electrodes from ganglion cells in the peripheral part and the central part of the retina in order to determine the differential sensitivity of these cells to increases in introcular pressure.

The overall objective of this program was to use scalp electrodes in the region of the inion to measure cortical potentials evoked by external electrical stimulation of the eye as a test for the occurrence of peripheral retinal ischemia.

The retinal ischemia was induced by compromising the retinal blood flow with increased intraocular pressure applied manometrically.

3B. Animal Selection

Rhesus (or closely related types) monkeys are usually chosen for all animal experiments whose data will be correlated with previous (and future) behavioral experiments to be applied to human operational situations. However, rhesus monkeys are unsuitable for use in gathering pilot data because of the difficulty in maintaining them for long periods of time to collect data from pilot experiments or the expense of keeping them for long periods of time. However, previous work has shown great similarities between the cat retina (and visual system) and that of the rhesus monkey, even though the cat retina lacks a fovea. The cat retina does have an area centralis, with ganglion cell receptive fields which resemble very closely those in the area in the monkey (and human) retina immediately adjacent to the fovea. The low cost of cats make it possible to do large numbers of pilot experiments. All of these factors made it advantageous to gather large amounts of data on the cat retina initially.

The animal was mounted in the optical stimulator with the eye immobilized by an ocular muscle clamp. A corneal contact lens was attached to correct refractive errors. An intraocular recording electrode was inserted through a small hole in the side of the eye, at the pars plana, to avoid detaching the retina, by a method which maintained the intraocular pressure at the desired level. A catheter was inserted through another location on the desired level. A catheter was inserted through another location on the pars plana to allow direct manometric control of the intraocular pressure.

3C. Anesthesia and Surgery

All experiments were carried out under either general inhalation anesthesia or I.V. administered pentabarbitol choloride anesthesia. All animals were initially anesthesized with ether. When a suitable depth of anesthesia was obtained either pentabarbitol was infused to keep the animal at a level sufficient to suppress any reflex responses to corneal stimulation or intratoe web pressure or a general inhalation anesthesia was used with a 70% nitrous oxide 30% oxygen mixture. An intravenous infusion of gallamine triethoxide (Flaxedil), 5-10 mg/cc of saline at the rate of 130 mg/kg body weight/hour. The animal was intubated and was respired artificially with a ventilator (Harvard Apparatus Company, Model 661). Inhalation anesthesia was maintained with a 70% nitrous oxide 30% oxygen mixture throughout the experiment. The expired pCO_2 was monitored continuously by a Beckman Model LB-1 Medical Gas Analyzer with the aid of an indicator alarm (Electrodyne MS-25). The CO_2 level was kept at 4.7%. In addition to the control of gas mixture flow furnished by the anesthesia machine, (Ohio Chemical and Surgical Instrument Company, Model 212B), a manometer was installed to avoid any damage to the animal's lungs from over pressure during the inspiration and exhalation part of the respiratory cycle.

The infusion of gallamine triethoxide with dextrose and saline was continued throughout the reporting session to assist in fixing the eye. A local anesthestic, (5% lidocaine ointment) was applied to the surface of the conjunctiva before any incision was made, and to all other incision pressure points.

Animals are maintained at normal body temperature by means of a heating pad. These life-support systems are adequate to maintain a cat in satisfactory physiological condition for up to 48 hours, although the experimental sessions were never more than 8 hours long, in order to insure uncomplicated recovery from the anesthesia.

In all experiments, the animals are under deep ether anesthesia during all surgical procedures. The level of ether anesthesia was sufficient to terminate spontaneous respiration and the animal required artificial inhalation. In addition, all incisions were filtrated with a local anesthestic. Only after surgery ended was the ether discontinued. Either a 70% nitrous oxide 30% oxygen breathing mixture or a sodium pentabarbitol infusion was used for a continuing anesthesia. The insertion of electrode through the pars plana involved no pain. This procedure is similar to operations that are often performed on humans with only a local anesthestic. During the experiment the heart rate was continuously monitored, and at no time were heart rate changes detected which would be associated with pain perception.

Although nitrous oxide, even at high, partial pressures, does not produce surgical anesthesia (Brown et al, 1927; Venes et al, 1927), it has been established that a 70% nitrous oxide 30% oxygen mixture in oxygen produces a high degree of sedation and analgesia in both cats and monkeys. It is an adequate anesthestic when only mildly noxious stimulants are present; for example, the direct stimulation of peripheral nerves at ferquencies up to 3 Hz., or foot pad shock, (Venes, et al, 1927).

Gallamine triethoxide is not required to relax the animal, but assisted in maintaining the high degree of immobility required to assure that both the electrical and visual stimulations were the same at all times during the experiment. It has been established that gallamine triethoxide has no effect on the retinal ganglion cell responses of cats and monkeys (Enroth-Cugell and Pinto, 1967). Because of these considerations, nitrous oxide and gallamine triethoxide have routinely been used for experiments of this type. Nitrous oxide has been used by us and others because it has only slight side effects in evoked visual responses as compared to strong central depression produced by other volatile anesthestics and barbituates (Van Norren and Padmos, 1977). The depressive action in the retina has also been seen with some of these other anesthestics as well (Van Norren and Padmos, 1977). Obviously it is important to minimize CNS effects from the anesthestic when studying the activity of the visual system, especially when using the evoked cortical responses.

The iris was dialated and accommodation relaxed with several doses of Duke mix (10% phenylephrine; 0.5 mydriacyl, 1:1) applied every hour.

3D. Optical Stimulation

The basic optical stimulator has been described in detail in previous reports and other publication (Wolbarsht 1978, 1980, Crocker, et al, 1968, Wagoner, et al, 1960). It has two channels with essentially equivalent pathways. Since the special features of this optical system are not relevant to the present experiment, it is not necessary to describe the equipment in detail. This equipment is capable of delivering reproducible light pulses to selected retinal areas. The spatial extent, duration, and wavelength of the stimulus can all be controlled independently. A Grass photoflash stimulator (Model PS-22A) was also used to give a visual stimulus which could be correlated with previous work on the visually evoked potentials as recorded in the cortex.

3E. Electrophysiological Recording Apparatus

The electrical stimulus was delivered to the eye through paired cheek and brow electrodes, or paired electrodes mounted at the inner and outer canthus of the eye. Occasionally a standard corneal contact lens was used for stimulation in order to minimize the stimulus artifact, the electrical stimulus was generated by a (Tektronix Type 161 Wave Form Generator and a Tektronix Type 162 Pulse Generator), with a power amplifier constructed locally from a design furnished by E.F. MacNichol, Jr. A circuit diagram of this power amplifier, is shown in Figure 1. The power amplifier was connected to the animal through a Grass Stimulus Isolation Unit (SI-1) in order to minimize artifacts in the recording system, which would interfere with the detection of the cortical responses. All physiological electrical responses were recorded by FET input stage amplifier of conventional design.

In preliminary experiments an incision through the skin along the mid line of the head was made to remove the underlying tissue. Tungsten wire recording electrodes were implanted in the skull along the midline, 60 and 80 percent of the distance from the inion and the nasion. Also conventional EKG electrodes were used on the shaved but intact scalp above the inion and at the points overlying those for the implanted electrode locations described above. Two types of stimulus electrodes were used, a corneal electrode built into a plastic contact lens (Grass E-2 Platinum Needle Electrode), and a stainless steel electrode placed on the mucus membrane near the corner of the eye. In some cases EKG electrodes were used on the shaved brow and lower lid. In both of these cases an ipsilateral cheek electrode was used.

The responses were processed with a Nicholet Signal averager with the following time constants unless noted on the figures: 12 x 640 ms, 0 delay, filter 0.02. All leads were capacity coupled.

The visual evoked potentials (VER) were obtained by stimulating the eye with either 300 ms or 10 ms pulses of light at a repetition rate of 1 per second through the 2 channel Maxwellian view optical system.

The intraocular pressure changes were obtained by lengthening or shortening the height of a column of saline connected to the vitreous cavity through a needle piercing the cornea or the pars plana.

4. RESULTS

4A. Electrical evoked responses from corneal stimulus electrodes.

EERs were recorded using a stimulus electrode implanted into plastic corneal contact lens. This gave an easily detected cortical response. The maximum EER was obtained in the stimulus voltage of about 0.550 V at a duration of 10 ms. The normal intraocular pressure in a cat is from 12 to 18 mm mercury 16 to 24 cm water. When the intraocular pressure was raised to 118 mm Hg 155 cm of water, both the visual evoked response and the electrical evoked response were eliminated. When the intraocular pressure was lowered to a more normal level, 18 mm Hg or below, both the visual evoked potential and the electrical evoked response returned. This raising of the intraocular pressure and lowering of it with complete return of the response could be repeated several times during a single recording session. The pressure cycling seemed to have no adverse effect on the eye as long as the elevated pressure phase was not maintained for more than five minutes.

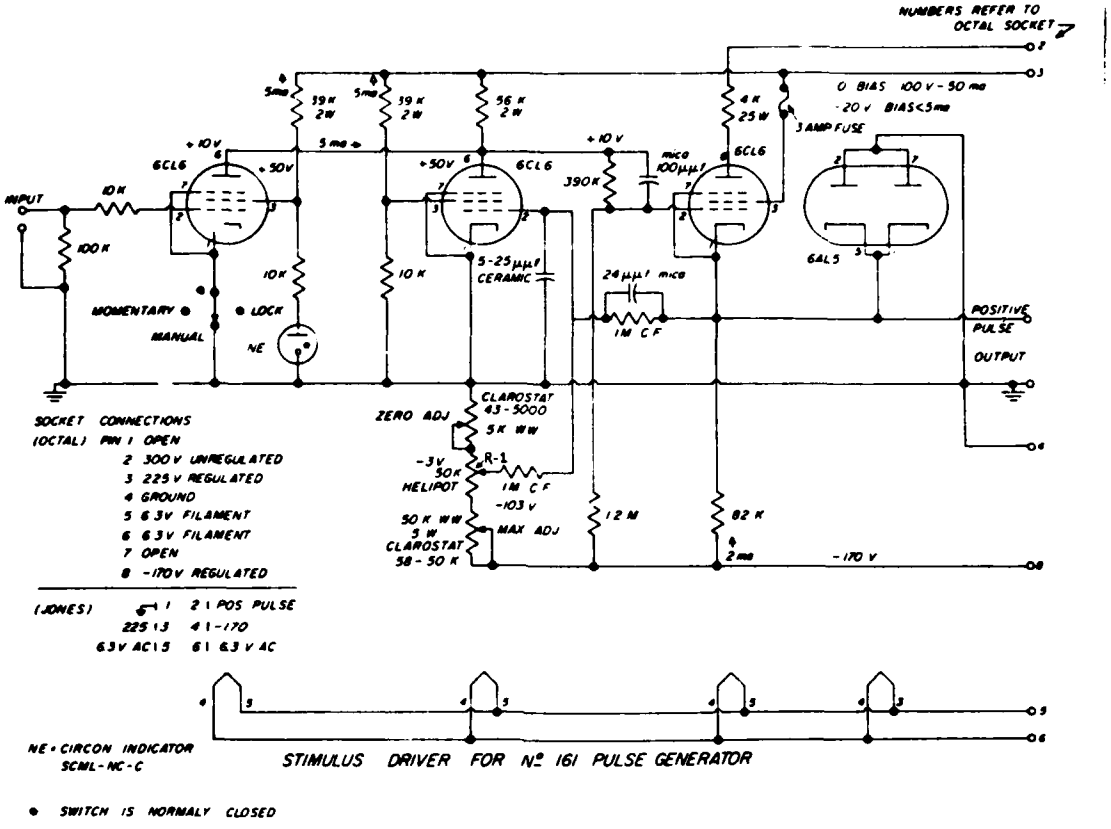

Figure 1 - Stimulus power amplifier. This circuit is based on a design by E.F. MacNichol, Jr., and is constructed on a chassis compatible with the Tektronix series pulse and wave length generators, and uses the type 160 power supply. The amplifier emits a pulse of 0 to 100 volts (controlled by resistor R1) whose duration is the same as the negative pulse delivered to input. This stimulus driver was designed to be used in conjunction with the Tektronix No. 161 Pulse Generator. It is capable of delivering a square wave pulse continuously variable in amplitude between 3v to 100v. The wave form has a rise and decay time of 2.5 seconds when working into a 5 kohm lead. This square wave form is preserved at 100v amplitude through 2.3k ohmload before 5% fall off is noticed. Below this load the output deteriorates rapidly. If there is no signal applied to the input of the first 6CL6, sufficient plate current flows to cause the output 6CL6 to be in the cut-off condition; thus the output is clamped by 6AL5 at approximtely ground potential. A negative potential of about 10v applied to the input (junction 100k and 10k) 6CL6 causes the plate current to decrease and thus the bias on output 6CL6 to be less, allowing the cathode potential of 6CL6 (output) to be positive of ground giving a sharp front pulse out. The feedback from the cathode of output 6CL6 to the grid of middle 6CL6 determines the top of the output pulse. The d.c. potential on this grid will be one half the difference between the potential of the output cathode and the potential on the slider of R-1. Since this is a precision output calibrated potentiometer the height of the pulse can be read directly in volts. The zero adjust should be placed approximately to the middle of its range or until the bottom of the wave form is approximately a straight line (about -3v). The position of maximum adjust will determine the maximum pulse height. This should be 100v above the zero base line (-103 to -106v on the bottom of Helipot). The pulse shape may be corrected to give a square front by the capacitor on the grid of the middle 6CL6. In the event the output is to be used in conjunction with an isolation transformer more satisfactory results will be realized if a 6AL5 limiting diode is used. The power to operate the unit is taken from the Tektronix No. 160 power supply and fed through a male octal connector located on the back of the unit. The 6 pin Jones connections will drive Grass stimulus isolation unit, SI-1.

The best responses were obtained with the stimulus artifact negative with respect to the response. Since the stimulus was electrically decoupled from the cat as much as possible, the stimulus artifact in the recording was low. Both polarities of the stimulus pulse had to be tried in order to obtain the maximum signal-to-noise ratio for the response. Since the electrical evoked response was eliminated by high intraocular pressure and reappears when the pressure is lowered, this implies if the electrical stimulus is indeed acting at or before the ganglion cell layer.

4B. Electrical evoked responses from stimulus electrodes at the inner and outer canthus.

The EER recorded with a stainless steel electrode placed on the mucus membrane at the inner and outer canthi had a higher threshold than that for corneal contact lens, 1.25 volts versus 0.950 volts for the corneal electrode. However, canthal electrodes appeared to be better for stimulating the more peripheral portions of the retina. This was measured by the disappearance of EER from this stimulus at a lower intraocular pressure than that required to abolish completely the response from the corneal contact lens stimulating electrode.

The responses for cheek and brow electrodes are more difficult to obtain consistently. However, results with EKG electrodes with well-moistened electrode paste and some kind of moisture shield (Saran Wrap) over the electrodes to eliminate evaporation gave the best and most consistent results. However, such an electrodemoisture shielding system might be difficult to arrange in an operational situation.

Recordings of the local electroretinogram (ERG) with tungsten electrodes inserted through the pars plana were helpful in determining which portions of the retina ceased function earliest with increases in intraocular pressure. The tungsten electrode was advanced visually through the opening on the pars plana until the tip just approached the retina, within 50 or 100 micrometers. In this manner, peripheral retinal locations lost their b-wave and later components at lower intraocular pressures than more centrally located recording sites. Initial attempts to use the intraocular electrodes as stimulus electrodes to stimulate preferentially different parts of the retina in order to determine the particular type of electrical evoked cortical response characteristic of different types of retinal stimulation were largely unsuccessful due to persistent and large electrical stimulus artifacts in this recording condition. This artifact eliminated most of the time domain in the response available for the conventional evoked response. However, some more work will certainly eliminate this problem.

The initial experiments in this study were directed towards the development of techniques for the most efficient and consistent recording of cortical responses to visual stimuli.

Once suitable electrodes were found and the optimal electrode locations established for the recording of the visually evoked response (VER), we proceeded to initiate electrical stimulation in a series of cats, using the VER as a control to ensure that the recording system was functioning.

Since the electrically evoked response (EER) is presumably initiated by the ganglion cells and conducted through similar pathways in the brain as the VER, we also used the VER as a control to establish the cessation of ganglion cell function upon raising the IOP. Finding an elimination of the EER under such conditions indicates that the EER is, indeed, a retinal phenomenon, rather than a direct optic nerve stimulation or artifact of some other sort.

Both systems of stimulation for EER with both electrodes in the antero-temporal dermis, or with a dermal reference electrode with a corneal contact lens stimulating electrode give similar responses. Responses from electrodes in the inner and outer canthi were readily obtainable and surprisingly similar in different cats. To all stimuli we also observed a clear "on" response and "off" response, which would "migrate" on the trace according to duration of the stimulus. The VER was consistently suppressed by raising the IOP to 155 cm H_2O, with return after the IOP was returned to normal. The optimal stimulus was in the neighborhood of 1 V, with a duration of about 10 msec. This was a true EER, since it was suppressed along with the VER when the IOP was raised. Also, it returned after the IOP was reduced to normal.

Interestingly, a similar EER was elicited through either polarity of stimulus, the only difference being an inversion of the stimulus artifact.

It was noted in one experiment that injection of lidocaine and pentabarbitol into the anterior chamber had little or no effect on the VER.

Our data show that the function of the peripheral retina can be detected by electrophysiological techniques. The experimental work during the present program was directed towards the verification that cortical responses seen following electrical stimulation of eye were verifiably from the peripheral retina rather than artifacts. Recording from retinal ganglion cells whose receptive fields are in the peripheral portions of the retina, and recordings from the visual cortex as seen by scalp electrodes over the inion both show clearly and reproducibly identifiable responses to electrical stimulation. The stimulating electrodes can be placed on the upper and lower lids (cheek and brow) or on the inner and outer canthi. Both responses are abolished when the intraocular pressure is raised. Figure 1 shows a normal electrical evoked response (EER) and in Figure 2 for comparison has a normal visual evoked response from the same eye. Figures 3 and 4 show responses from the same stimuli after raising the intraocular pressure.

5. CONCLUSIONS

No quantitative data has been gathered yet on the EER, and several important questions remain unanswered. For example, is the response gradually abolished as the intraocular pressure is raised, or as the peripheral circulation is compromised? And, also, it may be that both the VER and EER are abolished, not by oxygen lack or build-up of some metabolite due to stagnant or absent blood in the peripheral retina, but rather to deformation of the optic nerve at the disk while the intraocular pressure is raised. Our future research plans call for causing the carotid circulation on one side to be cut off so as to compromise the retinal blood supply without at the same time changing the nerve configuration at the disk due to changes in intraocular pressure. More retinal recordings in the center and periphery will aid in determining if those responses are abolished sequentially by the raised intraocular pressure.

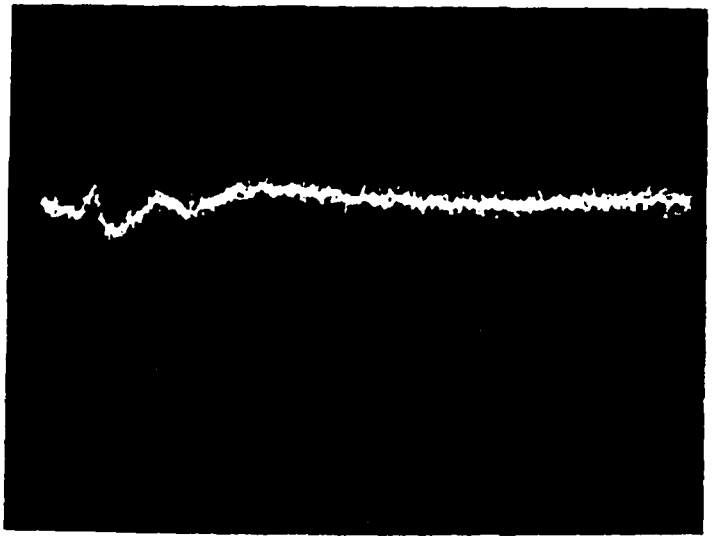

Figure 2 - Evoked cortical response to visual stimulation of the cat eye (VER). The multipeak response is normal, and highly reproducible. The intraocular pressure 15 mm Hg and the recording electrodes are on the skull midline anterior to inion.

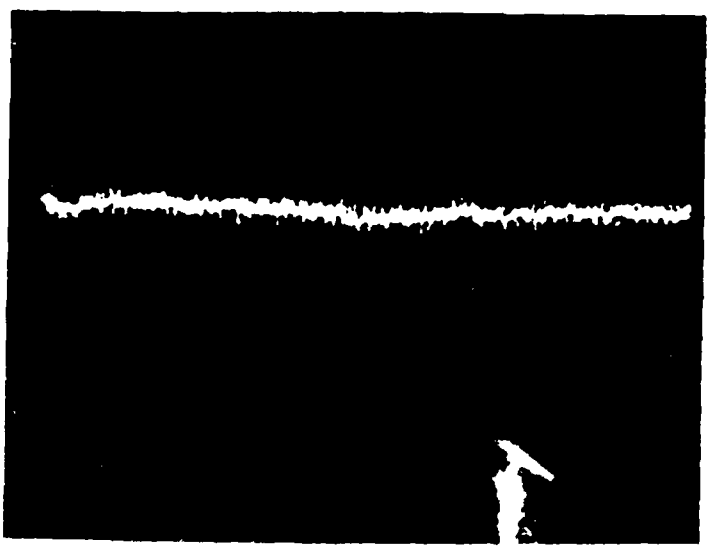

Figure 3 - Evoked cortical response to visual stimulation of the cat eye (VER). Intraocular pressure 150 mm Hg. The recording electrode location, stimulus, pulse, duration and intensity and parameter are the same as in Figure 2. The response returns to the level in Figure 2 when the pressure is returned to 15 mm Hg.

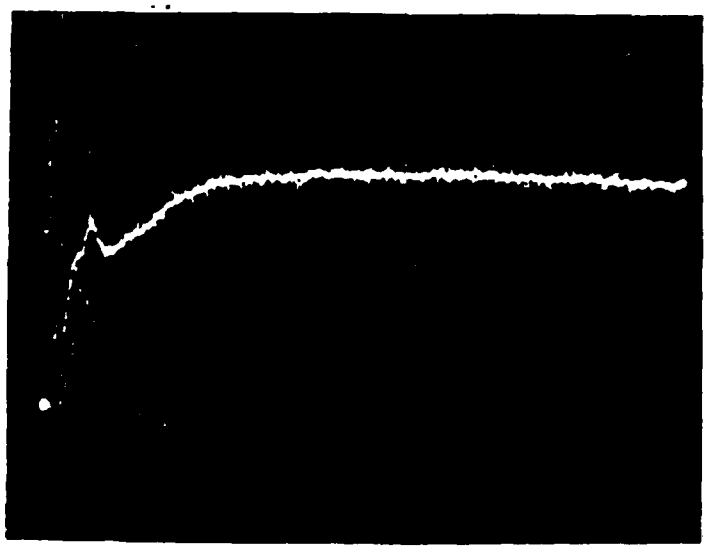

Figure 4 - Evoked cortical response to electrical stimulation of the cat eye (EER) at normal intraocular pressure. Intraocular pressure 15 mm Hg. Inner and outer canthus electrodes. 0.8 V, 2 ms stimulus pulse. Recording electrodes on the skull midline anterior to inion. The multipeak response is normal and highly reproducible.

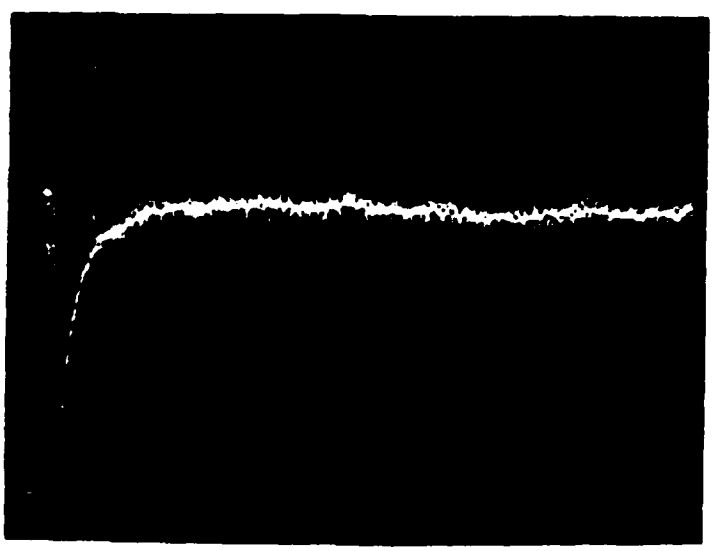

Figure 5 - Evoked cortical response to electrical stimulation of the cat eye (EER) at elevated intraocular pressure. Stimulus and recording conditions as in Figure 4. This response is recorded ten minutes after intraocular pressure has been raised to 120 mm Hg. All traces of the EER have disappeared. Elements of the neural response appeared within one minute after the intraocular pressure was returned to normal, as shown in Figure 6.

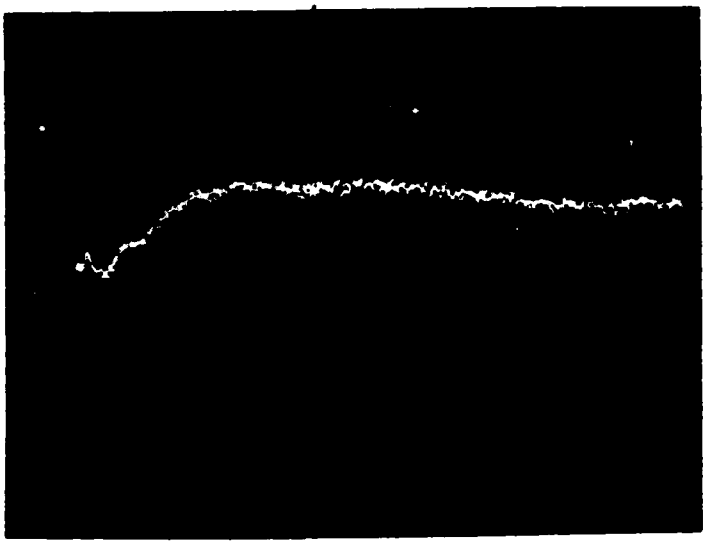

Figure 6 - Evoked cortical response to electrical stimulation of the cat eye (EER) after increased intraocular pressure. This response was recorded one minute after the intraocular pressure has been returned to normal (15 mm Hg) after remaining ten minutes at a pressure of 120 mm Hg. Stimulus and recording conditions as in Figure 4.

REFERENCES

Bertz, E.: Cerebral blood flow: Its measurement and regulation. Physiol. Rev. 52:595-630, 1972.

Brown, K.T., and Watanabe, K.: Neural stage of adaptation between the receptors and inner layer of monkey retina. Science 184:1113-1115, 1965.

Coburn, K.R.: Physiological end points in acceleration research, Aerospace Med. 41:5-11, 1970.

Cohen, M.: Continuous evoked responses as an indicator of "G" tolerance, pp. 135-140. IN: Research need relating to aircrew visual requirements (H. Rossenwasser, G.T. Chisum and P.E. Morway, eds.) Naval Air Development Center, Warminster, PA, NADC 79253–60, April, 1979.

Cohn, R.: Visual evoked responses in the brain injury monkey. Arch. Neurol. 21:321-329, 1969.

Dawson, W.W. and Radtke, D.: The electrical stimulation of the retina by in-dwelling electrodes. Investigative Ophthalmology and Visual Science. 16:249-252, 1977.

Donchin, E. and Lindsley, D.B. (eds.): Averaged evoked potentials: Methods, results, and evaluations, NASA-SP-191, Washington, D.C.: National Aeronautics and Space Administration.

Doolittle, J.H.: Accelerations in flight. Report 203:373-388. Annual report of NAC, Government Printing Offices, Washington, D.C., 1924.

Duane, T.: The effect of anoxia. Observations on the fundus oculi during blackout. AMA Arch. Ophthal. 51:343, 1954.

Duane, T.D.; Lewis, D.H.; Weeks, S.D.; and Toole, J.F.: The effects of applied ocular pressure and of positive acceleration on photic driving in man. NADC-MA-6214, Warminster, PA: Naval Air Development Center, 1962.

Fraser, T.M.: Human response to sustained acceleration. NASA-SP-103, Washington, D.C., National Aeronautics and Space Administration, 1966.

Gillingham, K.K.; and Krutz, R.W.: Effects of the abnormal acceleratory environment of flight. USAF-SAM Review 10-74, 1974.

Krutz, R.W.; Rositano, S.A.; and Mancini, R.E.: Comparison of techniques for measuring G_z tolerance in man. J. Appl. Physiol. 38:1143-1145, 1975.

Leverett, S.; Kirkland, V.E.; Schermerhorn, T.J.; and Newson, W.A.: Retinal circulation in man during G_z blackout. Proc. Aerospace Med. Ass'n., 1966.

Mercier, A.; and Duguet, J.: Physiopathology of the flyer's eye. USAF-SAM Special Publication. Randolph Field, Texas. USAF School of Aviation Medicine, 1947.

Motokawa, K.: Visual function and the electrical excitability of the retina. Tohoku Journal of Experimental Medicine, 51:145-153, 1949.

Motokawa, K. and Iwana, K.: The electrical excitability of the human eye as a sensitive detector of oxygen deficiency. Tohoku Journal of Experimental Medicine, 50:319-328, 1949.

Nelson, J.G. and Hrebien.: Real-time detection of steady-state evoked potentials. Frontiers of Computers in Medicine COMPMED 82 Conference Proceedings. In Press, 1982.

Richards, W. (Ed.) Symposium of electrophysiological techniques for studying visual function in man. J.O.S.A. 67:1451-1494; 1605-1606, 1977.

Tepas, D.I.; Armington, J.C.; and Kropfl, W.J.: Evoked potentials in the human visual system. Biological Prototypes and Synthetic Systems. 1:13-21.

Ward, B.: Electroretinogram during 100% + G_z gradient acceleration in dogs. Aerospace Med. 39:469-473, 1968.

Wolbarsht, M.L.; and Ringo, J.: Visual acuity and the balance between receptor density and ganglion cell receptive field overlap. Final Report, Naval Air Systems Command Contract N00019-79C-0370, 1980.

INTRACORTICAL INTERACTIONS FOR ORIENTATION CONTRAST

Jeremiah I. Nelson, Ph.D.
Dept. Ophthalmology PHL 811
NYU Medical Center
550 First Avenue
New York, NY 10016

Introduction

In Fig. 1[1], horizontal stripes in the circular areas appear tipped out of mutual alignment when presented in the context of a tilted, striped background. The manifest distortion of orientation perception by the presentation of surrounding contours has prompted some laboratories to investigate the effect of remote stimulation on single unit responsiveness in visual cortex, where most neurons are orientation selective, many exquisitely so. Contour patterns are not presented to the region of the visual field where stimulation excites the cortical cell under observation (the classic excitatory receptive field). A so-called contour adapting field of stripes is presented only beyond this region. The adapting field is found to greatly influence responsiveness of the test unit, typically inhibiting simple cell response, as first reported (for a single complex cell) by Blakemore & Tobin[2]. Unfortunately the receptive fields of simple and Type I hypercomplex cells include inhibitory as well as excitatory areas. Unless these areas, too, are excluded from stimulation it cannot be inferred that observed changes in responsiveness originate in a lateral inhibitory input from neighboring units. Worse still, the stronger, orientation non-selective inhibition from the receptive fields' inhibitory side bands may mask the properties of the lateral inhibition. We have sought to eliminate these difficulties in our studies of cat striate cortex.

Our findings provide a possible neurophysiological mechanism for one of psychology's oldest effects, the "optical illusions" of contour orientation.[3] These mechanisms involve intracortical interactions of surprising specificity and strength. Thus, the cortical area where the sensory coding of orientation is first performed seems also to contain mechanisms which systemmatically distort vision. Surely there must also be benefits. These most likely arise in situations where context influences how a stimulus is perceived (we consider below globality in stereoscopic depth perception). Spatially extensive interactions provide a basis for the distributed processing increasingly invoked by psychologists to explain higher perceptual processes, whether in the framework of Fourier theory or of an autocorrelation model[4]. The broader motivation for studying them is to proceed beyond local cue detection to the processing of sensory information. Only with principles of sensory processing at our disposal can we hope to mount an attack on the basis in brain of pattern recognition.

Orientation contrast illusions

Cats were prepared for electrophysiological recording and simple cells subserving central vision (all but two receptive fields within 7 deg of the area centralis) were selected for study, using conventional methods[5]. Receptive fields[6] were mapped using a conditioning (activated discharge) technique. Inhibitory as well as excitatory areas are revealed by this technique as modulations impressed against the steady discharge level elicited by the small, separate conditioning stimulus. Activated discharge profiles were subjected to statistical analysis to yield overall topographic maps of receptive field[7]. The availability of receptive field maps like that shown in Fig. 2 enable us to be rather certain that adapting field stimulation did not in fact fall on known receptive field regions, either excitatory or inhibitory. Results are presented below from remote stimulation experiments performed on the cell whose receptive field map is shown in Fig. 2

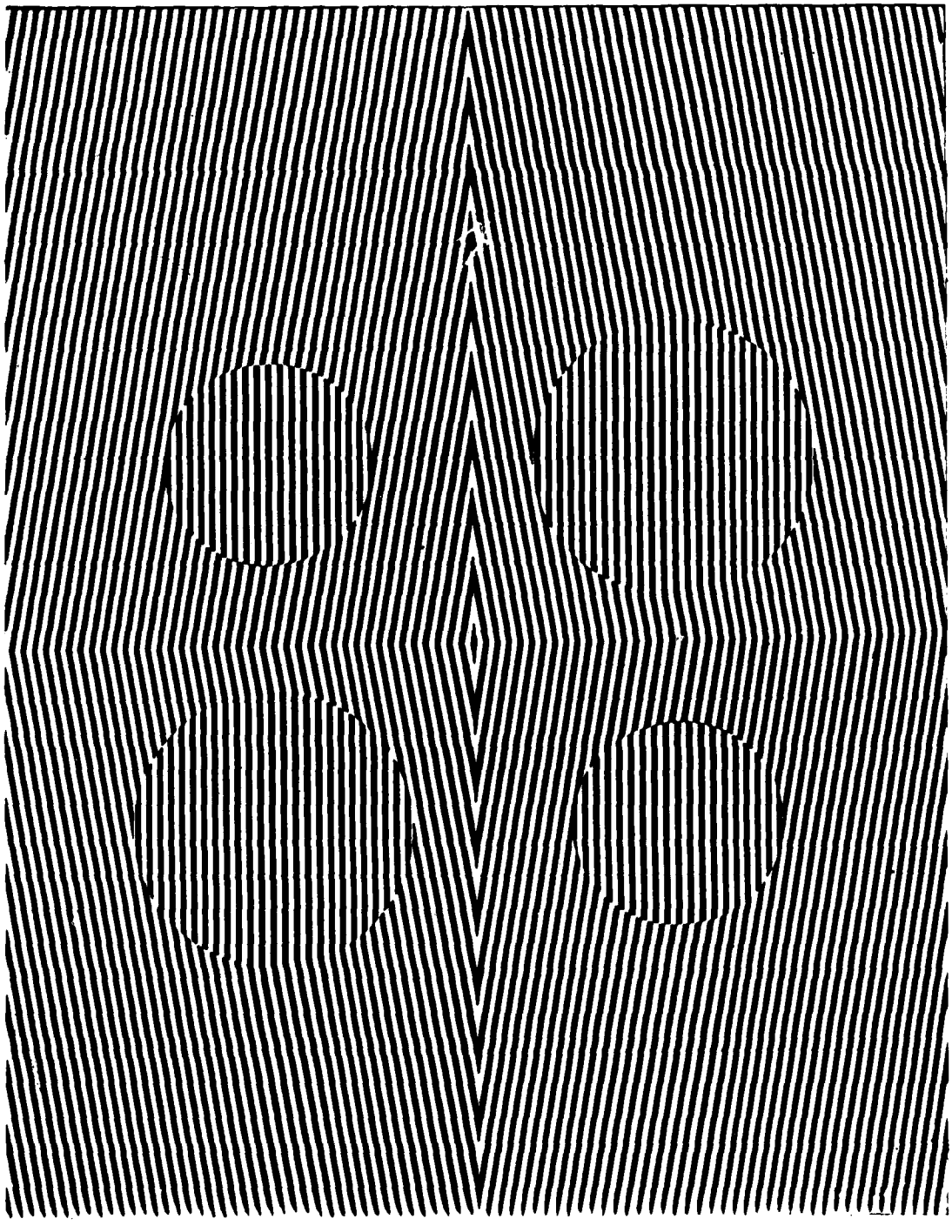

Figure 1 - Lines in the circular areas appear tipped out of alignment when presented in a context of inclined contours. This orientation contrast effect may be linked to intracortical interactions occurring among orientation-selective cortical neurons. These interactions disrupt sensory coding for orientation. Do they serve any useful purpose?

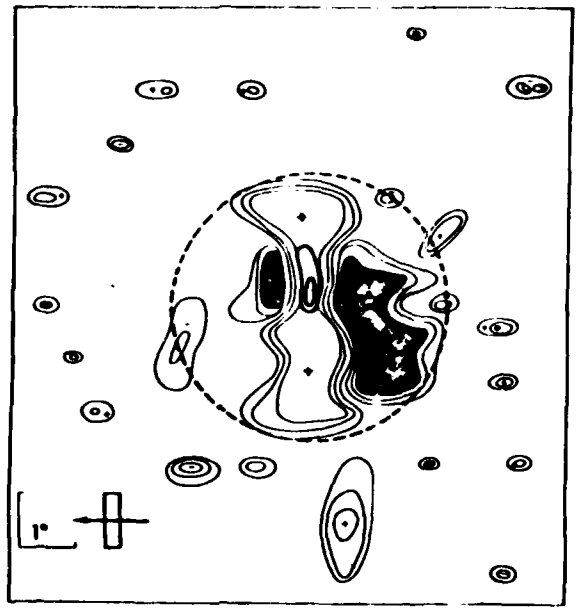

Figure 2 - Topographical map of conventional receptive field of a simple cell. The black areas are the inhibitory sidebands flanking the excitatory discharge center. The receptive field is drawn as if the cell preferred vertical bars. Orientation selectivity arises both because the excitatory discharge center is elongated and because the sidebands inhibit response to (mis-oriented) bars falling across them. Proceeding outwards, contour lines represent the limit of the receptive field at approximately the 10, 1 and 0.1% levels of statistical confidence. The excitatory area shows in addition the central areas (heavy lines) where response rose to 3 and to 5 times mean discharge level. Scattered islands occur randomly when the mapping process is repeated, and reflect noise in the single-unit discharge. The area within the circular dashed border was covered with cardboard to test the effects of stimulating many of this cell's neighbors while probing for a disturbance in the test cell.

When care is taken to map receptive field regions and to exclude all of them from adapting field stimulation, certain clear-cut results emerge: in agreement with a preliminary report for fewer cells[7], there is a remote influence of at least 10% strength in almost all cortical Area 17 cells tested (97% of all cells; the effect exceeded 70% in 23% of simple family cells and was generally weaker and more likely to be facilitatory under some conditions in complex cells[8]. For simple cells, this influence was predominantly inhibitory, and among these inhibited cells, the inhibition varied with the orientation of the adapting field stripes in 90% of the cells tested[9]. We term the effect **orientation domain inhibition** because it varies with stimulus orientation when other stimulus cue dimensions are held constant. Is this the contrast mechanism which has been modeled by psychophysicists?

A current, neurophysiologically-couched model of orientation contrast[10] is illustrated schematically in Fig. 3 (top). The contours of an illusion are represented according to orientation without regard for the details of their spatial position. Thus, across the orientation domain, there

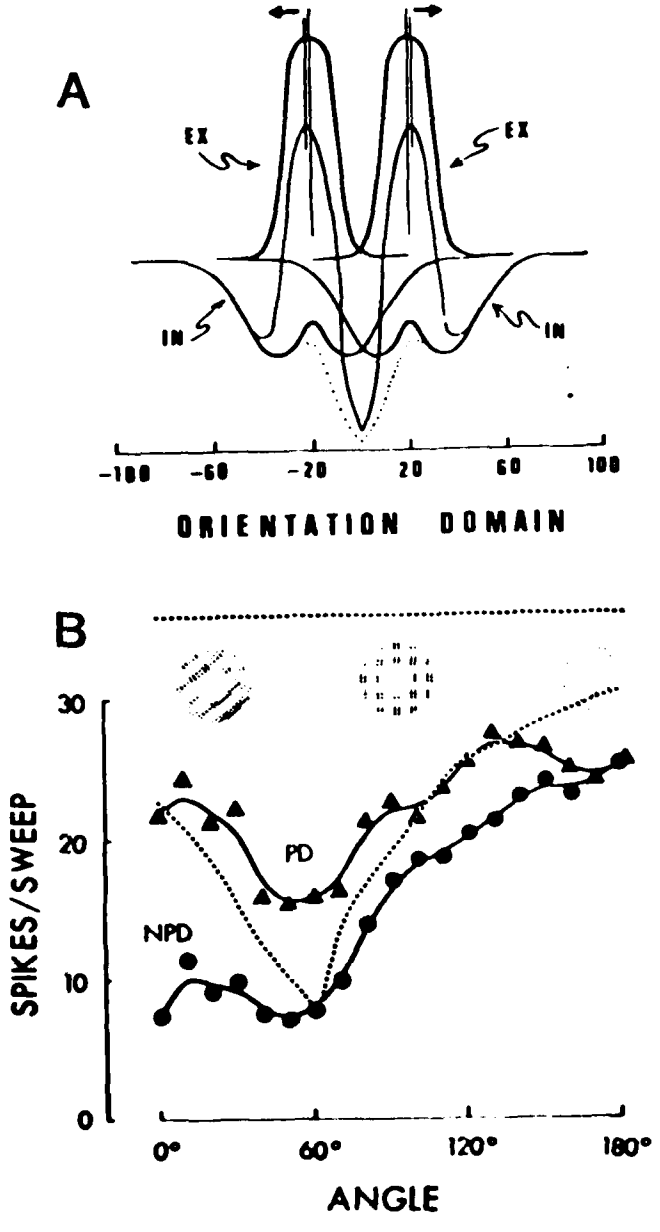

Figure 3 - (A:) Orientation domain inhibition model of orientation contrast (angle expansion illusions). EX, excitatory response profile (envelope) for many units along the orientation domain. IN, orientation domain inhibition, assumed to summate linearly (dotted line). Inhibition summates to its greatest value in the bisector between the two stimulated orientations. The linear combination of inhibition and excitation causes a displacement in the overall pattern of activity (arrows at top) appropriate to orientations more widely separated than those physically presented. An exaggerated difference in perceived orientation (orientation contrast) results. (B:) Orientation domain inhibition angle tuning curve recorded from cat simple cell in striate cortex. The test cell's preferred orientation lies at the bisector of ever-widening angles formed by two counter-rotating adapting fields. Inhibition is maximum for an acute angle of 50 - 60 deg; this angle would produce the maximum orientation contrast illusion according to models such as that in (A). Adapting fields: back-projected 0.32 cpd square wave gratings 47.4 deg across sweeping in preferred direction (PD) or non-preferred direction (NPD) for the conventional excitatory response. Horizontal line: control response, no adapting fields. Dotted curve: PD angle tuning curve predicted from linear summation of orientation domain inhibition functions observed with presentation of a single adapting field.

arise only two activity peaks corresponding to the two orientations displayed. Associated with each peak is a rather more broadly spreading trough of inhibition. The net profile of excitation across the orientation domain after these inhibitory and excitatory responses are combined displays peaks appropriate to a wider angle than that actually presented, and so the misperception of contour arises. This effect is termed **orientation contrast** because the difference in orientation is exaggerated. Two properties are central to models of the above sort: the inhibition must vary with orientation such that it is strongest in the vicinity of the optimal orientation for the conventional excitatory response, and, when two orientations are stimulated simultaneously, inhibition must summate to produce a maximum at tunings midway between the two orientations presented. In this way, the populations of neurons responding to the contours presented, and responsible for the sensory coding of their orientations, will experience an asymmetry in inhibitory inflow on their inside (bisector) vs. outside flanks. The distribution of activity within the population will be skewed. Note that models of this sort do not call for a distortion in the **shape** of any single unit's orientation tuning curve, as some have sought to demonstrate[11], but rather stipulate changes in tuning curve **height.** Neurophysiologically, neurons with certain optimal stimulus orientation preferences are suppressed in responsiveness; psychophysically, this may be tantamount to saying that contrast thresholds are elevated in selected orientation channels. Experiments in cat verify that the dominant effect is a change in responsiveness, and that the pattern of inhibition is in qualitative agreement with the model of Fig. 3 (top). This work is briefly presented below.

Selectivity for single orientations. To study domain inhibition in isolation, contour adapting fields were presented only to visual field regions lying beyond the circular border (i.e., beyond the receptive field) shown in Fig. 2. The adapting field inhibited the response of this simple-type neuron to a centrally-presented, optimal bar; this inhibition varied with orientation of the adapting field as shown by curves 1 and 2 (Fig. 4 A, B). This is not the experiment we might dream of performing, namely to sample at will a sequence of cells with regularly-progressing orientation tunings, and to measure the decrease in inhibition at tunings progressively more remote from the stimulated one. But this experiment is logically equivalent. The adapting field, rotated to successive orientations, must stimulate small populations of orientation-selective units further and further away in orientation from the unit under test.

To insure a maximal response from the largest number of cortical neurons, the adapting fields used in all experiments were drifted slowly across the visual field. When the field drifted in the direction preferred by this almost completely direction-selective neuron, an unexpected effect was observed: for adapting field orientations within ± 30 deg of optimal for the unit under test, there was relief from inhibition. This disinhibition has since been observed in 40% of simple cells displaying domain inhibition. In all cases, the disinhibition was much more orientation-selective than the main inhibitory effect, and well-centered on the optimal orientation[12]. It is inconceivable that the conventional central excitatory region of the receptive field contributed to this effect, as the diameter of the region completely shielded from adapting field stimulation was ten times the 0.6 deg width of the excitatory discharge center (central region of receptive field, illustrated for another cell in Fig. 2)[13]. This disinhibitory effect seems to be of considerable importance.

Selectivity with two orientations. The models of Blakemore et al. and Nelson[10] require that with two contour orientations presented at some acute angle, inhibition should be greatest for units whose optimal stimulus orientation would be the orientation of the angle's bisector. Consequently we presented two contour adapting fields at once, super-imposed at first at the optimal stimulus orientation of the neuron under test, and then counter-rotated so as to form a succession of over larger angles with each other. As the two adapting fields opened up to form acute,

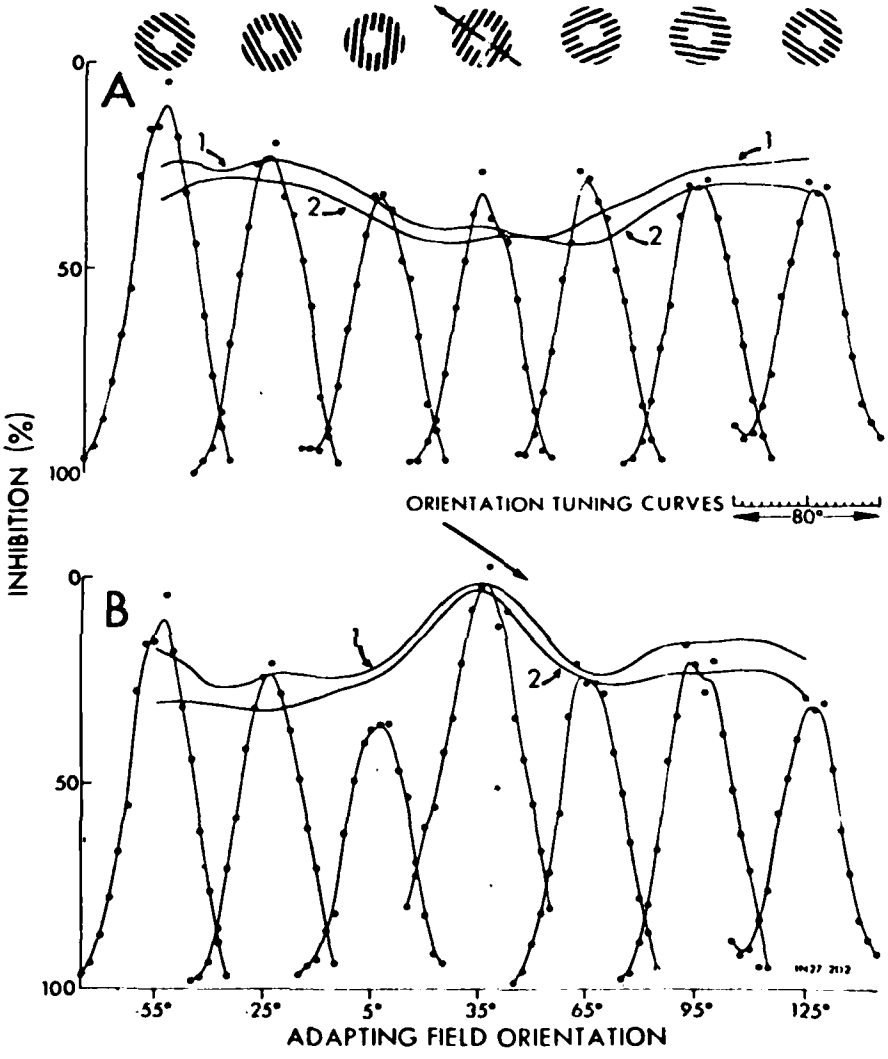

Figure 4 - Contour adapting fields distort tuning curve height. Two groups of orientation tuning curves (A,B) are shown for the simple cell whose receptive field is mapped in Fig. 2. Each orientation tuning curve was elicited by stimulating the central excitatory discharge region with a 5 x 1 deg moving light bar systemmatically rotated in 5 deg steps, while the surrounding area was stimulated with a contour adapting field held in one of seven orientations (X-esis), as schematized at the top of the Figure. Adapting fields were 0.92 cpd square wave gratings 23 deg across, sweeping at 2.65 deg/sec in the direction not preferred (A) or preferred (B) by this directionally-selective neuron (0 degs vertical). Height varies in accord with the tuning curve for orientation domain inhibition (1, repeated 12 hours later, 2).

orthogonal and finally obtuse angles with each other, they always framed at their bisector the optimal orientation of the test unit. When sampled at the bisector of a varying angle, orientation domain inhibition varies in strength; the "angle tuning curve" for domain inhibition is illustrated in Fig. 3 (bottom). These results, interpreted in accord with the above models of orientation contrast, suggest that the cat, too, sees orientation illusions. For the cat, the optimum acute angle should turn out to be 50 or 60 deg, about twice as great as the most effective angle in man[14].

Note that maximum inhibition occurs at 30 deg while maximum orientation contrast requires an angle of 60 deg. Were we to present two contours at a 30 deg angle, their **mutual** inhibition would be maximal. This inhibition is not the maximal attainable in the network, as the responses driving the inhibition suffer mutual reduction. Nor is the inhibition distributed in the optimal places for contrast. The place along the orientation domain able to receive the most inhibition will be one 30 deg away from as many contour orientations as possible. That place is the bisector of a 60 deg angle. We did in fact observe an inhibition here from two adapting fields which was approximately double the maximal attainable from either adapting field alone. Both the orientation selectivity and summation requirements of the contrast models are satisfied by orientation domain inhibition. With summation, inhibition is maximal at 60 deg; an inhibitory trough at the bisector is furthermore effectively disposed to asymmetrically distort the excitatory response envelope along the orientation domain (Fig. 3, top). The distortion in what students of sensory coding have termed the "cross-fiber firing pattern"[15] is assumed to be the neural correlate of the observed illusion. Note that for analyzing orientation contrast illusions, a significant part of the configuration lies along an axis where there is no physical contour in the figure. Interestingly, angle bisectors (as well as axes of symmetry) have proved useful in understanding orientation perception errors with figures more complex than isolated angles[16].

The inhibition tuning curves of Fig. 3 (bottom) for the angles formed by two adapting fields may be derived by summing two orientation domain inhibition tuning curves of the sort described previously for a single adapting field (Fig. 3 bottom, dashed line). Thus, while these interactions are specific to certain orientations and can be structured spatially (below), we can still say that the inhibitory pattern for the whole is merely the sum of the inhibitory responses to the parts. Most simple cells could contribute to orientation contrast. 40% of the simple family cells tested have an optimal angle **disinhibitory** pattern like this one, and so would display angle tuning curves for domain inhibition similar to that of Fig. 3 (bottom). But other simple cells have angle tuning curves appropriate for orientation contrast effects (exaggeration of perceived orientation differences) if one but considers the conventional excitatory response so carefully excluded from these experiments. The conventional excitatory response, with an average half-width at half-height of 14 to 18 deg in cat central vision[17] and a total width of perhaps 40 deg, provides a strong "relief from inhibition" in all cells, and so an angle tuning curve with a clear optimal angle must emerge, and stimulus contours forming such an angle must be distorted. Indeed, considering the strength of conventional excitation, disinhibition is almost superfluous as a component mechanism of orientation contrast. It must serve some additional purpose.

Shape or height? We next turned from the activity profiles of populations to the stimulus selectivity of a single unit. We sought to evaluate an isolated neuron's ability to code orientation in the presence of varying amounts of domain inhibition. To do this, the contour adapting field paused at selected orientations while the central activated discharge stimulus (typically 6 deg long) was rotated to elicit a conventional orientation tuning curve. Sensory coding errors demonstrably arise from modulation of activity across the domain; are individual tuning functions distorted as well?

As stimulus orientation varies, the peak responsiveness attainable by the test neuron must be limited by the amount of inhibitory inflow received. So the **peak height** of the two families of orientation tuning curves in Fig. 4 should coincide with the orientation domain inhibition tuning curves (curves 1 & 2, Fig. 4). This height change occurs and appears to be the dominant source of sensory coding error, implying that orientation selective channels are highly interactive, not independent. To ascertain the presence of additional shape changes, these tuning curves were replotted with heights normalized. In the absence of any adapting field, the tuning curves are very reproducible (for a cell of average selectivity, range ±2.55 deg, s= 1.6 deg, N=13). With the addition of an adapting field these curves become more variable (Fig. 5A, bottom), and there is a pattern to this variability (Fig. 5B): there is a slight peak shift away from the adapting field's orientation. Thus, when the adapting field's orientation is 30 to 60 deg clockwise from optimal, the unit's peak response occurs somewhat counterclockwise of its normal orientation.

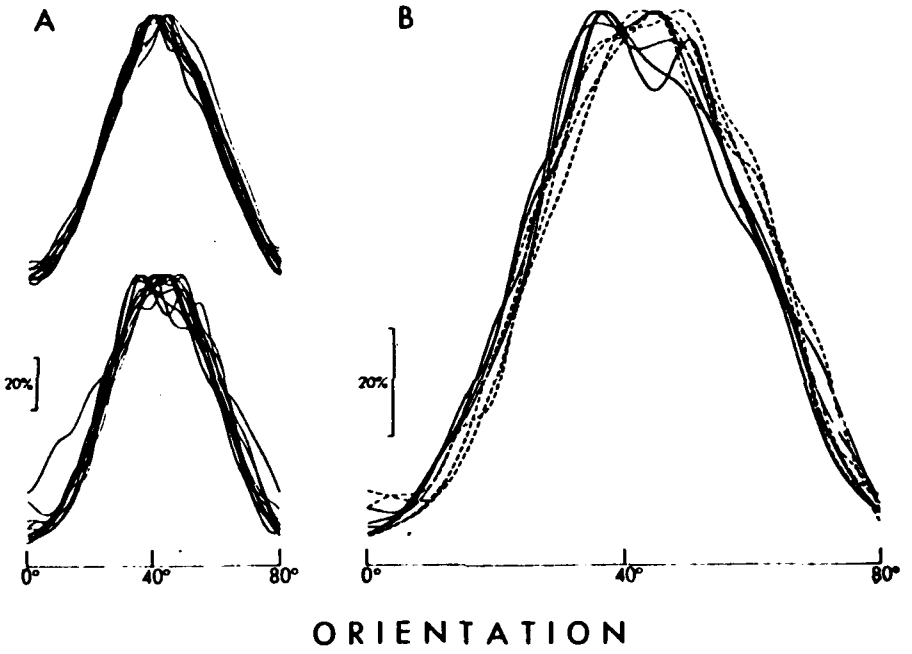

Figure 5 - (A:) top, orientation tuning curves are reproducible, but (bottom) much less so in the presence of contour adapting fields. (B:) Selected tuning curves obtained in the presence of adapting fields 30 or 60 deg clockwise (solid curves) or counter-clockwise (dashed) from the test unit's optimal stimulus orientation. Preferred- and non-preferred direction adapting field sweeps are shown for each orientation.

The peak shift effect cannot contribute to orientation contrast. On the contrary, it would produce the opposite effect, reasoned as follows: with orientation contrast, a contour presented somewhat counterclockwise both to vertical and to another inducing contour (itself perhaps 15 deg clockwise of vertical) should appear even more counterclockwise. Now consider a test unit with a vertical optimal stimulus orientation. After a peak shift, a somewhat counterclockwise contour optimally stimulates the test unit. Unfortunately, if the test unit continues to carry a fixed label of "vertical." In the psychophysical literature, such an apparent displacement **towards** the inducing stimulus has been variously termed "assimilation" or "confluxion." It is possible that this peak effect contributes to the weak contour **attraction** effects widely reported for very small angles[18].

Before assigning any perceptual role to the peak-shift effect, it must be noted that it is confined to the peak area of the tuning curve and the perturbation itself is extremely small, amounting to a change in activity of only 7%, in contrast to the overall **height** changes of 42% in this unit, and over 80% in several others. Neurophysiologically, we believe the effect arises because "single unit" tuning curves for many simple-type cells in fact carry a modest intracortical facilitatory contribution. This facilitation is the relief from inhibition seen Fig. 4B. Like the shape variability, the facilitatory effect is confined to perhaps a 30 deg interval centered around a unit's peak. Adapting fields positioned 30 to 60 deg to one side of optimal are able to inhibit neurons which would otherwise have made a facilitatory contribution to the response; symmetry of the curve is lost. In accord with this hypothesis, a unit without the relief from inhibition failed to display the peak shift effect. Prolonged stimulation technically required in this and other experiments[5] has shown that this facilitatory input is particularly susceptible to habituation, whose onset is marked by peak variability in tuning curves obtained conventionally without adapting fields.

An intracortical facilitatory process is perceptually useful to the organism, as it is capable of strengthening responses to contours which share certain alignments, orientations or positions in space. Such contours are likely to have arisen from a common object. We have been able to demonstrate the appropriate positional specificy for such a role.

Facilitation and perception

The relief from inhibition is due to a separate excitatory process, usually subliminal, but capable in some units of directly exciting the neuron. This excitatory input is most readily observed as a facilitatory modulation of conventional excitation driven by another, optimal stimulus. The facilitation is evident in Fig. 6A as peaks in responsiveness which coincide with the passage of individual stripes in the adapting field across the receptive field, in agreement with the "phase sensitivity" reported by others[19]. This regularity is in contrast to domain inhibition, which seems to originate isotropically around the receptive field. To test for structure in the areas of origin of the facilitation, we masked various quadrants and regions around the receptive field from stimulation. In this and other units, it proved possible to eliminate facilitation by masking merely a narrow strip of the visual field lying along the axial extension (optimal stimulus orientation) of the receptive field. Facilitatory regions occur beyond conventional receptive field regions, and may contribute to the puzzling modulations sometimes observed in conventional length-response curves[20]. Such length-response curves are obtained as an optimally-oriented bar is increased in length along the axial extent of the receptive field, and so comes to intrude upon the distant response-modulating regions we have studied here.

The importance to perception of a structured, selective facilitatory process is enormous. Contours are long, receptive fields are short. With intracortical facilitation, the otherwise isolated response of one neuron achieves the capability of augmenting the response of those other neurons which were themselves likely to have been stimulated by the same real-world object[21]. Coupled with non-facilitation of receptive fields in the wrong spatial position, and even active inhibition of units of "wrong" orientation tunings, we have the beginnings of a figure-ground **segmentation** mechanism[22]. This analysis may be transposed to another visual domain, binocular retinal disparity which is the cue to stereoscopic depth perception. A central technical problem in stereopsis is the suppression of false targets and the isolation of the correct disparity signal from repeating patterns such as Julesz's random-dot stereograms[23]. Mutual facilitation to provide visual field-wide coupling among like-tuned units, combined with mutual antagonism among units with dissimilar depth preferences (to remove local sensory coding ambiguity) has been hypothesized as the mechanism

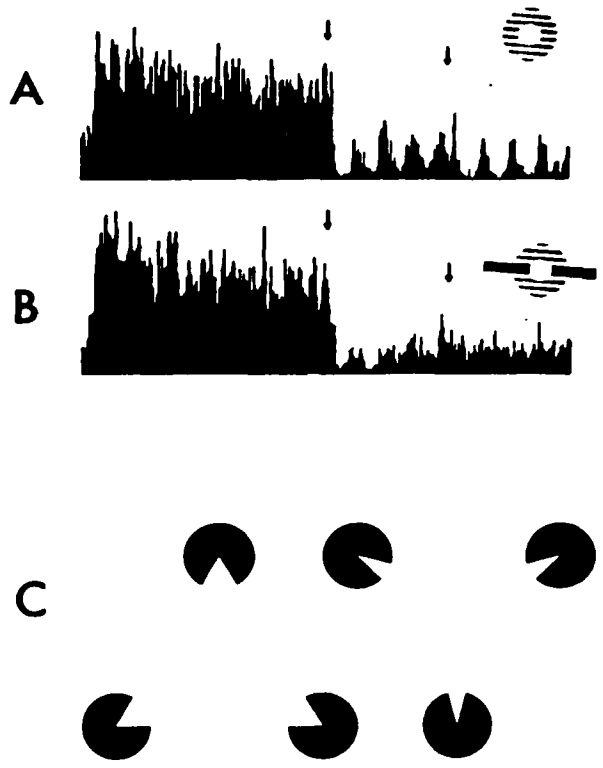

Figure 6 - Periodic relief from inhibition. (A:) Response decreases by 77% when adapting field is presented, moving in non-preferred direction (first arrow) and reversing sweep direction 2 sec later (second arrow; adapting field 0.57 cpd, 21 deg across). Periodic disinhibition corresponds to passage of individual stripes across the coaxial extensions of receptive field; it is blocked (B) when a 2.5 deg wide, very long opaque strip is placed across receptive field in the neuron's optimal stimulus orientation. Mask, 4 deg diameter; length-response data suggests the effect originates more than 5 deg from receptive field center. This effect may play an early role in the generation of subjective contours (C).

of stereoscopic globality[24]. Physiological evidence for these additional intracortical interactions has yet to be discovered[25].

Subjective contours (Fig. 6C) and the "moving visual phantoms" of Tynan & Sekuler[26] may well begin with intracortical interactions in the primary projection area. The facilitatory effect reported here would raise the activity of just those units with receptive fields lying along the subjective contour, yet no physical contour is there. Therein lies the appeal and power of subjective contours: unhindered by a cue conflict with real contours, the special contribution of higher centers to perceptual organization is left fully manifest. Perhaps even the curvature and other "field effects" sometimes seen in subjective contours (Fig. 6C) can be explained merely by the spatial domain spread functions of striate cortex interaction.

Some aspects of perception with both real and subjective contours still fail to find parallels in available neurophysiological data. We find no special effects among orthogonal contours, whereas they are strong inducers of subjective contours[27] and produce the orientation coding error known as the indirect effect[28]. Gaps or end-points in contours are extremely important for figure-ground segregation and the "effortless perception" of texture differences[29]. A gap between background and test fields has a profound effect upon both orientation contrast and the evoked potential[30],

yet there is no sign in cat striate cortex of sudden response non-linearities with various adapting field/stimulus separations.

Domain interactions and columns

It is tempting to regard domain interactions as the functional expression of cortical columnar structure[31]. "Columns" originally referred to an aspect of the cortex's radial organization, namely that an electrode penetration perpendicular to the somatosensory cortex could encounter units devoted **only to one** sensory submodality such as light skin touch or deep joint movement[32]; in certain special cases[33], this functional organization finds anatomical expression. Subsequently, tangential electrode penetrations in visual cortex revealed a different form of functional organization which probably plays a far greater role in cortical sensory processing.

Proceeding tangentially, successively encountered neurons sometimes display an orderly progression of orientation tunings[34]. We term this **sequence-slab** organization in distinction to the original, radial-aggregation meaning of "column." More recently, it has become possible to mark cells with elevated glucose uptake (and greater metabolic activity) using the deoxyglucose autoradiographic technique. When applied to the brain of an animal which was viewing only vertical contours prior to sacrifice, this technique reveals that like-tuned units have slab organization too[35]. Slabs of like-tuned units make it possible to snake broadly across the cortical surface and through the visual field while always remaining surrounded by "vertically-tuned" tissue. This may be termed **iso-slab** organization. A growing suspicion is that sequence-slab organization is the anatomical expression of domain inhibition, while iso-slab organization expresses domain facilitation. With regularity built into the tissue, random dendritic arborization at the cellular level would produce innervation with the selectivity we have observed in intracortical facilitatory and inhibitory interactions. Which cellular species is the interneuron? What factors lead to slab organization in the first place, and is there membrane specificity and contact inhibition to confine dendritic arborization within a slab? Increasing interactions among those studying cortical structure, function, and development are likely to provide answers to such questions, and to propel visual neurophysiology into the realm of visual perception.

Summary

Responses to visual stimulation presented in visual field regions remote from the classic receptive field have been reported from time to time and prove upon closer study to be remarkably prevalent and stimulus-specific. The remoteness of areas giving rise to the effects, as well as their stimulus specificity, suggest an origin in intracortical interactions. For simple cells in the orientation and spatial domains of the cat, inhibition occurs broadly among units of differing orientations but restricted (in central visual projection area) to a locale approximately 8 deg across. Facilitation is confined to units sharing similar orientation tuning, but may extend far out along the long axis (optimal orientation) of a receptive field. These interactions have been linked to the occurrence of orientation contrast illusions in contour perception. The selectivity of these interactions is probably shaped by the orderly functional architecture seen in sequence-slabs and iso-slabs (columns) of visual cortex. Indeed, the utility of the ordered interactions for perceptual processing may be a factor driving the evolution of ever-greater cortical surface area and the organization of this tissue into slabs or columns.

REFERENCES

[1] Blakemore, C. (1971). Program cover for the conference on **Contour Interaction in the Visual System**, Cambridge, January.

[2] Blakemore, C. & Tobin, E.A. (1972). Lateral inhibition between orientation detectors in the cat's visual cortex. Expl Brain Res. 15, 439-440.

[3] "Optical" illusions have proven to have little to do with the eye's optics. The term **figure illusions** is more appropriate. Figural illusions involving orientation have been well-studied since the nineteenth century:

Zollner, F. (1860). Ueber eine neue Art von Pseudoskopie und ihre Beziehungen zu den von Plateau and Oppel beschriebenen Bewegungsphanomenen. Poggend. Annalen 20, 500-523 & Plate VIII).

The optimal angle for getting the effect in man lies between 15 and 30 deg for a wide variety of configurations:

Berliner, A. & Berliner, S. (1948). The distortion of straight and curved lines in geometrical fields. Am. J. Psychol. 61, 153-166, 20 deg; Heymans, G. (1897). Quantitative untersuchungen Uber die Zollnersche und die Loebsche Tauschung. Z. Psychol. 14, 101-139, 30 deg; Over, R., Broerse, J. & Crassini, B. (1972). Orientation illusion and masking in central and peripheral vision. J. exp. Psychol. 96, 25-31, 15 deg; Wallace, G.K. & Moulden, B. (1973). The effect of body tilt on the Zollner illusion. Q. J1 exp. Psychol. 25, 10-21, 15-20 deg; White, K.G. (1971). Zollner illusion as perceptual enlargement of acute angle. Psychon. Sci. 24, 73-75, 22 deg.

The maximum effect is typically less than 4 deg, but can be greater with brief exposure times and short contours.

[4] Fourier:

Weisstein, N. & Harris, C.S. (1980). Masking and the unmasking of distributed representations in the visual system. In C.S. Harris, Ed., **Visual Coding and Adaptability.** Hillsdale, NJ: Erlbaum/Wiley, pp. 317-364.
((chapter pages unknown—have pre-print only.))

Autocorrelation:

Uttal, W.R. (1975). An autocorrelation theory of visual form detection: a computer experiment and a computer model.
Behavior Res. Methods & Inst. 7, 87-91.
W.R. Uttal, **An Autocorrelation Theory of Visual Form Detection.**
Hillsdale, NJ: Erlbaum/Wiley, 1975.

[5] Nelson, J.I., Kato, H. & Bishop, P.O. (1977). The discrimination of orientation and position disparities by binocularly activated neurons in cat striate cortex. J. Neurophysiol. 40, 260-283.

[6] The **receptive field** is a central concept in sensory (especially visual) neurophysiology today. Loosely, the receptive field is that region of the visual field where presentation will influence the responsiveness of the particular neuron under study.

The rationale of the present work is to delimit the extent of the classic or primary receptive field, and then show that with due care, influences may yet be observed from stimulation presented

beyond the primary field limits. A predominantly inhibitory influence is expected. This observation of a remote origin for the effect, along with other tests, argues for an intracortical origin for the influence.

While some workers have concentrated on only the excitatory areas of the receptive field, strictly the definition includes inhibitory as well as excitatory areas. For this work, where novel inhibitory influences are sought, it is important to determine and eliminate conventional inhibitory as well as excitatory areas. This has been done. Finally, the work requires a redefinition of the cortical receptive field: a receptive field is where you find it, and we have demonstrated new areas. However, in view of the probable difference in origins of the old and new areas, it is useful to maintain a distinction between the classic or primary receptive field and the new areas which have been studied here.

[7]
The details of how the maps were prepared are given elsewhere:
Nelson, J.I. & Frost, B.J. (1978). Orientation-selective inhibition from beyond the classic visual receptive field. Brain Res. 139, 359-365. Nelson, J.I. & Frost, B.J. (in prep.) Response to visual stimuli presented beyond the limits of topographically mapped cortical receptive fields. I. Maps.

[8]
The possibility remains that all simple cells display the effect but we twice failed to elicit it because the area masked from stimulation was so extensive. The masks were typically 6 deg across, while the average width of the excitatory discharge region was 0.6 deg. The area from which domain inhibition arises may be coextensive with—and sometimes limited to—the receptive field area.

[9]
Maffei & Fiorentini

(Maffei, L. & Fiorentini, A. (1976). The unresponsive regions of visual cortical receptive fields. Vision Res. 16, 1131-1139)

reported orientation selectivity in only 15% of 48 cells (28 simple, 20 complex) tested following shielding of only the conventional excitatory area from the contour adapting field. A large proportion of the inhibition they observed must therefore have arisen from inhibitory sidebands, whose response has been shown to be unselective for orientation:

Bishop, P.O., Coombs, J.S. & Henry, G.H. (1973). Receptive fields of simple cells in the cat striate cortex. J. Physiol. 231, 31-60; see esp. Fig. 3.

It seems unwarranted to attribute orientation domain inhibition itself to inhibitory sidebands, as tentatively suggested by Fries, Albus & Creutzfeldt:

Fries, W., Albus, K. & Creutzfeldt, O.D. (1977). Effects of interacting visual patterns on single cell responses in cat's striate cortex. Vision Res. 17, 1001-1008.

The regions giving rise to the two inhibitory effects may indeed overlap, yet their properties differ. Domain inhibition can in fact be elicited from regions which do not give rise to either sideband or endzone (hyper-complex) inhibition.

[10]
For models, see:

Carpenter, R.H.S. & Blakemore, C. Exp. Brain Res. 1973, 18, 287-303; Nelson, J.I. (1969). The misperception of contour. Ann Arbor, Mich.: University Microfilms, LD 00090.

More rigorously and recently:

Levine, D.S. & Grossberg, S. (1976). Visual illusions in neural networks: line neutralization, tilt after effect, and angle expansion. J1 theor. Biol 61, 477-504.

Andrews had earlier suggested a role for mutual inhibition in orient[illegible] misperception of single contours

(D.P. Andrews (1965). Perception of contours in the central fovea. Nature, Lond. 205, 1218-1220).

while Wallace made a similar suggestion for angles

(Wallace, G.K. (1969). The critical distance of interaction in the Zollner illusion. Percept. Psychophys. 5, 261-264.)

But is it perhaps MacKay who more than anyone, and before the neurophysiological discoveries of Hubel and Wiesel, argued for the fruitfulness of applying lateral inhibition concepts cortically to a wide range of contour effects; e.g.,

MacKay, D.M. (1961). Interactive processes in visual perception. In W.A. Rosenblith, Ed., **Sensory Communication.** New York: Wiley, Ch. 19.

[11]
Burns, B.D. & Pritchard, R. (1971). Geometrical illusions and the response of neurones in the cat's visual cortex to angle patterns. J. Physiol. 213, 599-616.

[12]
The narrow tuning of both classic excitation and domain facilitation may be reflected in the narrow "channel" tunings revealed psychophysically by sub-threshold **summation** paradigms (insightfully reviewed by Georgeson, M. (1979). Spatial Fourier analysis and human vision. In N.S. Sutherland, Ed., **Tutorial Essays in Psychology: A Guide to Recent Advances.** Hillsdale, NJ: Erlbaum, Ch. 2, 39-88.) Channels inferred from selective **adaptation** experiments have typically been much broader and, at least in the orientation domain, may reflect the broadly-tuned inhibitory mechanisms described here. For evidence and models linking selective adaptation and aftereffect to the domain inhibition mechanisms we believe cause simultaneous contrast, see:

Dealy, R.S. & Tolhurst, D.J. (1974). Is spatial adaptation an after effect of prolonged inhibition? J. Physiol. 241, 261-270.

Magnussen, S. & Kurtenbach, W. (1980). Adapting to two orientations: disinhibition in a visual after effect. Science 207, 908-909. Kurtenbach, W. & Magnussen, S. (1981). Inhibition, disinhibition and summation among orientation detectors in human vision. Exp. Brain Res. 43: 193-198.

Models:

Blakemore, C. & Sutton, P. (1969). Size adaptation: a new aftereffect. Science 166, 245-247.; Nelson, J.I. (1977). The plasticity of correspondence: after-effects, illusions and horopter shifts in depth perception. J1 theor. Biol. 66, 203-266.

[13]
Indeed, the disinhibitory effect increased when additional area around the receptive field was masked, leaving the adapting field contours even more remote from the receptive field. This suggests that conventional excitation is not the relevant input, and that the disinhibitory or facilitatory input arises from more remote regions than orientation domain inhibition, as with the double-opponent organization for motion possessed by many pigeon tectal neurons and perhaps by the cat suprasylvian cortex:

Frost, B.J. (1978). Moving background patterns alter directionally specific responses of pigeon tectal neurons.
Brain Res. 151, 599-603.

Frost, B.J., Scilley, P.L. & Wong, S.C.P., (1981). Moving background patterns reveal double-opponency of directionally specific pigeon tectal neurons.
Exp. Brain Res. 43, 173-185.

Von GrUnau, M. & Frost, B.J. (submitted). Double-opponent process mechanism underlying receptive field structure of directionally specific cells of cat lateral suprasylvian area.

[14]
Optimal orientation contrast occurs at large angles in man, for moving dot field stimuli:
Marshak, W. & Sekuler, R. (1979). Mutual repulsion between moving visual targets. Science 205, 1399-1401.
The shift to larger optimal angles may be due to the use of dots as well as to the motion per se, as dot stimuli greatly broaden the orientation selectivity curves observed in cat single units:
Henry, G.H., Dreher, B. & Bishop, P.O. (1974). Orientation specificity of cells in cat striate cortex. J. Neurophysiol. 37, 1394-1409.

[15]
It is the pattern of firing for a population of neurons ordered along the orientation domain which changes:
Erickson, R.P. (1968). Stimulus coding in topographic and non-topographic afferent modalities: On the significance of the activity of individual sensory neurons. Psychol. Rev. 75, 447-465.

[16]
Wenderoth, P. & Beh, H. (1977). Component analysis of orientation illusions. Perception 6, 57-75.

[17]
Nelson, J.I., Kato, H. & Bishop, P.O. (1977). The discrimination of orientation and position disparities by binocularly-activated neurons in cat striate cortex. J. Neurophysiol. 40, 260-283. ((17.6 deg))
Watkins, D.W. & Berkley, M.A. (1974). The orientation selectivity of single neurons in cat striate cortex. Expl Brain Res. 19, 433-446. ((13.9 deg))

[18]
Pointed out by Adam, J. (1964). A note on visual illusions of direction. Aust. J. Psychol. 16, 53-56. The unexpected attraction is also evident in data from Wallace, G.K. & Crampin, D.J. (1969). The effect of background density on the Zollner illusion. Vision Res. 9, 167-177.

[19]
Hammond, P. & MacKay, D.M. (1978). Modulation of simple cell activity in cat by moving textured backgrounds. J. Physiol. 284: 117P. Maffei & Fiorentini (*9).

[20]
(The "atypical" L-R curves were cut at the reviewers' suggestion from the published version of Orban, G., Kato, H. & Bishop, P.O., End-zone region in receptive fields of hypercomplex and other striate neurons in the cat. J. Neurophysiol. 1979, 42, 818-832.) P.O. Bishop, personal communication.

[21]
Domain facilitation could achieve "good continuation" processes such as Marr's theta-grouping:
Marr, D. (1976). Early processing of visual information. Phil. Trans. Roy. Soc. Lond. 275: 483-524
or Caelli's tangent vectors:
Caelli, T.M., Preston, G.A.N. & Howell, E.R. (1978) Implications of spatial summation models for processes of contour perception: a geometric perspective. Vision Res. 18, 723-734.

[22]
Dev, P. (1974). Segmentation processes in visual perception: a cooperative neural model. Univ. of Massachusetts, Amherst. **COINS Technical Report** 74 C-5.

[23] Julesz, B., **Foundations of Cyclopean Perception** (Chicago: Univ. Chicago Press, 1971). Julesz, B. (1960). Binocular depth perception of computer-generated patterns. Bell Syst. tech. J. 39, 1125-1162.

[24] For globality models based on intracortical interactions in the disparity domain analogous to those presented here in the orientation domain, see:

Nelson, J.I. (1975). Globality and stereoscopic fusion in binocular vision. J. theor. Biol. 49, 1-88.

Marr, D. & Poggio, T. (1976). Cooperative computation of stereo disparity. Science, N.Y. 194, 283-287.

Sugie, N. & Suwa, M. (1977). A scheme for binocular depth perception suggested by neurophysiological evidence. Biol. Cybernetics 26: 1-15.

Forshaw, R.B. (1979). The cooperative stereo algorithm: an empirical approach. Biol. Cybernetics 33: 143-149.

Hirai, Y. & Fukushima, K. (1978). An inference upon the neural networks finding binocular correspondence. Biol. Cybernetics 31: 209-217.

Marr and Poggio have also offered a model linking globality to low spatial frequency channels rather than to cooperativity (e.g., via intracortical interactions):

Marr, D. & Poggio, T. (1979). A computational theory of human stereo vision. Proc. R. Soc. Lond. B. 204, 301-328.

However, this model is disconfirmed by recent psychophysical evidence:

Schumer, R.A. & Julesz, B. (1982). Disparity limits in band pass random-grating stereograms. Paper presented at Annual Meeting, Association for Research in Vision & Ophthalmology, Sarasota, 2-7 May.

Single cells in striate and peristriate areas have been shown to respond to contours-in-depth conveyed by a random dot stereogram:

Poggio, G.F. (1980). Neurons sensitive to dynamic random-dot stereograms in Areas 17 and 18 of Rhesus monkey cortex. Paper presented at 10th Annual Meeting, Society for Neuroscience, Cincinnati, OH, 9-14 Nov 1980.

As global processing is needed to "pull out" these Cyclopean contours from the random dot stimulus, the ability of neurons to respond to the contours suggest that global processing can be seen at the cellular level, where it may arise through intracortical interactions of the sort studied here. Furthermore, these interactions may occur as early as the primary visual cortex (Area 17).

[25] As of this writing, the standing of domain interactions as a general principle of cortical organization for higher perceptual processing is as follows. Orientation domain interactions: strong neurophysiological evidence for both inhibition and facilitation, good psychophysical models for a role in sensory **coding errors**, but little understanding of the interactions' role (especially facilitation) in segmentation and **figural** processes generally. Retinal disparity domain: excellent psychophysical models for role in globality (an important bit of processing machinery in stereopsis); no one has sought to collect confirmatory neurophysiological evidence. Spatial frequency: neurophysiologically, claims have been made for columnar structure and even domain interactions:

De Valois, Karen K. & Tootell, Roger B.H. (1982). Spatial frequency inhibition in cat striate cortex cells. Paper presented at Annual Meeting, Association for Research in Vision & Ophthalmology, Sarasota, 2-7 May.

Fourier analysis is a widely useful tool in visual research, and a mirror image of (mathematically equivalent view of) the everyday spatial domain. However, the contention that the brain's perceptual achievements are won in the Fourier domain are controversial. Models for specific perceptual skills other than the details of grating detection thresholds are sadly lacking.

[26]
Kanizsa, G. (1976). Subjective contours. Sci. Amer. 234, (April), 48-52, 30 & 138.
Tynan, P. & Sekuler, R. (1975). Moving visual phantoms: a new contour completion effect. Science 188, 951-952.

[27]
Day, R.H. & Jory, M.K. (1978). Subjective contours, visual acuity and line contrast. In J.C. Armington, J. Krauskopf & B.R. Wooten, eds., Visual Psychophysics and Physiology, pp. 331-340, New York: Academic. Day, R.H. & Jory, M.K. (1980). A note on a second stage in the formation of illusory contours. Percept. Psycho. 27: 89-91.

[28]
Gibson, J.J. & Radner, M. (1937). Adaptation after effect and contrast in the perception of tilted lines. I. Quantitative studies. J. Exp. Psychol. 20, 453-467.

[29]
Julesz, B. (1981). Textons, the elements of texture perception, and their interactions. Nature 290: 91-97.

[30]
Tolhurst, D.J. & Thompson, P.G. (1975). Orientation illusions and after effects: inhibition between channels. Vision Res. 15, 967-972.
Ratliff, F. & Zemon, V. (1982 in press). Some new methods for the analysis of lateral interactions that influence the visual evoked potential. *In Evoked Potentials, Annals* N.Y. Acad. Sci.

[31]
Maffei, L. & Fiorentini, A. (1976). The unresponsive regions of visual cortical receptive fields. Vision Res. 16, 1131-1139.
Nelson, J.I. (1975). Globality and stereoscopic fusion in binocular vision. J. theor. Biol. 49, 1-88, esp. Fig. 17.

[32]
Mountcastle, V.B. (1957). Modality and topographic properties of single neurons of cat's somatic sensory cortex. J. Neurophysiol. 20: 408-434.

[33]
For simple radial columnar structure visible with conventional microscopic examination, see work on mouse "whisker barrels":

> Woolsey, T.A. & van der Loos, H. (1970). The structural organization of layer IV in the somatosensory region (S I) of mouse cerebral cortex. The description of a cortical field composed of discrete cytoarchitectonic units. Brain Res. 17, 205-242.

Evidence for systemmatic orientation and spatial frequency changes with tissue depth has also been presented:

> Bauer, R., Dow, B.M. & Vautin, R.G. (1980). Laminar distribution of preferred orientations in foveal striate cortex of the monkey. Exp. Brain Res. 41, 54-60.

This regularity does not appear in the central visual projection area of cat striate cortex:

> Lee, B.B., Albus, K., Heggelund, P., Hulme, M.J., & Creutzfeldt, O.D. (1977). The depth distribution of optimal stimulus orientations for neurones in cat area 17. Exp. Brain Res. 27, 301-314.

For claimed spatial frequency regularity with depth:

Maffei, L. & Fiorentini, A. (1977). Spatial frequency rows in the striate visual cortex. Vision Res., 17, 257-264.

As X and Y fiber types show laminar segregation, the different tunings may arise in separate parallel channels which do not interact at this stage. Consequently it is likely this observation does not reflect processing of the spatial frequency continuum (i.e., does not support interactions across the spatial frequency domain).

[34]
Hubel, D.H. & Wiesel, T.N. (1974). Sequence regularity and geometry of orientation columns in the monkey striate cortex. J. comp. Neurol. 158: 267-293.

Albus, K. (1975) A quantitative study of the projection area of the central and the paracentral visual field in area 17 of the cat. II. The spatial organization of the orientation domain. Exp. Brain Res. 24, 181-202.

[35]
Hubel, D.H., Wiesel, T.N. & Stryker, M.P. (1978). Anatomical demonstration of orientation columns in Macaque monkey. J. comp. Neurol. 177: 361-380.

CHEMICAL ASPECTS OF VISUAL TRANSDUCTION

by

Aaron Lewis
School of Applied and Engineering Physics
Cornell University
Ithaca, NY 14853

In this paper I will briefly review the postulated sequency of nucleotide changes in photoreceptor cells during the time course of visual transduction. The final and most important nucleotide change during visual transduction is the alteration of cyclic guanasine monophosphate (cGMP) to guanasine monophosphate (GMP). This reaction is simply the breaking of a bond which is the only difference between cGMP and GMP. Such biochemical reactions occur in many systems which transduce chemical signals and are usually controlled by a hormone induced, membrane bound adenylate cyclase enzyme.[1] However, in rod outer segments there is nearly universal agreement that this reaction is caused by an enzyme called phosphodiesterase (PDE) which is turned on by rhodopsin light absorption.

How does rhodopsin turn on PDE and what is the role of cyclic nucleotide alterations in visual excitation? This is an area of intensive research. At first it was shown that one rhodopsin activated at least 1000 PDE molecules which, once turned on, converted many cGMP to GMP.[2] This, of course, caused much excitement since clearly such a process could be the elusive, but required, amplification step in vision if the timescales for cyclic nucleotide transformation were appropriate. Recently, however, it has been suggested[3] that the activation of PDE does not occur directly, instead experiments indicate that there is another protein turned on in large numbers by excited rhodopsin. This protein has been dubbed "transducin" since it would be the essential element in the transduction step.

In order to understand the role of transducin and other observed light induced biochemical alterations in rod outer segments such as the conversion of GTP→GDP, a flow scheme is shown below. This scheme integrates cyclic nucleotide alterations into a plausible mechanism.

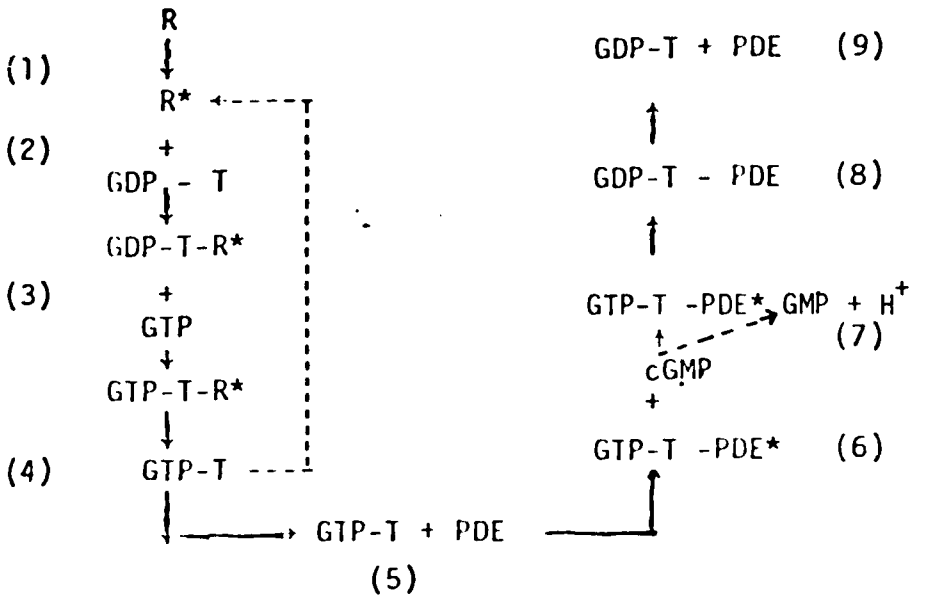

The first step in all these changes is the conversion of rhodopsin by light to an activated state, R* this is shown in the scheme above as (1). At this point in (2) membrane bound R* reacts with the protein transducin which in the dark has complexed to it GDP and is free in the ROS cytoplasm. This forms a GDP-T-R* complex which reacts in (3) with GTP causing the GDP of the complex then exchanges for GTP in the cytoplasm of ROS. Then the GTP-T-PDE* reacts with cGMP forming GMP plus a H+ and giving back the GTP-T-PDE* activated complex which is

ready to catalyze another cGMP→GMP reaction. Eventually reaction with H_2O in (7) hydrolyzes GTP from the GTP-T-PDE* forming GDP-T-PDE in (8) and inactivating PDE. This leads in (9) to the splitting of the complex giving GDP-T + PDE and the GDP-T is then ready for another series of reactions with R*.

In summary, the two observables in light activated ROS are a reduction in cGMP levels to GMP and a reduction in GTP concentration to GDP as a result of the final step in T and PDE inactivation. As a result of this reaction the R* is cleaved in (4) from the GTP-T-R* complex and is free to react with another GDP-T complex to catalyze the exchange of GDP with GTP. This is depicted by the dashed line in the above scheme and is the amplification step in the hypothesis since the R* catalyzed exchange has been shown by radioactively labelled GTP to take place on approximately $\simeq$1000 transducin molecules.

Once GTP-T is formed, the T is capable of reacting in (5) with the enzyme phosphodiesterase (PDE) to form a GTP-T-PDE* complex which activates PDE. The complex with PDE then reacts to convert cGMP→GMP + H^+. It is clear that a focus of future experiments will have to be to detect the timescales of the cGMP→GMP and the GTP→GDP reactions under physiological conditions. Such kinetic experiments are crucial if we are to determine whether the cyclic nucleotide cascade discussed above is a plausible component of the excitation processes in visual transduction or whether these reactions could be connected to the control of the sensitivity of the cell to light.

REFERENCES

1. J.S. Pober and M.W. Bitensky, Adv. Cyclic. Nucleotide Res. **11**, 265, (1979).

2. A. Lewis in Advances in Infrared and Raman Spectroscopy ed. R. Hestor and R. Clarke, Vol. X, Heydyn, N.Y. 1981, p. 432.

3. B. K. Fung, J.B. Hurley and L. Stryer, Proc. Natl. Acad. Sci. (U.S.A.) **78**, 152 (1981).

SPECTRALLY SELECTIVE ADAPTATION EFFECTS

Gloria Twine Chisum, Ph.D.
and
Phyllis E. Morway

Naval Air Development Center
Warminster, Pennsylvania 18974

Technological developments of recent years have increased the number of monochromatic stimuli to which flight crew members are exposed. In the case of Head-Up Displays, nearly-monochromatic stimuli arise from cathode ray tube phosphors or from laser stimuli in the Holographic Head-Up Displays. In the case of Helmet-Mounted Displays, stimuli from either a cathode ray tube phosphor, light emitting diodes or holographic images also provide nearly-monochromatic spectral stimuli. In the case of eye protective devices, the spectral quality of the visual field is broader band, but now rather than intermittent spectral stimuli, the spectral stimuli are present for longer periods of time and the entire visual field is viewed through a spectrally distorting filter. Thus, for perhaps the duration of a mission the visual field is one viewed through spectrally distorting filters. Still another source of spectral stimulation is from lighting. For a number of years the naval aviation environment has been lit by red light for the primary purpose of preserving dark adaptation for performance of low light level or night tasks. Periodically the use of red lighting has been reassessed, and proposals have been made for low-level white lighting and for other types of light. One type of lighting which is currently receiving increasing attention is low pressure sodium vapor lights. The attractiveness of this light stems both from the nearly monochromatic character of the light and for the relatively low power consumption required to provide the relatively highly luminous output of the light. We have undertaken a series of experiments directed at determining the effects of spectrally distorted stimuli on performance of visual tasks. In the experiment described here, the effect of adaptation to white, red and sodium vapor, or yellow, lights on recovery of dark adaptation was measured by the time required to discriminate visual acuity targets of two levels of acuity under low light level conditions.

APPARATUS

A diagram of the optical system used to present the visual stimuli is shown in Figure 1. The optical system is composed of three optical channels, Ch 1, Ch 2 and Ch 3. The light sources in two of the channels are tungsten filament lamps, T1 and T2. The light source in the third channel is a low pressure sodium lamp (SOX 18 W), SL. The light beams in each of the three channels pass through collecting lenses at L_1, collimating lenses at L_2, and are brought to a focus by L_3 at the apertures A_1. The beams are again collimated by lenses L_4. From this point, the beams are conducted to the eyepoint, EP, by various means which allow the three beams to combine and present a single visual field to the observer. The Ch 1 beam is focused by L_5 at the A_2 aperture, again collimated by L_6 and reflected at a right angle from the beam splitter B_3 into the ocular of the system. The Ch 2 beam is focused by L_5, at A_2, passes through the beam splitter B_1 to the collimating lens L_6. The beam splitter B_2 reflects the beam at a right angle into the ocular. The Ch 3 beam comes to focus at A_2 after being reflected at a right angle from the mirror, M. Another right angle reflection from B_1 passes the beam through the collimating lens, L_6, to B_2 where a third right angle reflection directs the beam into the ocular. The ocular is mounted in the wall of a light-tight chamber in which the observer is seated. To the eye of the observer positioned at EP by a dental impression bite plate, the last lens of the ocular is seen in Maxwellian view as an evenly illuminated 60° field when no field stop is placed in the collimated portion of the beam.

Control of the presentation of the beams is provided by a leaf camera shutter and a paddle shutter located at S. The target, G, is located in the collimated portion of Ch 2 between lenses L_4 and L_5. The G is produced by one of two gratings of parallel, opaque lines separated by clear spaces equal to the lines. The G is mounted so it can be oriented either horizontally or vertically in the view of the observer. Resolution of the grating patterns requires a visual acuity, of either 0.33 or 0.13 (the reciprocal of the visual angle in minutes). The target illumination is provided by the tungsten lamp T_1 and controlled in intensity by neutral density filters F_1. A field stop placed between L_4 and L_5 eliminates the field surrounding the target.

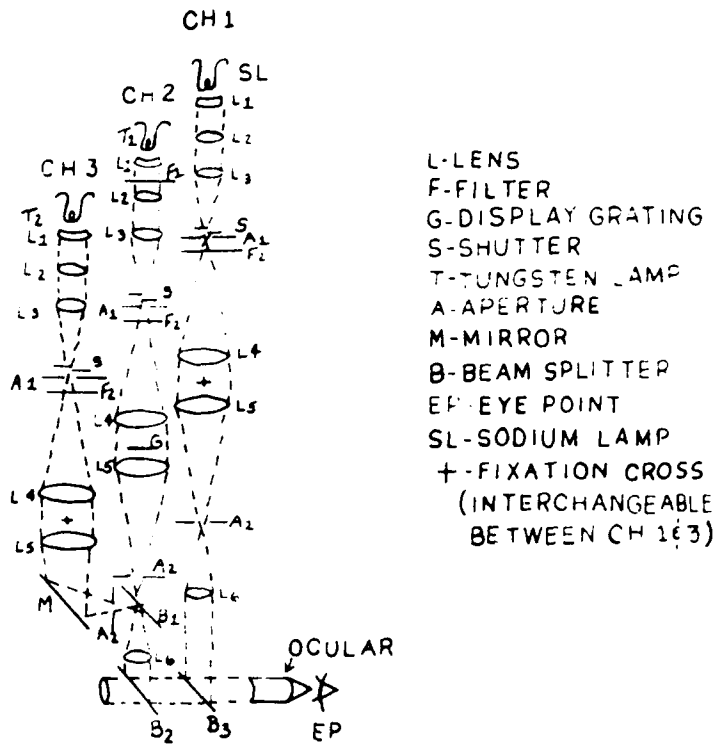

Figure 1 - Optical System *Schematic Diagram*

The gaze of the O is directed by the fixation cross, +, located in the collimated portion of either Ch 1 or Ch 3 between L_4 and L_5. The choice of beams is dependent upon which beam is serving as the adapting source. When Ch 3 serves as the red or white adapting source, Ch 1 provides the source for the fixation cross. When the sodium lamp in Ch 1 serves as the adapting source, Ch 3 provides the source for the fixation cross. The adapting and fixation sources are made interchangeable by means of filters F_2. There are also filters at this location which serve to equate the intensity of the white and yellow sources to that of the red source, which is the dimmest of the three sources.

The red source is produced by attenuating the tungsten lamp, T_2 with a Navy standard red filter #3215-250. In Ch 1, the source is attenuated by a 6200 Å interference filter and 0.5 neutral density filter to equate the source to the Ch 3 red filter to produce the light for the fixation cross, and by neutral density filters along to produce the adapting source. A field stop placed between L_4 and L_5 in Ch 1 and Ch 3 eliminates the field surrounding the fixation cross.

An observer positioned at EP initially sees a fixation cross followed by a 60° visual field of the desired adapting source. The adapting field is replaced at the approximate time by a fixation cross and a target centered in the 60° field. The cross is positioned to the left of the target with the right arm of the cross extending into the target.

The stimulus sequencing, grating orientation, luminance adjustments and data recording are controlled automatically by a programmable digital logic system shown schematically in Figure 2. The observer controls consist of a foot switch, FS, which is used to initiate a trial sequence, and two response button, R, which are used to indicate target detection and orientation. The electro-mechanical controls consist of three shutter controls, S_1, S_2, & S_3, which effect the presentation of the adapting beam, the fixation cross and the target, a filter positioning motor, F which introduces the filters which control the display luminance, and a stepping motor, G, which positions the target in either a horizontal or vertical position. Sequencing of the operation of the electro-mechanical devices and inputs to the data recorder are mediated by the digital logic system. The data recording system is a Digital Equipment Corp. MINC-23 micro data processor. Completion of a response by the 0 triggers the system to record the number, filter wheel position, response time and response correctness.

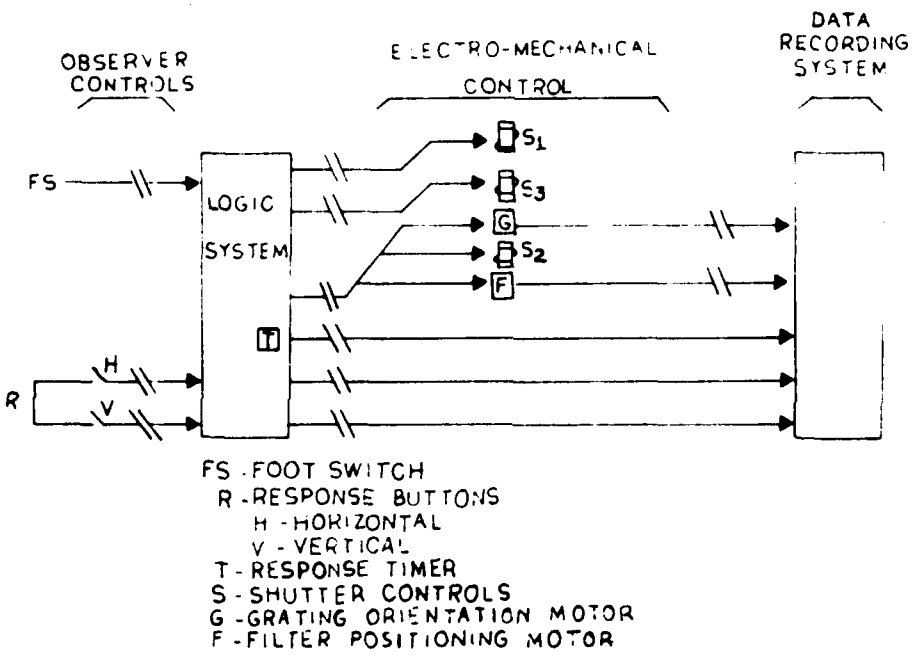

Figure 2 - Stimulus Control System Schematic Diagram

CALIBRATION

The radiances of the unfiltered visual field presented by each beam were measured with an EG&G model 580/585 spectroradiometer, and the luminances were calculated. The transmittance of the interference filter and the red filter were measured with a Perkin Elmer Model 402 UV-Visible spectrophotometer. The transmittances of the neutral density filters used to adjust the luminances of the yellow and white sources to match the dimmest red source and the luminances of the targets were measured with the Spectra Pritchard Model 1980A-PL Photometer and the Gardner Laboratory XL 211 Hazemeter. The filter combinations determined in this manner were placed in the optical system. The accuracy of the calculated photometric matches were verified

and any minor adjustments were made by means of a psychophysical procedure. The adjustments eliminated just detectable differences between beams and between filter conditions in a beam.

The area calibrations were accomplished by mounting a calibrated telescope in front of the ocular of the optical system. The calibrations in visual angle were made by rotating the telescope around the focal point of the ocular and reading the scale of the mount which was calibrated to 15" of arc. The cross hairs of the telescope were set at the edge of the stimulus to be measured and setting of the telescope mount scale was noted. The mount was then rotated so that the cross hairs intersected with the opposite edge of the stimulus dimension being measured and the scale was noted again. This procedure was repeated 10 times. The difference between the means of the two readings provided a measure of the visual of the visual angle of the stimulus. The 60° field of view, the target and the fixation cross were measured in this manner. This procedure also allowed the target and fixation cross to be centered in the 60° field of view.

PROCEDURE

All observers, (O), were reqiured to have at least 20-30 vision and normal color vision. To assure this, the Snellen Eye Chart, the Farnsworth-Munsell 100-Hue Test and the Dvorine Pseudo-Isochromic Plates were administered prior to an O's first experimental session. The experiments design is shown in Table 1. All conditions, A-H were presented in a random blanced order to the observers. Two acuity gratings requiring resolutions of 0.33 and 0.13 were presented following an adapting light of yellow, red or white or no light adaptation, the control condition (conditions G and H).

Table I. Experimental Design

ADAPTING LIGHT	DISPLAY GRATING ACUITY REQUIREMENTS	
	0.33	0.13
YELLOW	A	B
RED	C	D
WHITE	E	F
NO LIGHT	G	H

One-half of the data for one condition were collected during each experimental session. The visual fields are shown in Figure 3. At the start of a session, the 0 was seated in a light-tight chamber and allowed to dark adapt for 10 minutes. A buzzer alerted the 0 at the completion of this period. At the same time, a fixation cross was presented at the ocular. By means of a dental impression bite board, the 0 positioned himself at the ocular and fixated the cross. When the 0 was properly positioned and accommodated, he pressed the foot switch which initiated a randomly selected one minute presentation of a 60° adapting field of either a red, white, yellow (sodium) or no light. At the end of the one minute adapting period, simultaneously, the adapting field disappeared and the target appeared centered in the ocular, adjacent to the fixation cross. The 0 was required to determine the horizontal or vertical orientation of the display grating and to respond by pressing the proper button on the hand switch. As soon as a response was made, the paddle shutter closed the target from the 0's view. The filter condition was changed and a pre-set random coder operated to adjust the target orientation. The target paddle shutter re-opened and the 0 was again presented with a target to which he responded. This sequence was repeated five times with each target dimmer than the preceding one. Following the fifth response, the leaf camera shutters closed from the 0's view both the fixation cross and the target, and the timing circuit started a one minute re-adaptation period. At the completion of the re-adaptation period, the buzzer sounded and the entire sequence of the adaptation followed by five targets was repeated. A completed experimental condition usually consisted of 16 adaptation-target sequences for a total of 80 responses per session. To avoid fatigue, all experimental sessions lasted approximately one hour. Complete data were collected for three observers.

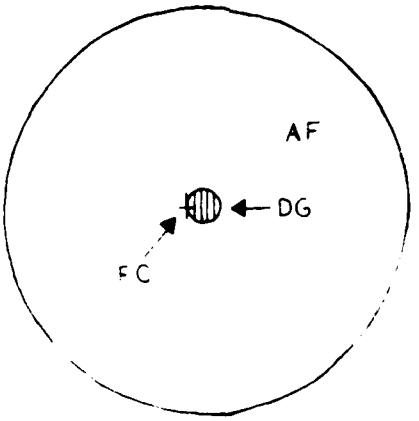

AF - ADAPTING FIELD

DG - DISPLAY GRATING

FC - FIXATION CROSS

Figure 3 - Visual Fields Schematic Diagram

RESULTS

The results for the three observers individually and for all observers are shown in Figures 4 through 7. The time required to resolve the 0.33 visual acuity target was, not surprisingly, longer than that required to resolve the 0.13 acuity target, and the time required to resolve the targets following light adaptation was longer than that required to resolve the targets with no pre-adapting condition. In general, the yellow light adaptation was followed by more rapid recovery than either the red or white adaptation. For one observer, DM, there is essentially no difference between the three light adaptation conditions and one observer, DD, showed a marked reversal of the recovery times for the dimmest 0.33 acuity target. The pattern of significant differences for these data is shown in Table III.

Table II shows the Analysis of Variance Summary table for the response time data. The main effects and those interactions for which the F ratios are significant are shown in the table. Target acuity produced the most significant effect. Target luminance, as would be expected, and the adapting conditions also produced significant effects. A significant portion of the variance is also attributable to the observers. Inspection of figures five and six reveals the reason for this significant main effect, as well as the significant interaction between observer and the adapting conditions. The interactions between the target luminance and the adapting conditions are due in a major way to the relative response times at the lowest display luminance. For two observers there was reversal of the relative positions and for one a shift in the magnitude of the differences. Recognizing that combining the data for the three observers is not statistically correct, comparison of the individual data with the combined data indicates that the combined data contributes to a conceptualization of the effect being studied and does not distort the results if it is remembered that there are significant individual differences. The mean response times for all observers is shown in the right side of Table II. It is readily seen in this table that the difference in the response times to the 0.13 acuity target are not significantly different. There are significant differences in the response times to the 0.33 acuity target. The patterns of these differences is shown in Table III where the significant differences between individual pairs of means for individual observers and for all observers are reported. Resolution of the display following white adaptation was in general slower than that following any of the other adapting conditions. The most obvious differences are between the dark adapted, or control, condition and each of the light adapted conditions. Though there appears to be slightly faster re-adaptation following the yellow light adaptation, the only instance in which the difference between the red and yellow adapting conditions is significant in the one case where observer DD showed the significantly longer response time to the dimmest target following the yellow adaptation. Examination of the error scores in Table IV shows that observer DD made more errors than either of the other observers. His longest error score is in responses to the dimmest 0.33 target following the yellow adapting condition. He obviously had the greatest difficulty with the foveal acuity conditions, particularly following the chromatic adaptation.

DISCUSSION

The results of the experiment reported here suggest that recovery of dark adaptation occurs more quickly following narrow wavelength band adaptation as opposed to broader wavelength adaptation. The light used in the yellow adapting conditions, Figure 8, was composed of a narrow band width centered at 580 nanometers with very weak emission in the longer wavelength region and a weak emission at 490 nanometers due to an enhancement gas in the sodium vapor. The results also suggest that recovery of dark adaptation following the sodium vapor light adaptation is also more rapid than either white or red adaptation. The apparent advantage of the sodium light over the red light is possibly due to the narrow spectral band output of the sodium lamp.

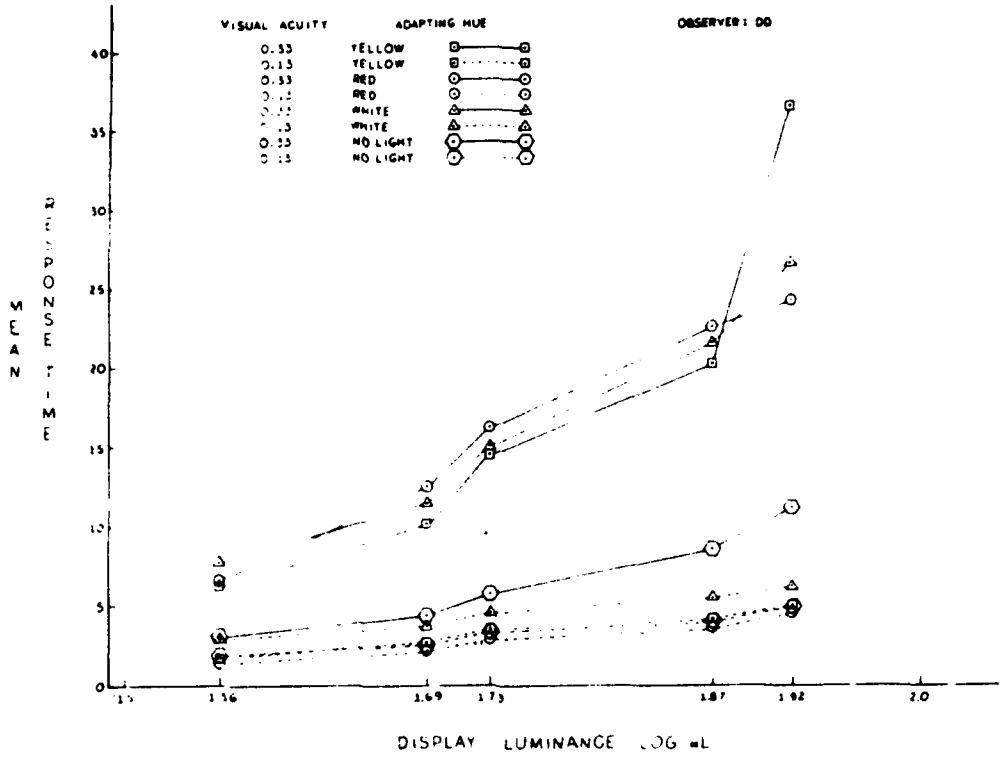

Figure 4 - Response Times – Observer DD

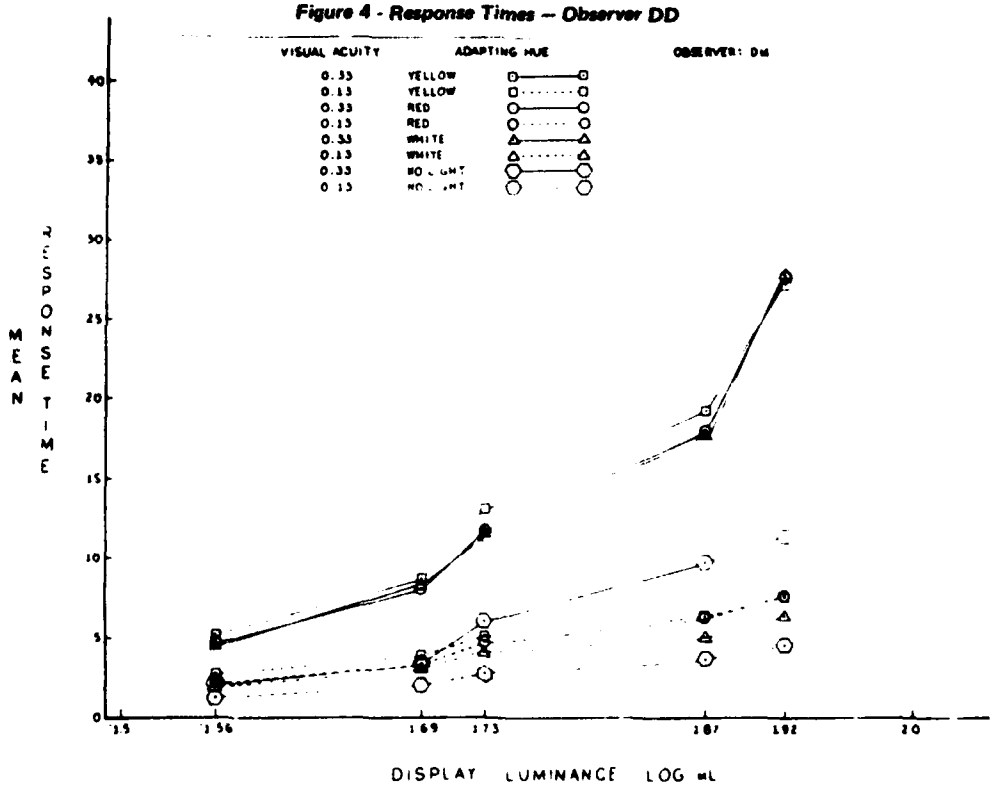

Figure 5 - Response Times – Observer DM

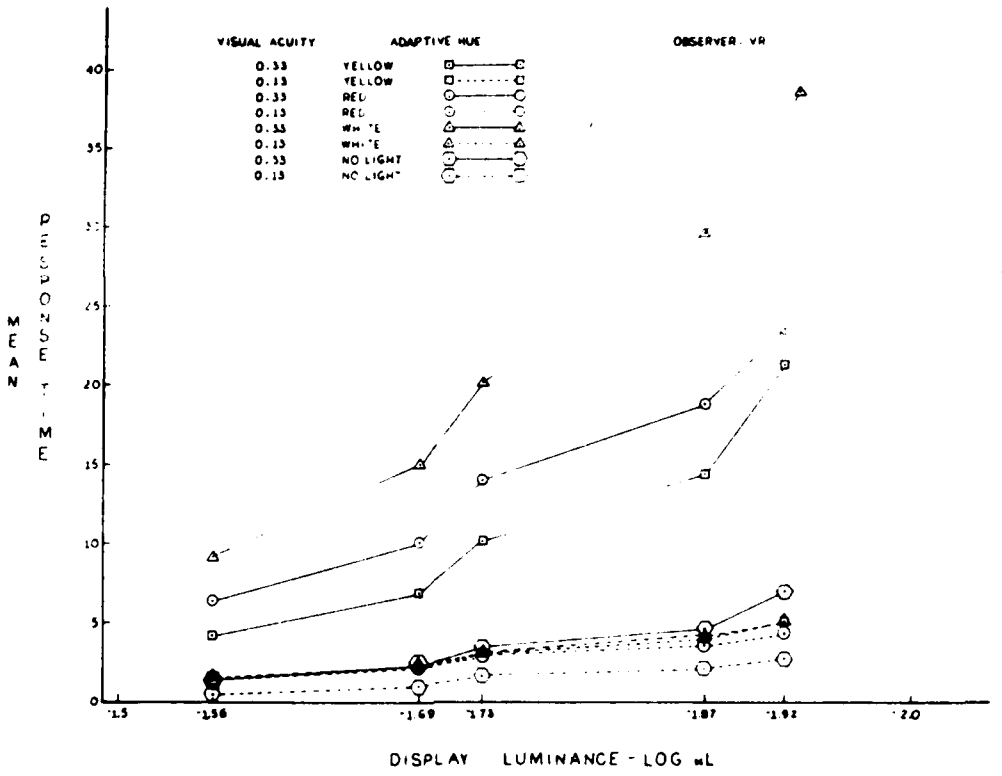

Figure 6 - Response Times – Observer VR

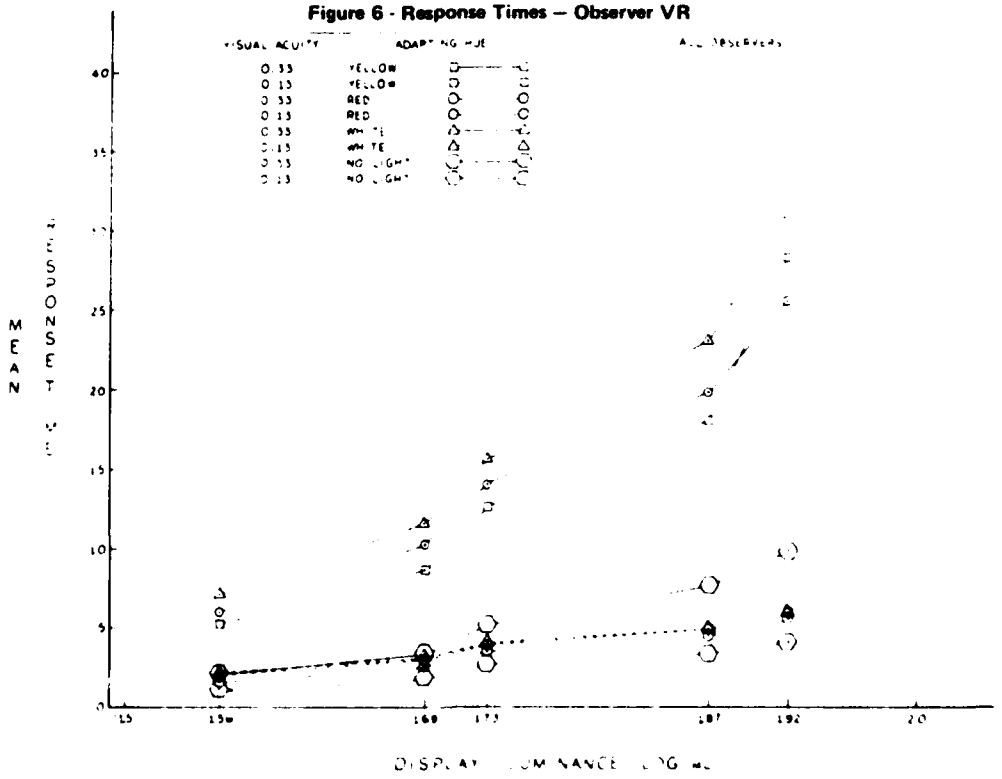

Figure 7 - Response Times – All Observers

Table II. Analysis of Variance Summary Table and Mean Response Times – All Observers

ANALYSIS OF VARIANCE
SUMMARY TABLE

Source Of Variance	DF	F
Target Acuity (G)	1	1666.00**
Target Luminance (L)	4	269.96**
Observer (O)	2	7.16**
Adapting Light (A)	3	151.61**
LxA	12	8.54**
OxA	6	14.57**
LxOxA	24	1.56*
Error	1919	
Total	3839	

*P 0.05
**P 0.001

MEAN RESPONSE TIMES - ALL OBSERVERS

TARGET ACUITY	ADAPT LIGHT	-1.56	-1.69	-1.73	-1.87	-1.92
0.33	W	7.2	11.6	15.6	23.0	31.0
	Y	5.3	8.7	12.6	18.0	28.3
	P	6.0	10.3	14.0	19.8	25.5
	D	2.1	3.4	5.1	7.7	9.9
0.13	W	2.2	3.1	4.0	4.9	5.9
	Y	2.0	3.0	3.9	4.9	5.9
	R	1.7	2.6	3.5	4.5	5.6
	D	1.2	1.9	2.7	3.4	4.1

Table III. Significant Mean Difference for Individual Pairs of Means for Individual Observers and All Observers – 0.33 Acuity

ADAPTING LIGHT	ADAPTING LIGHT														
	WHITE					YELLOW					RED				
	DISPLAY LUMINANCE - LOG mL														
	-1.56	-1.69	-1.73	-1.87	-1.92	-1.56	-1.69	-1.73	-1.87	-1.92	-1.56	-1.69	-1.73	-1.87	-1.92
YELLOW		V A	V* A*	V* A*	D* V* A*										
RED				V* A*	V* A*					D* A					
DARK	V A*	D V* A*	D V* A*	D* V* M A*	D* V* M* A*	A*	A*	D V M A*	D* V* M* A*	D* V* M* A*	A*	D V A*	D* V* A*	D* V* M A*	D* V* M* A*

TARGET ACUITY - 0.33

D,V,M - OBSERVERS

A - ALL OBSERVERS

* - P<.01

Table IV. Error Scores

TARGET ACUITY	ADAPT. LIGHT	OBSERV.	-1.56	-1.69	-1.73	-1.87	-1.92
0.33	W	D	1	3	7	10	5
		M					
		V			1	2	3
	Y	D		1	3	6	12
		M					
		V	1	1		3	2
	R	D	3	7		7	4
		M					1
		V		2	3	3	7
	D	D			1	4	3
		M	1		3	5	
		V				1	3
0.13	W	D	1				
		M					
		V			1		1
	Y	D	1				2
		M					
		V				1	3
	P	D	1	1	2		2
		M					
		V					
	D	D				1	
		M			1		
		V					

AD-A122 076 RESEARCH PROGRAM REVIEW AIRCREW PHYSIOLOGY(U) NAVAL AIR 2/2
DEVELOPMENT CENTER WARMINSTER PA AIRCRAFT AND CREW
SYSTEMS TECHNOLOGY DIRECTORATE G T CHISUM ET AL.
UNCLASSIFIED JUN 82 NADC-82232-60 F/G 6/19 NL

END

FILMED
DTIC

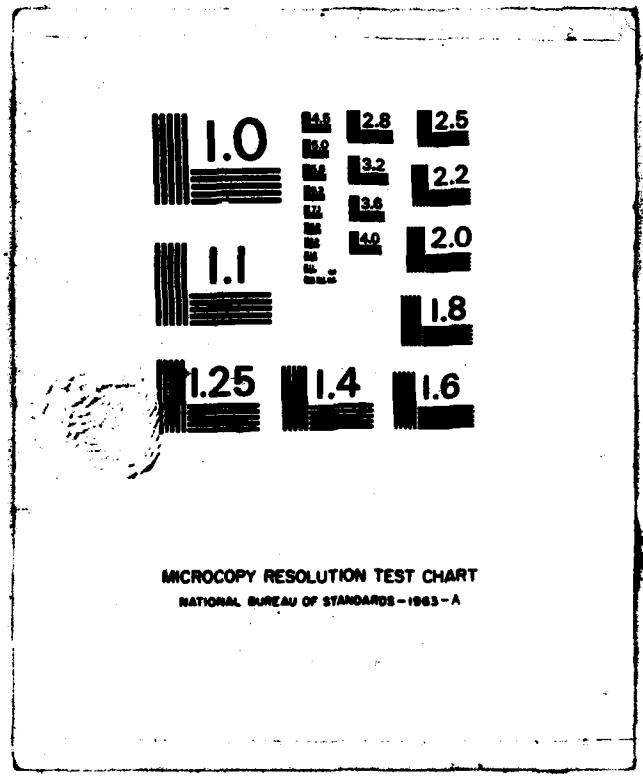
1.0
1.1
1.25
1.4
1.6
2.8
2.5
3.2
2.2
3.6
2.0
4.0
1.8
MICROCOPY RESOLUTION TEST CHART
NATIONAL BUREAU OF STANDARDS - 1963 - A

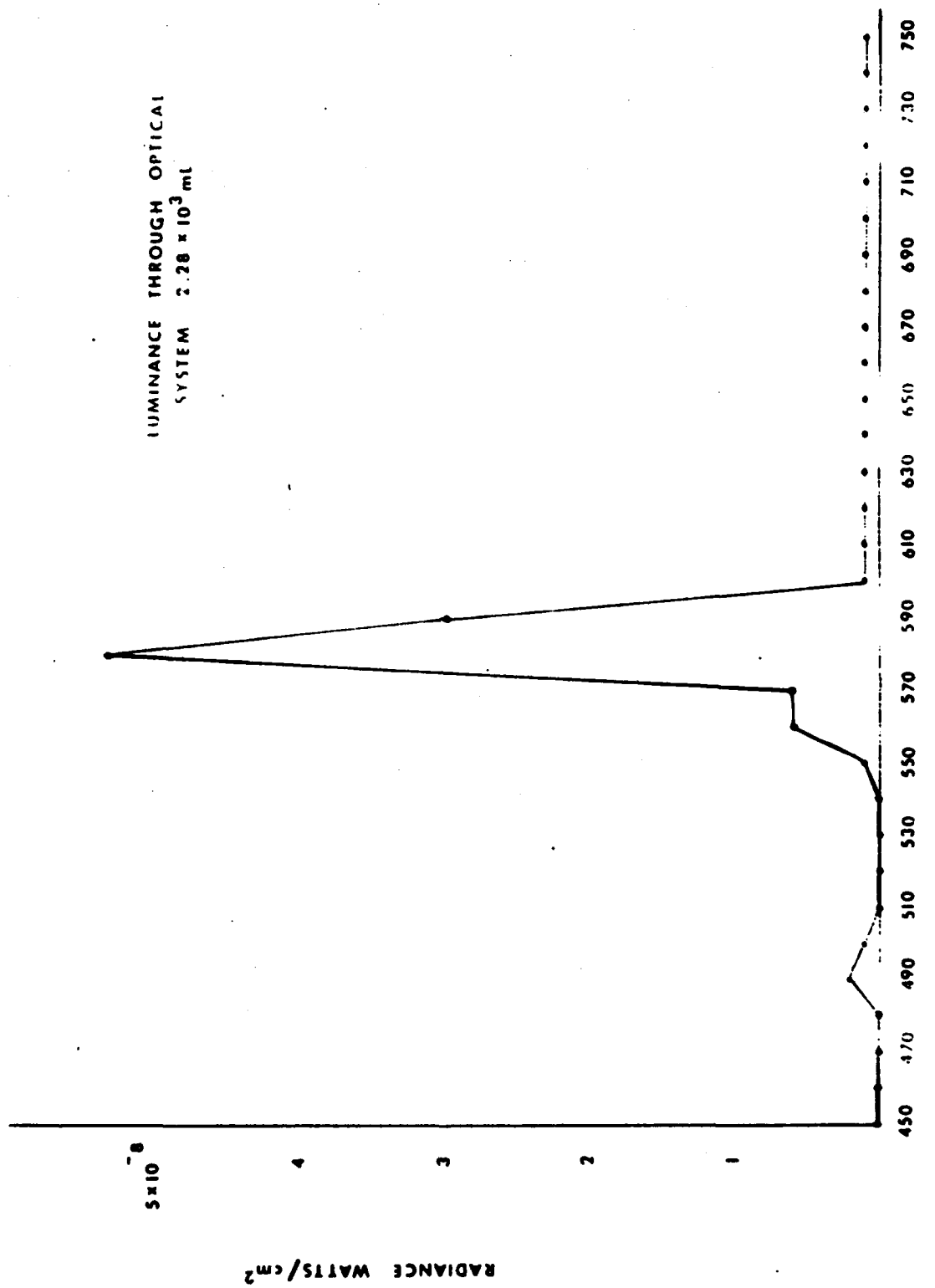

Figure 8 - Sodium Lamp Emission

The red light is produced by filtering a broad spectral output lamp, and the filter which is used has a relatively broad spectral transmittance which begins at 600 nanometers (Figure 9).

The operational significance of the findings of this exeriment relate to the high luminance production with relatively low power consumption of the SOX (Sodium Vapor Lamp) as compared with the red light where the spectral band of the light is achieved by filtering a broad spectral output light with a red filter. A large portion of the power used in producing the light is wasted.

The data reported here are a part of the total projected data for the experiment. We are collecting data for two additional observers, and hope to have the complete data in hand within a month.

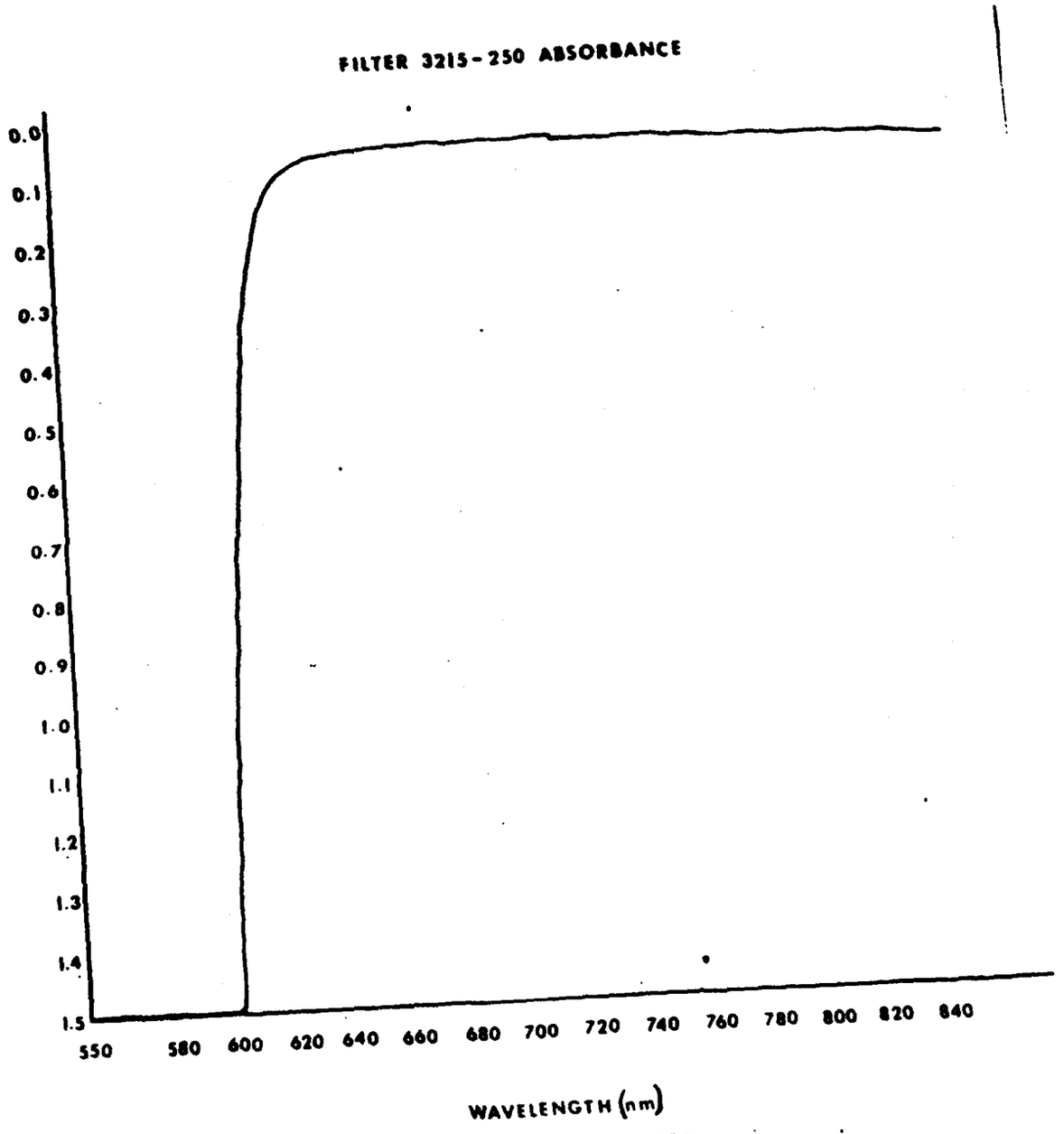

Figure 9 - Transmittance of Standard Navy Red Filter

DISTRIBUTION LIST (Cont'd)

	No. of Copies
Dr. Milton Whitcomb, Committee on Hearing Bioacoustics and Biomechanics, National Academy of Sciences, Washington, DC 20418	1
CAPT James E. Goodson (Code L5), Naval Aerospace Medical Research Laboratory, Pensacola, FL 32512	1
Major Roger W. Wiley, Bio-Optical Division, US Army Aeromedical Research Laboratory, Fort Rucker, AL 36362	1
Dr. A. Terry Bahill, Biomedical Engineering Program, Dept. of Electrical Engineering, Carnegie-Mellon University, Pittsburgh, PA 15213	1
Dr. Leonard Matin, Dept. of Psychology, Schermerltorn Hall, Columbia University, New York, NY 10027	1
U.S. Air Force School of Aerospace Medicine, Brooks Air Force Base, Texas 78235	1
U.S. Army Aeromedical Research Lab., P.O. Box 474, Ft. Rucker, AL 36362	2
U.S. Army Armament & Development Command, Aberdeen Proving Ground, Aberdeen, MD 12005	1
U.S. Army Natick Laboratories, Natick, MA 01761	1
NASA-AMES Research Center, Moffett Field, CA 94035	1
Chief of Naval Material, MAT 0723, Washington, DC 20360	1
National Aeronautical & Space Administration, Lewis Research Center, Cleveland, OH 44135	1
Federal Aviation Agency, 6500 S. MacArthur, P.O. Box 25082, Oklahoma City, OK 73125	1
Naval Biodynamics Laboratory, Box 29407, New Orleans, LA 70189	1
Naval Air Material Research Laboratory, New Orleans, LA 70189	4
NASA-Lewis Research Center (Library), Cleveland, OH	1

DISTRIBUTION LIST

NADC-82232-60

AIRTASK NO. WR0410101
Work Unit No. DG104

	No. of Copies
Director, Defense Technical Information Center, Bldg. 5, Cameron Station, Alexandria, VA 22314	12
Chief of Naval Operations (OP-98E) Navy Department, Washington, D.C. 20350	1
Chief of Naval Research, 800 N. Quincy St., Arlington, VA 22217	2
(1 for Code 440)	
(1 for Code 441)	
National Library of Medicine, Bethesda, MD 20014	1
Commanding Officer, Naval Medical Research and Development Command, National Medical Center, Bethesda, MD 20014	9
(3 for Code 71)	
(3 for Code 7113)	
(1 for Code 7130)	
(2 for Code 42)	
Commanding Officer, Naval Aerospace Medical Research Laboratory, Naval Air Station, Pensacola, FL 32508	2
Commanding Officer, Naval Aerospace Medical Institute, Naval Air Station, Pensacola, FL 32508	1
Commander, Operational Test & Evaluation Force, Naval Base, Norfolk, VA 23511	1
Commanding Officer, Naval Training Equipment Center, Orlando, FL 32813	2
Commanding Officer, Naval Submarine Medical Center, Naval Submarine Base, New London, Groton, CT 06340	1
Commander, Naval Air Systems Command, Washington, DC 20361 (00D4)	14
(2 for retention)	
(8 for AIR-32R)	
(1 for AIR-340B)	
(1 for AIR-531)	
(1 for AIR-5311C)	
(1 for AIR-5313)	
Commanding Officer, Naval Health Research Center, P.O. Box 85122, San Diego, CA 92138	1

DISTRIBUTION LIST (Cont'd)

	No. of Copies
Commander, Naval Safety Center, Naval Air Station, Norfolk, VA 23511	1
Commander, Naval Air Test Center, Patuxent River, Md 20670	
Air Force Aerospace Medical Research Lab., AMRL/DAL Library, Wright-Patterson Air Force Base, OH 45433	2
Air University Library, Maxwell Air Force Base, Montgomery, AL 36122	1
Headquarters, TAC/SPGA, Langley Air Force Base, Hampton, VA 23665	
Science & Technology Div., Library of Congress, 110 2nd St., S.E., Washington, DC 20540	1
Dr. James A. Bynum, US Army AMRL, P.O. Box 476 Fort Rucker, AL 36362	1
LTC John K. Crosley, US Army AMRL, Fort Rucker, AL 36362	1
Dr. Siegfried Gerathewohl, Federal Aviation Administration Washington, DC 20591	1
Dr. John J. O'Hare, Office of Naval Research, Code 442, Arlington, VA 22217	1
Ms. Helen Paulsen, USN Submarine Base, Box 900, Groton, CT 06340	1
Dr. Lawrence Stark, 226 Minor Hall, University of California, Berkeley, CA 94720	1
Mr. Dennis Breglia, Naval Training Equipment Center, Code N-731, Orlando, FL 32813	1
Mr. John H. Allen, Naval Training Equipment Center, Code N-731, Orlando, FL 32813	1
Dr. Jeremiah Nelson, Dept. of Ophthalmology, PHL 811, New York University Medical Center, 550 First Avenue, New York, NY 10016	1
Prof. Aaron Lewis, School of Applied and Engineering Physics, Cornell University, Ithaca, NY 14853	1
Dr. Myron L. Wolbarsht, Department of Ophthalmology, Duke University Medical Center, Durham, NC 27710	1

DISTRIBUTION LIST

NADC-82232-60

AIRTASK NO. WR0410101
Work Unit No. DG104

	No. of Copies
Director, Defense Technical Information Center, Bldg. 5, Cameron Station, Alexandria, VA 22314	12
Chief of Naval Operations (OP-98E) Navy Department, Washington, D.C. 20350	1
Chief of Naval Research, 800 N. Quincy St., Arlington, VA 22217 (1 for Code 440) (1 for Code 441)	2
National Library of Medicine, Bethesda, MD 20014	1
Commanding Officer, Naval Medical Research and Development Command, National Medical Center, Bethesda, MD 20014 (3 for Code 71) (3 for Code 7113) (1 for Code 7130) (2 for Code 42)	9
Commanding Officer, Naval Aerospace Medical Research Laboratory, Naval Air Station, Pensacola, FL 32508	2
Commanding Officer, Naval Aerospace Medical Institute, Naval Air Station, Pensacola, FL 32508	1
Commander, Operational Test & Evaluation Force, Naval Base, Norfolk, VA 23511	1
Commanding Officer, Naval Training Equipment Center, Orlando, FL 32813	2
Commanding Officer, Naval Submarine Medical Center, Naval Submarine Base, New London, Groton, CT 06340	1
Commander, Naval Air Systems Command, Washington, DC 20361 (00D4) (2 for retention) (8 for AIR-32R) (1 for AIR-340B) (1 for AIR-531) (1 for AIR-5311C) (1 for AIR-5313)	14
Commanding Officer, Naval Health Research Center, P.O. Box 85122, San Diego, CA 92138	1

DISTRIBUTION LIST (Cont'd)

	No. of Copies
Commander, Naval Safety Center, Naval Air Station, Norfolk, VA 23511	1
Commander, Naval Air Test Center, Patuxent River, Md 20670	
Air Force Aerospace Medical Research Lab., AMRL/DAL Library, Wright-Patterson Air Force Base, OH 45433	2
Air University Library, Maxwell Air Force Base, Montgomery, AL 36122	1
Headquarters, TAC/SPGA, Langley Air Force Base, Hampton, VA 23665	
Science & Technology Div., Library of Congress, 110 2nd St., S.E., Washington, DC 20540	1
Dr. James A. Bynum, US Army AMRL, P.O. Box 476 Fort Rucker, AL 36362	1
LTC John K. Crosley, US Army AMRL, Fort Rucker, AL 36362	1
Dr. Siegfried Gerathewohl, Federal Aviation Administration Washington, DC 20591	1
Dr. John J. O'Hare, Office of Naval Research, Code 442, Arlington, VA 22217	1
Ms. Helen Paulsen, USN Submarine Base, Box 900, Groton, CT 06340	1
Dr. Lawrence Stark, 226 Minor Hall, University of California, Berkeley, CA 94720	1
Mr. Dennis Breglia, Naval Training Equipment Center, Code N-731, Orlando, FL 32813	1
Mr. John H. Allen, Naval Training Equipment Center, Code N-731, Orlando, FL 32813	1
Dr. Jeremiah Nelson, Dept. of Ophthalmology, PHL 811, New York University Medical Center, 550 First Avenue, New York, NY 10016	1
Prof. Aaron Lewis, School of Applied and Engineering Physics, Cornell University, Ithaca, NY 14853	1
Dr. Myron L. Wolbarsht, Department of Ophthalmology, Duke University Medical Center, Durham, NC 27710	1